

Ion-Neutral Chemistry of Importance to Astrophysical  
and Cosmological Environments

by

Oscar Martinez Jr.

B.S., Chemistry

University of Maryland, Baltimore County, 2005

B.A., Modern Languages and Linguistics (Russian)

University of Maryland, Baltimore County, 2005

A thesis submitted to the  
Faculty of the Graduate School of the  
University of Colorado in partial fulfillment  
of the requirements for the degree of  
Doctor of Philosophy  
Department of Chemistry and Biochemistry

2010

This thesis entitled:

Ion-Neutral Chemistry of Importance to Astrophysical  
and Cosmological Environments

Written by Oscar Martinez Jr.

has been approved for the Department of Chemistry and Biochemistry

by

---

Veronica M. Bierbaum

---

Theodore P. Snow

Date\_\_\_\_\_

The final copy of this thesis has been examined by the signatories, and we find that both the content and the form meet acceptable presentation standards of scholarly work in the above mentioned discipline.

Martinez Jr., Oscar (Ph.D., Physical Chemistry)

Ion-Neutral Chemistry of Importance to Astrophysical and Cosmological Environments

Thesis directed by Dr. Veronica M. Bierbaum and Dr. Theodore P. Snow

## Abstract

Scientific studies have led to a more thorough understanding of processes directing the evolution of the Universe. In addition to observational studies with telescopes, terrestrial laboratory studies now contribute to the knowledge encompassed by astronomy and astrophysics. The laboratory-astrophysics experiments performed for this thesis focused on topics ranging from the birth of the first stars and galaxies to chemical processes important to the interstellar medium (ISM).

Models attempt to derive a better understanding of certain cosmological and astrophysical environments. Their reliability, however, depends heavily on the accuracy of data employed. Our contributions to laboratory astrophysics are based on the use of a flowing afterglow-selected ion flow tube (FA-SIFT) supported by *ab initio* calculations to study ion-neutral reaction kinetics.

Studies for this thesis began with carbon cation,  $C^+$ . This species, ubiquitous throughout dense-translucent and molecular-cloud regions of the ISM, is extremely reactive and is shown to lead to more complex organic species. We have measured reactions of ground-state  $C^+$  with abundant interstellar neutrals. Our measurements will increase the accuracy in models of the ISM.

After the big bang, star and galaxy formation was not possible until the early Universe sufficiently cooled to enable protogalactic collapse. This process did not occur until a sufficient concentration of the first molecule,  $H_2$ , enabled efficient cooling. The dominant mechanism of  $H_2$  formation during this epoch was associative detachment (AD). Because of high uncertainties in existing measurements, we have remeasured the rate constant of the AD reaction and obtained a significant improvement for cosmological models. We have also characterized the chemistry of  $H^-$  with prototypical chemical reactants, effectively mapping reactivity trends for hydride.

The recent detection of anions in the ISM suggests that these species must play a role in the evolution of astrophysical environments. However, in contrast to their positive counterparts, relatively little is known about anion chemistry. We contribute a number of studies of anionic species, continuing the characterization of the reactions of these species and their role in astrochemistry. A number of carbanions, relevant to interstellar chemistry, were studied with the most abundant atomic species of the interstellar medium, H atom.

For my family

## Acknowledgements

I wouldn't be here, if it were not for the help, support, and guidance from a few folks. First off, Veronica Bierbaum and Ted Snow deserve a sizeable chunk of my thanks. They have been everything you could hope for in mentors – patient, kind, caring, and supportive. They have helped me past hurdles, and have taught me well! Additionally, I thank the rest of my defense committee: Don David, Jose Jimenez and Barney Ellison.

My fellow labmates, Nick Demarais, John Garver, and Zhibo Yang, have been a source of help, advice, and entertainment. Zhibo has helped tremendously with experimental work and even more so with computational work. Nick has learned well and will have to continue the good tradition. Among other things, John always has a knack for amusing discussion. I would also like to extend gratitude to the members of our sister labs, i.e. the Ellison, Weber, and Lineberger groups for sharing guidance, supplies and friendship. Last among this list of friends is Akin, whom I thank for the free support and guidance that only a friend can give.

A number of people at the CIRES integrated instrument development facility have been key to my success. Don David is amazing at troubleshooting and fixing practically everything. Ken Smith, Craig Joy, Jim Kastengren, and Wayne Winkler have all worked on repairing or improving a variety of things relevant to my instrument. Lastly, Dennis Steffey has a wonderful knack for fixing a material I have been responsible for breaking more than once – glass! I owe similar gratitude to a number of people at the JILA facilities. I thank Mike Whitmore and James Fung-A-Fat for their electronic prowess. Julie Phillips, at the scientific reports office, deserves a special thanks for reading and improving my papers and this thesis.

My undergraduate mentors deserve recognition for providing the guidance responsible for getting me here in the first place. Bradley Arnold and Joel Liebman both gave me a start in their research and were careful enough not to scare me off. Once at the University of Colorado, a number of people at the Colorado Diversity Initiative were here to give me an initial boost and support throughout my graduate career. Mark Hernandez has been a terrific mentor. Barbara Kraus and Kristin Lopez have given me a number of opportunities to serve as a mentor and provide outreach.

Numerous funding agencies have been kind enough to share the wealth in the form of a stipend or support. These include the Alliance for Graduate Education and the Professoriate (AGEP), the National Aeronautics and Space Administration (NASA) and its Graduate Student Researchers Program (GSRP). Also, Farid Salama at the NASA Ames Research Center (ARC) deserves recognition for being my GSRP scientific mentor and making me a part of his group during my internship at the ARC.

Lastly, my families also deserve considerable recognition. My wife Sarah and son Marcos have lent their patience and kind support while having their husband/father in graduate school. My in-laws were kind enough to let me steal their daughter to Colorado (more or less). Lastly, my parents have always supported the coolness of science.

Thanks to all!

**Table of Contents**

<b>Chapter 1.</b>	Lab-Astrophysics Applications of the FA-SIFT	
1.1	Introduction	1
1.2	Astrophysical Background	3
1.3	Ion-Neutral Reactions	10
1.4	Ion-Neutral Reaction Mechanisms	12
1.5	Chemical Models	12
1.6	FA-SIFT	13
1.7	FA-SIFT/ISM Relevance	14
1.8	Experimental Work of this Thesis	15
1.8.1	Carbon Cation	15
1.8.2	Hydride ( $H^-$ ) – Cosmological and Astrophysical Relevance	16
1.8.3	Organic Anions	17
1.8.4	Nitrogen-Containing Carbon-Chain Anions	18
1.9	Conclusion	18
1.10	References	21
<b>Chapter 2.</b>	Experimental Methods	
2.1	Introduction	25
2.2	Flowing Afterglow-Selected Ion Flow Tube	25
2.3	Ionization and SIFT Regions	27
2.3.1	Electron and Chemical Ionization	29
2.3.2	Cold-Cathode Discharge	30
2.4	Reaction Flow Tube and Neutral Atom Sources	32
2.4.1	Hydrogen Atoms	33
2.4.2	Nitrogen and Oxygen Atoms	34
2.5	Detection Region	37

<b>2.6</b>	Traditional Flowing Afterglow	37
<b>2.7</b>	Reaction Kinetics	38
<b>2.8</b>	Collision Rate Constants	45
<b>2.9</b>	Computational Support	47
<b>2.10</b>	References	48
<b>Chapter 3.</b>	Gas-Phase Study of $C^+$ Reactions of Interstellar Relevance	
<b>3.1</b>	Introduction	49
<b>3.2</b>	Experimental Methods	51
<b>3.3</b>	Results and Discussion	52
<b>3.3.1</b>	$C^+ + NH_3$	54
<b>3.3.2</b>	$C^+ + CH_4$	56
<b>3.3.3</b>	$C^+ + O_2$	58
<b>3.3.4</b>	$C^+ + H_2O$	60
<b>3.3.5</b>	$C^+ + C_2H_2$	61
<b>3.4</b>	Conclusions	63
<b>3.5</b>	References	67
<b>Chapter 4.</b>	Study of the Associative Detachment Reaction of Hydride Ion with Hydrogen Atom	
<b>4.1</b>	Introduction	69
<b>4.2</b>	Experimental Methods	70
<b>4.3</b>	Discussion	73
<b>4.4</b>	Implications of Our Results	78
<b>4.5</b>	References	79
<b>4.6</b>	Appendix	81

<b>Chapter 5.</b>	<b>H<sup>-</sup> Reactivity Overview</b>	
5.1	Introduction	84
5.2	Experimental Methods	85
5.3	Results and Discussion	87
5.3.1	Proton Abstraction	89
5.3.2	Atom Abstraction/Addition	91
5.3.3	Associative Detachment	94
5.3.4	S <sub>N</sub> 2/E2 Reactions	95
5.3.5	Unreactive Neutral Reagents	97
5.4	Conclusions	98
5.5	References	99
<b>Chapter 6.</b>	<b>Experimental and Theoretical Studies of Reactions Between H Atoms and Carbanions of Interstellar Relevance</b>	
6.1	Introduction	101
6.2	Experimental Methods	103
6.3	Theoretical Calculations	103
6.4	Results and Discussion	104
6.4.1	Reactions of group I: deprotonated nitriles [CH <sub>2</sub> CN <sup>-</sup> , CH <sub>3</sub> CHCN <sup>-</sup> , and (CH <sub>3</sub> ) <sub>2</sub> CCN <sup>-</sup> ]	108
6.4.2	Reactions of group II: deprotonated acetaldehyde (HC(O)CH <sub>2</sub> <sup>-</sup> ), acetone (CH <sub>3</sub> C(O)CH <sub>2</sub> <sup>-</sup> ), and ethyl acetate (CH <sub>3</sub> CH <sub>2</sub> OC(O)CH <sub>2</sub> <sup>-</sup> )	109
6.4.3	Reactions of group III: deprotonated methanol (CH <sub>3</sub> O <sup>-</sup> ), acetic acid (CH <sub>3</sub> CO <sub>2</sub> <sup>-</sup> ), and glycine (NH <sub>2</sub> CH <sub>2</sub> CO <sub>2</sub> <sup>-</sup> )	110
6.4.4	Anion-H-atom reaction efficiencies	115
6.5	Conclusions	115
6.6	References	117

<b>Chapter 7</b>	<b>Experimental and Theoretical Studies of Reactions Between H Atoms and Nitrogen-Containing Carbon-Chain Anions</b>	
7.1	Introduction	119
7.2	Experimental Methods	120
7.3	Theoretical Calculations	122
7.4	Results and Discussion	122
7.4.1	Reactions of $C_nN^-$ ( $n = 1-6$ )	125
7.4.2	Reactions of $C_nN_2^-$ ( $n = 1, 3, 4, \text{ and } 5$ )	137
7.4.3	Reactions of $C_nN_3^-$ ( $n = 2 \text{ and } 4$ )	138
7.4.4	Astrophysical Implications	143
7.5	Conclusions	144
7.6	References	146
<b>Bibliography</b>		148

## Tables

<b>Table 1.1</b>	Detected interstellar and circumstellar molecules listed in order of detection and color-coded by type.	2
<b>Table 3.1</b>	Reaction rate constants and branching ratios for $C^+ + NH_3$ .	55
<b>Table 3.2</b>	Reaction rate constants and branching ratios for $C^+ + CH_4$ .	57
<b>Table 3.3</b>	Reaction rate constants and branching ratios for $C^+ + O_2$ .	59
<b>Table 3.4</b>	Reaction rate constants and branching ratios for $C^+ + H_2O$ .	62
<b>Table 3.5</b>	Reaction rate constants and branching ratios for $C^+ + C_2H_2$ .	64
<b>Table 3.6</b>	Recommended reaction rate constants and branching ratios for reactions of $C^+$ with $NH_3$ , $CH_4$ , $O_2$ , $H_2O$ , and $C_2H_2$ .	66
<b>Table 4.1</b>	Rate constants for the reaction of $H^- + H \rightarrow H_2 + e^-$ .	76
<b>Table 4.2</b>	Experimental data for $H^- + H$ reaction using the $Cl^- / H$ atom multipoint concentration calibration.	81
<b>Table 4.3</b>	Experimental data for $H^- + H$ reaction using the $Cl^- / H$ atom two-point concentration calibration.	82
<b>Table 4.4</b>	Experimental data for $H^- + H$ reaction using the $OH^- / H$ atom multipoint concentration calibration.	83
<b>Table 5.1</b>	Hydride / neutral molecule reactions.	86
<b>Table 6.1</b>	Reactions between anions and H atoms	105
<b>Table 7.1</b>	Kinetic data for reactions between $C_nN^-$ ( $n=1-6$ ) and H atom.	123
<b>Table 7.2</b>	Kinetic data for reactions between $C_nN_2^-$ ( $n=1, 3-5$ ) and H atom.	124
<b>Table 7.3</b>	Complete computational results for reactions between $C_nN^-$ ( $n=1-6$ ) and H atom.	126
<b>Table 7.4</b>	Complete computational results for reactions between $C_nN_2^-$ ( $n=1, 3-5$ ) and H atom.	129
<b>Table 7.5</b>	Complete computational results for reactions between $C_nN_3^-$ ( $n=2$ and $4$ ) and H atom.	142

## Figures

<b>Figure 1.1</b>	Orion Nebula showing the varied composition of the interstellar medium.	5
<b>Figure 1.2</b>	Dense molecular cloud cross-section illustrating a cloud-classification scheme.	8
<b>Figure 1.3</b>	Species density vs. total hydrogen column density.	9
<b>Figure 2.1</b>	Flowing Afterglow-Selected Ion Flow Tube.	26
<b>Figure 2.2</b>	Mass spectrum of SIFTed cation $C^+$ .	28
<b>Figure 2.3</b>	Mass spectrum showing reactant-ion depletion and the formation of primary and secondary product ions.	28
<b>Figure 2.4</b>	Schematic representation of electron impact for $C^+$ production.	31
<b>Figure 2.5</b>	Schematic representation of cold-cathode discharge ionization.	31
<b>Figure 2.6</b>	Schematic showing generation of N and O atoms using microwave discharge.	35
<b>Figure 2.7</b>	Titration plot for determination of N and O atom concentrations.	36
<b>Figure 2.8</b>	Semilogarithmic plot of ion signal vs. reaction distance for $C^+ + CH_4$ .	40
<b>Figure 2.9</b>	Product ion extrapolation plot for reaction of $C^+ + CH_4$ .	43
<b>Figure 5.1</b>	$H^- + N_2O$ reaction coordinate plot.	92
<b>Figure 5.2</b>	$H^- + CO_2$ reaction coordinate plot (a) H atom attacking O of $CO_2$ (b) H atom attacking C of $CO_2$ .	93
<b>Figure 5.3</b>	$H^- + CH_3Cl$ reaction coordinate plot	96
<b>Figure 6.1</b>	Correlation plot between the logarithm of the reaction efficiency and experimental exothermicity.	107
<b>Figure 6.2</b>	Relaxed potential energy surface scan of the entrance channel of the $CH_3O^- + H$ reaction.	112
<b>Figure 6.3</b>	Relaxed potential energy surface scan of the entrance channel of the $CH_3CO_2^- + H$ reaction.	113
<b>Figure 7.1</b>	The reaction coordinate plot (in kcal/mol, 0 K) for $CN^- + H$ in which H atom binds to C (blue line) and N (green line), respectively.	132

<b>Figure 7.2</b>	The reaction coordinate plot (in kcal/mol, 0 K) for $C_2N^- + H$ in which H atom binds to	
	(a) C1,	134
	(b) C2, and	134
	(c) N3, respectively.	135
<b>Figure 7.3</b>	The reaction coordinate plot (in kcal/mol, 0 K) for	
	(a) $NCNCN^- + H$ and	139
	(b) $C(CN)_3^- + H$ .	140

## Publications

- 1) Martinez Jr., O., Betts, N. B., Villano, S. M., Eyet, N., Snow, T. P., and Bierbaum, V. M. "Gas Phase Study of C<sup>+</sup> Reactions of Interstellar Relevance" *The Astrophysical Journal* **2008**, 686 1486.
- 2) Snow, T. P., Stepanovic, M., Betts, N. B., Eichelberger, B. R., Martinez Jr., O., and Bierbaum, V. M. "Formation of Gas-Phase Glycine and Cyanoacetylene via Associative Detachment Reactions" *Astrobiology* **2009**, 9 1001.
- 3) Martinez Jr., O., Yang, Z., Betts, N. B., Snow, T. P., and Bierbaum, V. M. "Experimental Determination of the Rate Constant for the Associative Detachment Reaction H<sup>+</sup> + H → H<sub>2</sub> + e<sup>-</sup> at 300 K" *The Astrophysical Journal Letters* **2009**, 705 L172.
- 4) Yang, Z., Eichelberger, B., Martinez Jr., O., Stepanovic, M., Snow, T. P., and Bierbaum, V. M. "The Influence of Spin Effects on the Gas Phase Reactions of Carbanions with N and O Atoms" *Journal of the American Chemical Society* **2010**, 132 5812.
- 5) Martinez Jr., O., Yang, Z., Snow, T. P., and Bierbaum, V. M. "Gas Phase Reactions of Hydride Anion, H<sup>-</sup>" *The Astrophysical Journal* **2010**, 720 173.
- 6) Yang, Z., Eichelberger, B. R., Carpenter, M. Y., Martinez Jr., O., Snow, T. P., and Bierbaum, V. M. "Experimental and Theoretical Studies of Reactions Between H Atoms and Carbanions of Interstellar Relevance" *The Astrophysical Journal* **2010**, 723 1325.
- 7) Yang, Z., Martinez Jr., O., Snow, T. P., and Bierbaum, V. M. "Gas Phase Ion-Neutral Reactions of Carbon-Nitrogen Chain Anions" – In Preparation.
- 8) Demarais, N., Martinez Jr., O., Yang, Z., Snow, T. P., and Bierbaum, V. M. "Gas-Phase Reactions of Deprotonated Benzene, Naphthalene, and Anthracene of Interstellar Relevance" – In Preparation.

## Chapter 1

### Lab-Astrophysics Applications of the FA-SIFT

#### 1.1 Introduction

Interstellar space, occupying the immense volume in between stars, is as complex as it is vast. Astronomical observations have shown this space encompasses a variety of physical and chemical conditions of gas (99% by mass), grains (ice and dust particles  $\sim 1\%$  by mass), and electromagnetic energy. This matter is collectively known as the interstellar medium (ISM) and represents 10% of the known matter of the galaxy (Spitzer, 1978; Gerlich & Smith 2006). The ISM is extremely diverse, with particle densities ranging from 1 to  $\sim 10^6 \text{ cm}^{-3}$  and temperatures ranging from 10 to  $10^5 \text{ K}$ . A number of processes are responsible for the overall nature of the ISM. Among these, chemical processes are one of the forces driving the evolution of the interstellar medium.

The emergence of chemistry in relation to astronomy and astrophysics began with the startling discovery in the 1930s of the existence of molecules in space. Development of high-resolution optical spectroscopy led to the discovery of the first molecules in space, CH, CN, and  $\text{CH}^+$  (Swings & Rosenfeld 1937; McKellar 1940; Adams 1941; Douglas & Herzberg 1941). A logical question soon followed: *How are molecules formed in space?* Overlap of the fields capable of answering this and related questions, astronomy and chemistry, led to the development of a field in its own right, i.e., astrochemistry (IAU S197 1999; IAU S231 2005; Shaw 2006; IUPAC 42<sup>nd</sup> Congress Symposium 2009). Since then, more than 160 molecules (shown in Table 1.1) have been discovered in interstellar and circumstellar environments (cf. Woon 2010) and advances continue to be made in understanding the chemistry of space.

**Table 1.1** Detected interstellar and circumstellar molecules listed in order of detection. Atoms in molecules are color-coded by type: grey font = hydrogen (and deuterium), black font = carbon and silicon, blue font = nitrogen and phosphorus, red font = oxygen and sulfur, green font = chlorine and fluorine, purple font = magnesium, sodium, aluminum, potassium, iron, and lithium, red box = cation, blue box = anion. Detections of species with an asterisk remain controversial.

CH	CN	<span style="border: 1px solid red; padding: 2px;">CH<sup>+</sup></span>	OH	NH <sub>3</sub>	H <sub>2</sub> O	H <sub>2</sub> CO
CO	H <sub>2</sub>	HCO <sup>+</sup>	CH <sub>3</sub> OH	HC <sub>3</sub> N	HCN	HCOOH
SiO	CS	CH <sub>3</sub> CN	OCS	NH <sub>2</sub> CHO	H <sub>2</sub> S	HNCO
CH <sub>3</sub> CHO	CH <sub>3</sub> CCH	CH <sub>2</sub> NH	H <sub>2</sub> CS	HNC	SO	CH <sub>3</sub> OCH <sub>3</sub>
CH <sub>3</sub> NH <sub>2</sub>	N <sub>2</sub> H <sup>+</sup>	C <sub>2</sub> H	CH <sub>2</sub> CHCN	CH <sub>3</sub> CH <sub>2</sub> OH	HC <sub>3</sub> OCH <sub>3</sub>	SO <sub>2</sub>
HDO	SiS	NS	NH <sub>2</sub> CN	HCO	C <sub>3</sub> N	H <sub>2</sub> CCO
C <sub>2</sub>	HNO	CH <sub>3</sub> CH <sub>2</sub> CN	HC <sub>7</sub> N	HC <sub>5</sub> N	HC <sub>9</sub> N	C <sub>4</sub> H
NO	OCN	CH <sub>3</sub> SH	HNCS	C <sub>2</sub> H <sub>4</sub>	<span style="border: 1px solid red; padding: 2px;">HCS<sup>+</sup></span>	<span style="border: 1px solid red; padding: 2px;">HOCO<sup>+</sup></span>
<span style="border: 1px solid red; padding: 2px;">HOC<sup>+</sup></span>	CH <sub>3</sub> C <sub>3</sub> N	SiH <sub>4</sub>	CH <sub>3</sub> C <sub>4</sub> H	c-SiC <sub>2</sub>	C <sub>3</sub> H	HCl
C <sub>3</sub> O	c-C <sub>3</sub> H <sub>2</sub>	C <sub>6</sub> H	<span style="border: 1px solid red; padding: 2px;">HCNH<sup>+</sup></span>	MgNC	C <sub>5</sub> H	<span style="border: 1px solid red; padding: 2px;">H<sub>3</sub>O<sup>+</sup></span>
C <sub>2</sub> S	C <sub>3</sub> S	(CH <sub>3</sub> ) <sub>2</sub> CO	NaCl	AlCl	KCl	AlF
PN	CH <sub>3</sub> NC	C <sub>3</sub>	c-C <sub>3</sub> H	CH <sub>2</sub> CN	HC <sub>2</sub> CHO	C <sub>5</sub>
SiC	C <sub>2</sub> H <sub>2</sub>	SiC <sub>4</sub>	CO <sub>2</sub>	CH <sub>2</sub>	CP	l-C <sub>3</sub> H <sub>2</sub>
HC <sub>2</sub> N	NH	CH <sub>4</sub>	C <sub>2</sub> O	HCCNC	SiN	HNCCC
<span style="border: 1px solid red; padding: 2px;">SO<sup>+</sup></span>	NH <sub>2</sub>	<span style="border: 1px solid red; padding: 2px;">CO<sup>+</sup></span>	<span style="border: 1px solid red; padding: 2px;">HC<sub>3</sub>NH<sup>+</sup></span>	H <sub>2</sub> CN	NaCN	N <sub>2</sub> O
MgCN	C <sub>8</sub> H	<span style="border: 1px solid red; padding: 2px;">H<sub>3</sub><sup>+</sup></span>	<span style="border: 1px solid red; padding: 2px;">H<sub>2</sub>COH<sup>+</sup></span>	C <sub>7</sub> H	CH <sub>3</sub> COOH	HC <sub>11</sub> N
HF	c-C <sub>2</sub> H <sub>4</sub> O	LiH	C <sub>5</sub> N	SiC <sub>3</sub>	SH	CH <sub>3</sub>
CH <sub>2</sub> OHCHO	SiCN	C <sub>4</sub> H <sub>2</sub>	C <sub>6</sub> H <sub>2</sub>	C <sub>6</sub> H <sub>6</sub>	CH <sub>2</sub> CHOH	AlNC
FeO	HOCH <sub>2</sub> CH <sub>2</sub> OH	NH <sub>2</sub> CH <sub>2</sub> COOH <sup>*</sup>	N <sub>2</sub>	CH <sub>2</sub> CHCHO	CH <sub>3</sub> CH <sub>2</sub> CHO	SiNC
HC <sub>4</sub> N	CO(CH <sub>2</sub> OH) <sub>2</sub> <sup>*</sup>	CH <sub>2</sub> CCHCN	c-H <sub>2</sub> C <sub>3</sub> O	CH <sub>3</sub> CONH <sub>2</sub>	CH <sub>3</sub> C <sub>6</sub> H	CH <sub>2</sub> CNH
<span style="border: 1px solid red; padding: 2px;">CF<sup>+</sup></span>	CH <sub>3</sub> C <sub>5</sub> N	<span style="border: 1px solid blue; padding: 2px;">C<sub>6</sub>H<sup>-</sup></span>	O <sub>2</sub>	<span style="border: 1px solid blue; padding: 2px;">C<sub>4</sub>H<sup>-</sup></span>	HCP	<span style="border: 1px solid blue; padding: 2px;">C<sub>8</sub>H<sup>-</sup></span>
CH <sub>2</sub> CHCH <sub>3</sub>	PO	CNCHO	CCP	<span style="border: 1px solid blue; padding: 2px;">C<sub>3</sub>N<sup>-</sup></span>	NH <sub>2</sub> CH <sub>2</sub> CHN	PH <sub>3</sub>
<span style="border: 1px solid blue; padding: 2px;">C<sub>5</sub>N<sup>-</sup></span>	HCNO	AlO	HOCN	C <sub>2</sub> HOCHO	C <sub>3</sub> H <sub>7</sub> CN	HSCN
HSCN	AlOH	<span style="border: 1px solid blue; padding: 2px;">CN<sup>-</sup></span>	<span style="border: 1px solid red; padding: 2px;">OH<sup>+</sup></span>	C <sub>60</sub>	C <sub>70</sub>	

## 1.2 Astrophysical Background

While astrochemistry is concerned with all facets of chemistry in space, particular attention has been devoted to the chemistry of interstellar clouds. Since interstellar clouds are on a size scale between solar systems and galaxies, their chemistry drives physical processes such as structure and star formation, heating and cooling, radiation flux, and ultimately, galactic evolution. Spectroscopic tools are used to probe and determine the constituents, temperatures, radiation fluxes, and kinetic properties within regions of space (Tielens 2005; Kwok 2006; Rehder 2010).

Hydrogen is the most abundant element in the ISM and is mostly in atomic form in the diffuse ISM and in molecular form in dense clouds. Helium has about 10% of the abundance of hydrogen. Next in abundance are the elements carbon, nitrogen, and oxygen, at  $10^{-3}$  to  $10^{-4}$  the abundance of hydrogen. Other elements exist at much lower densities.  $H_2$  is the most abundant molecule followed by CO ( $10^{-4}$  the abundance of  $H_2$ ). Other elements exist in “trace amounts.” However, because of the vastness of the ISM, total amounts are still appreciable. Savage & Sembach have given a summary of abundances for a variety of elements in a range of ISM environments (1996).

Most molecular detections in space are made using radio astronomy. Rotational transitions of molecules emit and absorb radiation in meter to submillimeter wavelengths, which is then detected using ground, airborne, and satellite observatories (Wall et al. 1999). While the technique can unambiguously assign spectra to a specific molecule, detection requires a molecule to have a dipole moment and is thus limited to these species. However, because of its sheer abundance,  $H_2$  can be detected by its quadrupolar rotational spectrum.

Radio astronomy is also limited to species in the gas phase. Assignment becomes increasingly difficult with the increasing complexity of a molecule. However, species up to 13 atoms in size have been detected. In addition, buckyballs,  $C_{60}$  and  $C_{70}$ , have recently been detected because their high symmetry simplifies their spectra.

Spectroscopy at other wavelengths can sometimes also be used to identify and detect species. Absorption spectra use a background star as a light source. Hydrogen, for example, can be detected by absorption and emission in visible and ultraviolet (UV) wavelengths. However, because of low densities, populations of excited-state species are low. Consequently there are fewer lines in the visible spectrum since most lines associated with electronic ground-state transitions appear in the UV. Organic compounds can be detected via their absorption and emission at infrared (IR) wavelengths. Additionally, IR spectroscopy can be used to peer through dusty or icy sightlines since small particulates are invisible at IR wavelengths. Although evidence points to the existence of many additional molecules, including larger species, detections are currently limited by the complexity of spectra, column densities, signal-to-noise problems, and detection efficiency. A variety of compilations of spectroscopic data exist that contain reference spectra for species observed in addition to spectra that have been made public (Müller et al. 2001, 2005; Lovas et al. 2009; CDMS 2010; Woon 2010).

The coupling of spectroscopic methods allows for the mapping of regions of space and the interstellar medium. Regions can be mapped and classified by temperature, composition, density, and states of matter (neutral, ionized, atomic, and molecular). Matter in the ISM condenses into clouds. An image of the Orion Nebula, shown in Figure 1.1, shows the variety of interstellar cloud conditions, dense through diffuse. It is in these clouds that a majority of the chemistry in space occurs.



**Figure 1.1** Orion Nebula showing the varied composition of the interstellar medium.  
Photo Credit: the National Aeronautics and Space Administration and the Space Telescope Science Institute (STSI).

Interstellar clouds are classified by their defining characteristics using spectroscopic observations. Snow and McCall have suggested a classification scheme for interstellar clouds (Snow & McCall 2006). Defining characteristics of cloud types are based on relative densities of abundant nuclei. For example, a total number density for hydrogen nuclei is defined as  $n_{\text{H}} = n(\text{H}) + 2n(\text{H}_2)$ . A local fraction of nuclei in terms of number densities of hydrogen nuclei is then defined as  $f_{\text{H}_2}^{\text{n}} = 2n(\text{H}_2)/n_{\text{H}}$  where  $n_{\text{H}} = n(\text{H}) + 2n(\text{H}_2)$ .

Diffuse atomic regions, typically at the periphery of interstellar clouds, encounter the brunt of interstellar radiation. In these regions gaseous matter can be both fully dissociated as atoms and ionized. Diffuse clouds are defined by the local fraction given in the example above, with  $f_{\text{H}_2}^{\text{n}} < 0.1$ , indicating the predominance of hydrogen in atomic form. Temperatures in these regions range from 30–100 K, with particle densities ranging from 10–100  $\text{cm}^{-3}$ . These regions are probed by UV and visible (vis) wavelength spectroscopic methods.

Along a particular sightline into a cloud, matter along the periphery shields internal matter from cosmic radiation and neutral species can exist. This shielding is represented by the dust-extinction parameter,  $A_{\text{v}}$ , a logarithmic expression of the extinction at visual wavelengths in units of stellar magnitudes. With higher extinction, temperatures can plummet and conditions support the existence of dense regions with molecular species. Dense molecular clouds are the densest regions ( $>10^4 \text{ cm}^{-3}$ ) in the ISM still classified as clouds. Because of high extinction, temperatures here are lower, ranging from 10–50 K. These regions are strongly molecular in nature,  $f_{\text{CO}}^{\text{n}} > 0.9$  [where  $f_{\text{CO}}^{\text{n}} = n(\text{CO})/n_{\text{c}}$  and  $n_{\text{c}} \approx n(\text{C}^+) + n(\text{C}) + n(\text{CO})$ ], and are probed by infrared absorption and millimeter-wavelength emission. Furthermore, star formation occurs in these dense regions as continued condensation, triggered by a shock or gravitational attraction, initiates star formation (Hollenbach & Thronson 1987).

Between diffuse atomic and dense molecular regions, there exist diffuse molecular and translucent regions. A schematic representation of a simple dense molecular cloud, shown in Figure 1.2, outlines the four regions and includes the defining and relevant information for each one. Of course, conditions such as these can change when stars within stellar nurseries hatch and begin to emit radiation from within a cloud. Supernovae and collisions with other clouds, among many other physical processes, can also dramatically change cloud conditions. Additionally, “cloud-region barriers” can permeate one another, allowing for the exchange of media within. While stellar radiation may not permeate the core of a dense molecular cloud, cosmic ray particles can. Cosmic ray particles are capable of dissociating and ionizing atoms and molecules with which they interact. Figure 1.3 highlights relative cloud conditions, showing conditions of cloud types and states of abundant species.

Dust in the ISM is composed of heavy elements like Si, Fe, O, and C. Dust particles have a mean size of  $\sim 0.1 \mu\text{m}$  (deduced from scattering, polarization, and absorption of radiation). Relative radiation depletions give indications of grain composition, and grains fall into one of two categories: one in which grains are mostly composed of carbon, and another where grains are mostly metal silicates. Grains in dark clouds develop icy mantles, most of which are made of water, although CO, CO<sub>2</sub> and CH<sub>3</sub>OH ices also exist. The grains provide a surface and ices provide a medium for chemistry to occur. For a review of this chemistry and its ability to form complex organic molecules see Millar and Williams (1993) and Herbst and van Dishoeck (2009).

Additionally, a variety of absorption features have been attributed to polycyclic aromatic hydrocarbons (PAHs) (Allamandola et al. 1989). PAHs are fused rings of carbon (10–50 atoms large). PAHs are also assumed to cluster into grainlike particles. Because of their size, PAHs

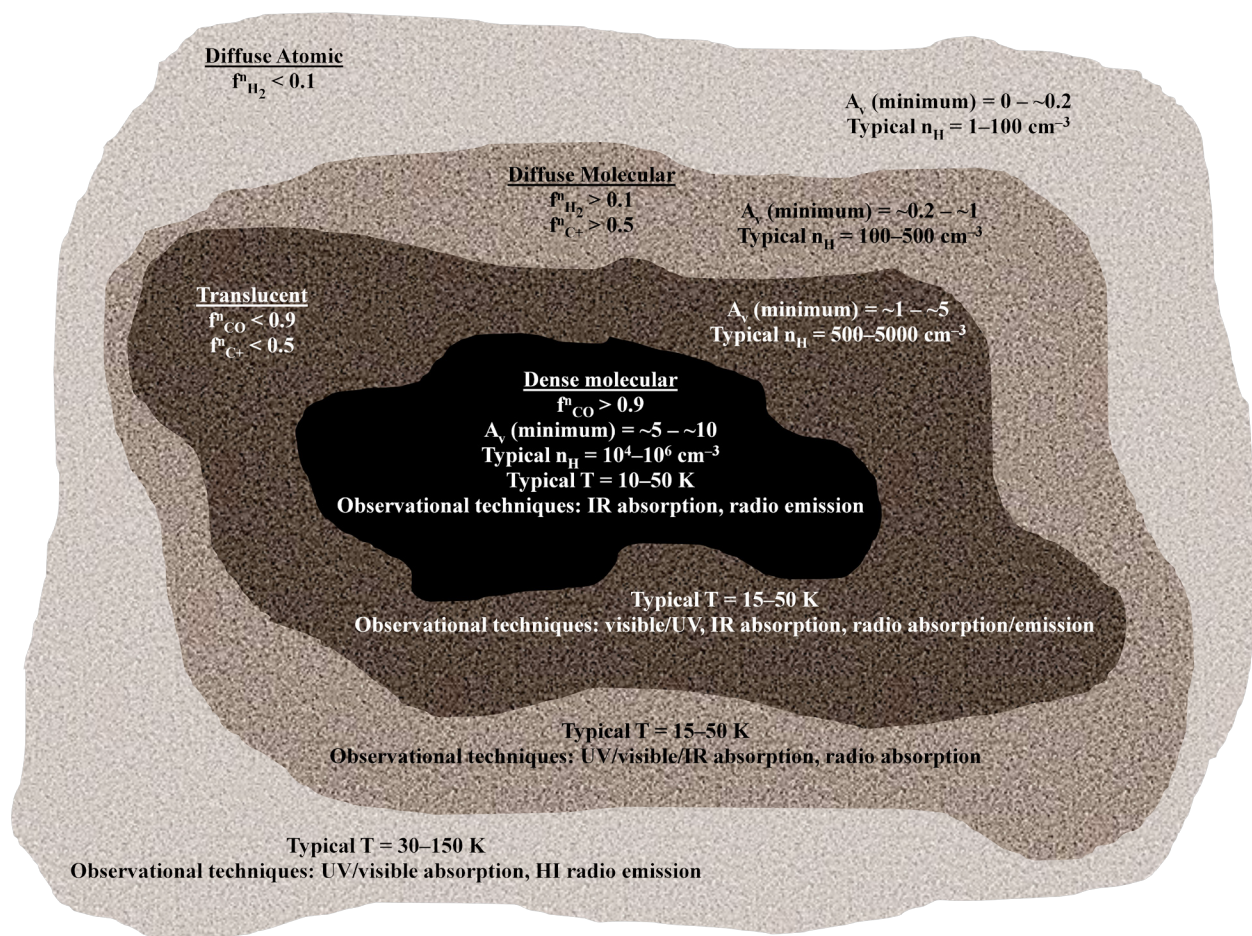


**Figure 1.2** Dense molecular cloud cross-section illustrating the cloud-classification scheme proposed by Snow & McCall (2006). Shown are the diffuse atomic, diffuse molecular, translucent, and dense molecular cloud regions and their properties.

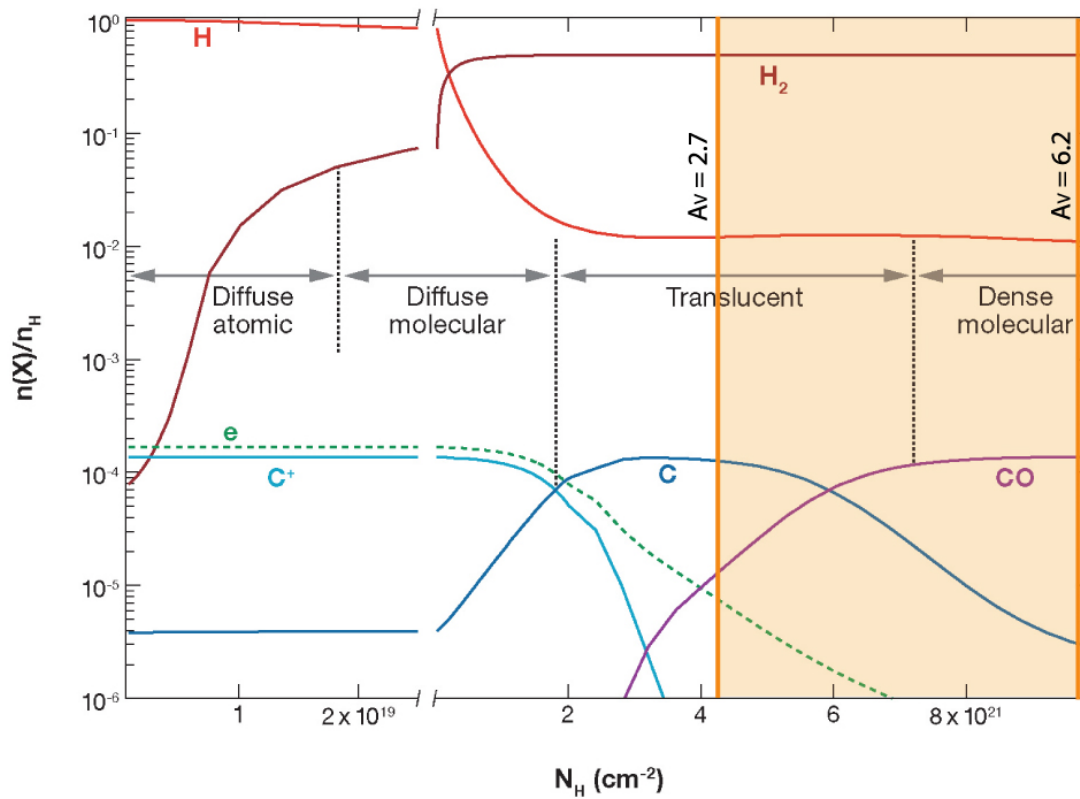


**Figure 1.3** Species density (normalized to total hydrogen) vs. total hydrogen column density (Snow and McCall 2006).

can accommodate a considerable amount of interstellar radiation, absorbing and distributing excess energy into many degrees of freedom, in addition to radiative emission of excess energy. A large amount of carbon in the Universe is assumed to be locked into PAHs. Also, they have been implicated as carriers of both the diffuse interstellar bands (DIBs) and unidentified infrared bands (UIRs) (Tielens and Snow 1995; Peeters et al. 2004).

DIBs, absorption features in the visible spectrum, have been dubbed the longest-standing spectroscopic mystery in all of astronomy (Herbig, 1995). The broad absorption features were first detected by Mary Lee Heger (1922). A number of candidates for the carriers of these features have been suggested, however no conclusive identification has been made to date. Carriers, however, are believed to be organic in nature and possibly quite complex (hence support for PAHs and other molecules such as carbon chains) (Snow 2001). The laboratory astrophysics program at the University of Colorado at Boulder supporting the work in this thesis was originally founded in support of the DIBs project to examine the viability and chemistry of species with promise as DIBs carriers.

### **1.3 Ion-Neutral Reactions**

Ion-neutral reactions occur without the activation barrier used to describe traditional reactions; they also have high reaction rates (Friedman 1968). Long ago, theory arrived at an accurate description of the simple mechanism behind these reactions. Simply put, attraction between an ion and a dipole of a neutral reactant or an ion and an induced dipole in a neutral reactant results in a strong long-range force that leads to a collision (Langevin 1905). Collisions, however, do not always proceed to products. Reactions in the gas phase are still dependent on the energies involved (i.e., reaction enthalpies); therefore not every collision leads to products.

In general, only exothermic reactions can form products (Solomon & Klemperer 1972; Herbst & Klemperer 1973). Since these reactions can occur in low-energy environments, they are the major type of reaction that occurs in low-temperature regions of space like the ISM. Although much chemistry can occur on the surface of grains or in matrices of ice, most chemistry in the ISM occurs in the gas phase; additionally, although radical-neutral reactions also have large rates and possess little-to-no temperature dependence, ion-neutral reactions are generally considered to be more important in interstellar processes (Dalgarno & Black 1972; Solomon & Klemperer 1972; Herbst & Klemperer 1973; Klemperer 1997, Herbst 2001).

Ion-neutral reactions are likely responsible for molecule formation in the interstellar medium (Watson 1973; Solomon & Klemperer 1972; Herbst & Klemperer 1973; Dalgarno & Black 1976; Watson 1976, 1977). They are capable of synthesizing small-to-large neutral and ionic species in varied environments (Smith 1992). In fact, large reaction networks can form a variety of molecules that have been detected (Smith & Adams 1989; Smith 1992; Herbst 1993, 1995, 2005). These networks can also be used to predict the viability of species in certain ISM regions. Moreover, they also show the interdependence of a variety of reaction mechanisms in forming and destroying both ions and neutrals.

Reaction networks have also shown viable pathways for the synthesis of prebiotic molecules (e.g., Snow et al 2009). A majority of the molecules discovered are organic in nature. Carbon exists in a variety of forms, including atomic, molecular, diamond, PAH, chains, clusters, and carbonaceous solids. Because of its high abundance in the Universe and due to its reactivity, carbon is key to the formation of prebiotic molecules (Henning & Salama 1998; Ehrenfreund & Charnley 2000). The relatively new field of astrobiology is dedicated to the study of the nature

and formation of life in the Universe (Chyba & Hand 2005). (NASA has even initiated an astrobiology institute to continue the advancement of the field.)

#### 1.4 Ion-Neutral Reaction Mechanisms

A number of different chemical mechanisms for two-body-gas-phase reactions can occur between an ion and a neutral in the ISM (Dalgarno & Black 1976). An association product between an ion and a neutral must rid itself of excess energy and can only be formed either by emitting radiation or an electron. Radiative emission of a photon is known as radiative association ( $X^{+/-} + Y \rightarrow XY^{+/-} + h\nu$ ); emission of an electron is called associative detachment ( $X^- + Y \rightarrow XY + e^-$ ). Additionally, there are charge transfer ( $X^{+/-} + Y \rightarrow Y^{+/-} + X$ ) and ion-atom exchange reactions ( $X^{+/-} + YZ \rightarrow XY^{+/-} + Z$ ). Anions can be formed by radiative attachment of an electron ( $X + e^- \rightarrow X^- + h\nu$ ). Cations (and electrons) are typically formed by photoionization ( $X + h\nu \rightarrow X^+ + e^-$ ). A number of other reactions are responsible for ion destruction: dissociative recombination ( $XY^+ + e^- \rightarrow X + Y$ ), radiative recombination ( $X^+ + e^- \rightarrow X + h\nu$ ), and photodetachment ( $X^- + h\nu \rightarrow X + e^-$ ).

#### 1.5 Chemical Models

Models have been developed to provide insight into a variety of physical processes (cosmological, astrophysical, etc.) (cf. Dalgarno & Black 1976; Galli & Palla 1998; Herbst 2001; Snow & McCall 2006). Models are evaluated for steady-state abundances, accounting for the formation and destruction mechanisms of constituents. Additionally, they are based on physical parameters such as radiation flux, fields, initial concentrations, temperature, density, shocks, etc. (Le Teuff et al. 2000). Useful models rely on accurate parameters, particularly reaction-rate constants, to provide meaningful data. Several studies have emphasized the importance of

reaction-rate constants to chemical models (Markwick-Kemper 2005; Glover et al. 2006; Wakelam et al. 2006).

Many ion-neutral kinetic databases have been in use for many years. Compilations are available in the literature (Ikezoe et al. 1987; Anicich 1993a, 1993b; Sablier & Rolando 1993; Snow & Bierbaum 2008). Additionally, online databases have been compiled by NIST (Chemical Kinetics Database) and groups at the University of Manchester (Woodall 2007; UMIST 2010) and at Ohio State (Herbst 2010). These online databases have been extensively used by modelers. Comparison of these databases has shown that a number of discrepancies exist between different sources (Wakelam et al. 2006). However, the *KInetic Database for Astrochemistry* (KIDA 2010) has been recently launched and is helping to bring consistency in the literature using available data. While the online database cites the literature, it also relies on experts in the field to provide recommendations for important reactions.

## 1.6 FA-SIFT

Experimental work on ion-neutral kinetics advanced dramatically in the 1960s with the invention of the flowing afterglow (FA) instrument by Ferguson, Fehsenfeld, and Schmeltekopf (1969). Originally designed to study chemistry relevant to the Earth's ionosphere, the technique flourished and has subsequently proved to be valuable to other fields, including astrophysics. FA provided an ion source with high ion densities of cations and anions with a well-defined thermal energy distribution. A variety of reactant ions could be synthesized and reacted with an equally diverse assortment of neutral species (atomic and molecular).

Introduction of the selected ion flow tube (SIFT) by Adams & Smith (1976) soon followed. The technique allows for the selection of ions of a specific polarity and mass-to-

charge ratio. It eliminated problems associated with plasma production along with much of the ambiguity of reactant identity.

The present arrangement of the FA-SIFT dedicated to laboratory astrophysics at the University of Colorado at Boulder includes a variety of ion sources, such as electron ionization, cold-cathode discharge, and Penning ionization. The method is adaptable to a variety of sources. Future plans include adaptation of a laser-induced acoustic desorption (LIAD) to include species with low vapor pressures (Perez et al. 2000). Multiple sources allow for a variety of gas-phase syntheses of common or exotic ions. In addition to the introduction of molecular neutrals, the current setup allows for the introduction of H, N, and O reactant atoms, the most abundant atomic species in the ISM.

### **1.7 FA-SIFT/ISM Relevance**

While experiments in the FA-SIFT do not occur under conditions identical to those in the ISM, they remain relevant nonetheless. First, room temperature ( $\sim 300$  K) measurements of the FA-SIFT are at a considerably higher temperature than exists in some regions of the ISM. However, theoretical Langevin treatment of ion-neutral reactions is temperature independent, and many experimental ion-neutral reactions have shown no temperature dependence (Snow & Bierbaum 2008). Temperature and pressure effects are generally understood in the laboratory.

Second, reactions in the FA-SIFT occur at considerably higher pressure than those pressures in the ISM. Bimolecular reaction rate constants and branching ratio determinations, however, should be pressure and concentration independent (experimental determinations are checked for this feature). However, pressure effects do take place when reactions involve association. Association reactions occur by several mechanisms. The associative intermediate

can radiate excess energy, the associative intermediate can have enough internal degrees of freedom (limited to large species) to accommodate and distribute the energy, or a third body can collisionally cool and stabilize a reactive intermediate. For reactions of the latter type observed in the FA-SIFT, collisional cooling by the carrier gas (He) is the means by which associative intermediates are stabilized. Because of low densities, association reactions in the ISM will occur by photon emission (radiative association). Temperature and pressure-dependent studies remain important and development of future experiments, methods, and instruments will allow these studies.

## **1.8 Experimental Work of this Thesis**

A variety of astrophysically (and cosmologically) relevant experiments were carried out for the bulk of this thesis. Experiments used the FA-SIFT instrument in both flowing afterglow and SIFT modes. Each project was completed with a specific relevance in mind, relating to either cosmological or astrophysical problems. Following are brief summaries of the projects detailed throughout this thesis.

### **1.8.1 Carbon Cation**

Carbon cation ( $C^+$ ) is a prevalent interstellar ion that is included in multiple chemical pathways leading to different astrobiologically relevant molecules.  $C^+$  is also tied to PAH production via reactions that involve acetylene. New measurements using the FA-SIFT technique are presented of the rate constants and product branching ratios for the gas phase reactions of  $C^+$  with  $NH_3$ ,  $CH_4$ ,  $O_2$ ,  $H_2O$ , and  $C_2H_2$  (Martinez et al. 2008). Results were obtained using two instruments that were separately calibrated and optimized; in addition, low ionization

energies were used to ensure formation of ground-state  $C^+$ , the purities of the neutral reactants were verified, and mass discrimination was minimized.

### 1.8.2 Hydride ( $H^-$ ) – Cosmological and Astrophysical Relevance

Cosmological models rely on the associative detachment (AD) reaction-rate constant for  $H^- + H$  to correctly predict the time scale for first galaxy and star formation after the big bang. The AD reaction is thought to be the most prominent mechanism for  $H_2$  formation in the early Universe. Formation of  $H_2$ , the first molecule, resulted in the additional cooling required to allow condensation resulting in star and galaxy formation. Previous measurements of the rate constant were uncertain by a factor of two, resulting in unsatisfactory uncertainty from models in which they were incorporated. We have determined the rate constant for the AD reaction of hydride ions with hydrogen atoms ( $H^- + H \rightarrow H_2 + e^-$ ) at 300 K to be  $2.0 (\pm 0.6) \times 10^{-9} \text{ cm}^3 \text{ s}^{-1}$ , where our error bars represent the total absolute error and include  $1\sigma$  of the measured values (Martinez et al. 2009). Experiments were carried out in a flowing-afterglow instrument using the well-characterized reactions of  $Cl^- + H$  and  $OH^- + H$  to calibrate the concentration of hydrogen atoms. Our measurement represents a significant improvement over previous determinations; it will reduce uncertainties in cosmological models that rely on this reaction-rate constant. Additionally, our higher reported value indicates earlier star and galaxy formation than previously thought.

Following the cosmologically relevant AD reaction experiments was a series of experiments to characterize the reactivity of  $H^-$ . Few reactions were previously measured, and little was known of the reactivity of  $H^-$ . Rate constants were measured at 300 K for the reactions of the hydride anion,  $H^-$ , with neutral molecules  $C_2H_2$ ,  $H_2O$ ,  $CH_3CN$ ,  $CH_3OH$ ,  $(CH_3)_2CO$ ,

$\text{CH}_3\text{CHO}$ ,  $\text{N}_2\text{O}$ ,  $\text{CO}_2$ ,  $\text{O}_2$ ,  $\text{CO}$ ,  $\text{CH}_3\text{Cl}$ ,  $(\text{CH}_3)_3\text{CCl}$ ,  $(\text{CH}_3\text{CH}_2)_2\text{O}$ ,  $\text{C}_6\text{H}_6$ , and  $\text{D}_2$  using a flowing-afterglow instrument (Martinez et al 2010). Experimental work was supplemented by *ab initio* calculations that provided insight into the viability of reaction pathways. Our reported rate constants should prove useful to models of astrophysical environments where conditions support the existence of both  $\text{H}^-$  and neutral species. The variety of neutral reactants studied includes representative species from prototypical chemical groups, effectively mapping reactivity trends for the hydride anion.

### 1.8.3 Organic Anions

The recent detection of molecular anions in the interstellar medium has underscored the need for laboratory studies of negative ion chemistry. Hydrogen atoms are the most abundant atomic species in the ISM, and the chemistry of H atoms with anions may contribute to molecular synthesis in interstellar clouds. This work is a combined experimental and computational study of a series of anions reacting with H atoms by AD (Yang et al. 2010). The anions include deprotonated nitriles ( $\text{CH}_2\text{CN}^-$ ,  $\text{CH}_3\text{CHCN}^-$ , and  $(\text{CH}_3)_2\text{CCN}^-$ ), acetaldehyde ( $\text{HC(O)CH}_2^-$ ), acetone ( $\text{CH}_3\text{C(O)CH}_2^-$ ), ethyl acetate ( $\text{CH}_3\text{CH}_2\text{OC(O)CH}_2^-$ ), methanol ( $\text{CH}_3\text{O}^-$ ), and acetic acid ( $\text{CH}_3\text{CO}_2^-$ ). Experimental measurements of the reaction-rate constants were made with the FA-SIFT technique. *Ab initio* theoretical calculations were carried out to explore the reaction mechanism and investigate the factors influencing reaction efficiencies, which are largely proportional to reaction exothermicities. Other factors influencing reaction efficiencies include the charge density on the reactive site of the anion, the characteristics of the potential energy surfaces along the approach of the reactants, and angular momentum conservation of the anion–H atom collision.

### 1.8.4 Nitrogen-Containing Carbon-Chain Anions

Nitrogen-containing carbon-chain species represent an important group of neutral and ionic species in the ISM. The detection of some corresponding anions,  $C_nN^-$  ( $n = 1, 3,$  and  $5$ ), highlights the importance of laboratory studies of their chemistry, especially with the ISM's most abundant atomic species, hydrogen atom. This work is a combined experimental and computational study of a series of nitrogen-containing carbon-chain anions reacting with H atoms (Yang et al., in preparation). The anions include  $C_nN^-$  ( $n = 1 - 6$ ),  $C_nN_2^-$  ( $n = 1, 3, 4,$  and  $5$ ), and  $C_nN_3^-$  ( $n = 2$  and  $4$ ), and reactions mainly proceed through associative detachment ( $A^- + H \rightarrow AH + e^-$ ) or fragmentation pathways. Experimental measurements of the reaction rate constants were made with the FA-SIFT technique. *Ab initio* theoretical calculations were carried out to explore the reaction mechanisms and investigate the factors determining reactivities. Reaction is mainly determined by the characteristics of the potential energy surfaces along the approach of the reactants. In addition, angular momentum conservation of the anion-H atom collision may have a universal effect of decreasing the reaction efficiencies. Our results indicate  $C_nN^-$  ( $n = 1 - 6$ ) and  $C_nN_2^-$  ( $n = 1, 3, 4,$  and  $5$ ) can be destroyed in reactions with H atoms by either forming the corresponding neutral monohydride compound or fragmenting into smaller anionic and neutral species. However,  $C_nN_3^-$  ( $n = 2$  and  $4$ ) anions are unreactive, such that they may exist in the H atom rich regions in the ISM.

### 1.9 Conclusion

The ISM is not entirely an empty vacuum as many once believed. Although ISM clouds are significantly more tenuous than their Earthly counterparts, both the time scales and the immense volume overcome the scarce reactant density. Ion-neutral reactions allow for a tremendous amount of chemistry at such vast scales. Additionally, many ion-neutral reactions

are highly relevant to understanding circumstellar and planetary atmospheres (cf. Glassgold 1996; Anicich & Huntress 1986).

The FA-SIFT lends itself well to studying ion-neutral reactions pertinent to many facets of astrophysics. The instrument couples well to a variety of ion sources, giving it the ability to study a variety of astrophysically relevant ions. In addition to reacting ions with neutral molecules, the method has had much success with studying reactant ions, neutrals, and atomic species that are ubiquitous throughout the ISM. The neutral atoms include H, N, and O atoms; all are readily studied with the FA-SIFT.

The FA-SIFT has been used in the experiments of this thesis. Kinetic measurements were performed to significantly improve upon former measurements with significant error. Results from kinetic experiments addressed reactions of  $C^+$  with several interstellar neutrals. Improved measurements of these reactions allow for more accurate models of interstellar clouds. Additionally, cosmological models of the early Universe benefit from the refinement of the kinetic measurement of the AD reaction of  $H^-$  leading to  $H_2$ , the most effective coolant after the big bang that was capable of seeding star and galaxy formation. Continued studies of  $H^-$  mapped out its reactivity with a variety of prototypical chemical neutrals, all of which have been discovered in regions likely to have a strong presence of  $H^-$ .

Finally, the recent discovery of anions in the ISM has prompted us to expand our knowledge of anion reactions and their contribution to astrochemistry. To date, however, there exists only limited work on gas-phase-anion-neutral reactions. A large portion of the work in this thesis aimed at expanding the anion reaction knowledge base. A better understanding of the reactions of organic anions with the most abundant neutral, H atom, should lead to a fundamental

understanding of their reactivity trends. Likewise, additional anion-hydrogen atom experiments were carried out to understand the reactivity of bare carbon-chain anions and nitrogen-containing carbon-chain anions, species that are extremely stable and undoubtedly present in the ISM.

## 1.10 References

- Adams, W. S. 1941, *ApJ*, 93, 11.
- Adams, N. G. & Smith, D. 1976, *Int. J. Mass Spectrom. Ion Proc.*, 21, 349.
- Allamandola, L. J., Tielens, A. G. G. M., & Barker, J. 1989, *ApJ Suppl. Ser.*, 71, 733.
- Anicich, V. G. 1993a, *ApJ Supp.*, 84, 215.
- Anicich, V. G. 1993b, *J. Phys. Chem. Ref. Data.*, 22, 1469.
- Anicich, V. G., & Huntress, W. T., Jr. 1986, *ApJS*, 62, 553.
- Chemical Kinetics Database, NIST, 2000, Standard Reference Database 17, Version 7.0 (Web Version), Release 1.5, <http://kinetics.nist.gov/kinetics/index.jsp>.
- CDMS 2010, <http://www.astro.uni-koeln.de/cdms/>.
- Chyba, C. F. & Hand, K. P. 2005, *Annu. Rev. Astron. Astrophys.*, 43, 31.
- Dalgarno, A., & Black, J. H. 1976, *Rep. Prog. Phys.*, 39, 573.
- Douglas, A. E. & Herzberg, G. 1941, *ApJ*, 94, 381.
- Ehrenfreund, P., & Charnley, S. B. 2000, *Annu. Rev. Astron. Astrophys.*, 38, 427.
- Ferguson, E. E., Fehsenfeld, F. C., & Schmeltekopf, A. L. 1969, *Adv. Atom. Mol. Phys.*, 5, 1.
- Friedman, L. 1968, *Ann. Rev. Phys. Chem.*, 19, 273.
- Galli, D., & Palla, F. 1998, *A&A*, 335, 403.
- Gerlich, D. & Smith, M. 2006, *Phys. Scr.*, 73, C25.
- Glassgold, A. E. 1996, *Annu. Rev. Astron. Astrophys.*, 34, 241.
- Glover, S. C., Savin, D. W., & Jappsen, A. -K. 2006, *ApJ*, 640, 553.
- Heger, M. L. 1922, *Lick. Obs. Bull.*, 337, 141.
- Henning, Th., & Salama, F. 1998, *Science*, 282, 2204.
- Herbig, G. H. 1995, *Ann. Rev. Astron. Astrophys.*, 33, 19.
- Herbst, E. 1993, *Rep. Prog. Phys.*, 56, 1209.
- Herbst, E. 1995, *Annu. Rev. Phys. Chem.*, 46, 27.
- Herbst, E. 2001, *Chem. Soc. Rev.*, 30, 168.
- Herbst, E. 2005, *J. Phys.: Conf. Ser.*, 4, 17.

- Herbst, E. 2010, <http://www.physics.ohio-state.edu/~eric/>.
- Herbst, E., & Klemperer, W. 1973, *ApJ*, 185, 505.
- Herbst, E. & van Dishoeck, E. F. 2009, *Ann. Rev. Astron. & Astrophys.*, 47, 427.
- Hollenbach, D. J., & Thronson, Jr., H. A., eds. 1987, *Interstellar Processes*, Reidel, Dordrecht.
- Ikezoe, Y., Matsuoka, S., Takebe, M., & Viggiano, A. 1987, *Gas Phase Ion-Molecule Reaction Rate Constants Through 1986*, Maruzen, Tokyo.
- IAU Symposium 197 1999, *Astrochemistry: From Molecular Clouds to Planetary Systems*, ed. Minh, Y. C. & Van Dishoeck, E. F., Sheridan Books, Chelsea, MI.
- IAU Symposium 231 2005; *Astrochemistry: Recent Successes and Current Challenges*, eds. Dariusz, C. L., Blake, G. A., & Herbst, E., Cambridge University Press, Cambridge, U.K.
- IUPAC 42<sup>nd</sup> Congress Symposium, *Astrochemistry*, Glasgow, Scotland, U.K., 2-7 August 2009.
- KIDA (*KInetic Database for Astrochemistry*) 2010, <http://kida.obs.u-bordeaux1.fr/>.
- Klemperer, W. 1997, Faraday Lecture, *Proc. Roy. Inst.*, London, 209.
- Kwok, S. 2006, *Physics and Chemistry of the Interstellar Medium*, ed. Murdzek, J., University Science Books, Sausalito, CA.
- Langevin, P. 1905, *Annal. Chim. Phys.*, 5, 245.
- Le Teuff, Y. H., Millar, T. J., & Markwick, A. J. 2000, *A&A Suppl. Ser.*, 146, 157.
- Lovas, F. J., Bass, J. E., Dragoset, R. A., & Olsen, K. J. 2009, *NIST Recommended Rest Frequencies for Observed Interstellar Molecular Microwave Transitions*, <http://www.nist.gov/phylab/data/micro/index.cfm>.
- Markwick-Kemper, A. J. 2005, in *Proc. IAU Symp. 231, Astrochemistry: Recent Successes and Current Challenges*, ed. D. C. Lis, G. A. Blake, & E. Herbst (Cambridge Univ. Press: Cambridge), 204.
- Martinez, O., Jr., Betts, N. B., Villano, S. M., Eyet, N., Snow, T. P., & Bierbaum, V. M. 2008, *ApJ*, 686, 1486.
- Martinez, O., Yang, Z., Betts, N. B., Snow, T. P., & Bierbaum, V. M. 2009, *ApJL*, 705, L172.
- Martinez, O., Yang, Z., Demarais, N. J., Snow, T. P., & Bierbaum, V. M. 2010, *ApJ*, 720, 173.
- McKellar, A. 1940, *Publ. Astron. Soc. Pac.*, 52, 187.
- Millar, T. J., & Williams, D. A., eds. 1993, *Dust and Chemistry in Astronomy*, Institute of Physics, Bristol.
- Müller, H. S. P., Schlöder, F., Stutzki, J., & Winnewisser, G. 2005, *J. Mol. Struct.*, 742, 215.

- Müller, H. S. P., Thorwirth, S., Roth, D. A., & Winnewisser, G. 2001, *A&A*, 370, L49.
- Peeters, E., Allamandola, L. J., Hudgins, D. M., Hony, S., & Tielens, A. G. G. M. 2004, *Proceedings: Astrophysics of Dust*, ed. Witt, A. N., Clayton, C. G., Draine, B. T., 309, 141.
- Perez, J., Ramirez-Arizmendi, L. E., Petzold, C. J., Guler, L. P., Nelson, E. D., & Kenttamaa, H. I. 2000, *Int. J. Mass Spectrom.*, 198, 173.
- Rehde, D. 2010, *Chemistry in Space: From Interstellar Matter to the Origin of Life*, Wiley-VCH, Weinheim, Germany.
- Sablier, M. & Rolando, C. 1993, *Mass Spectrom. Rev.*, 12, 285.
- Savage, B. D., & Sembach, K. R., 1996, *Annu. Rev. Astron. Astrophys.*, 34, 279.
- Shaw, A. M. 2006, *Astrochemistry: from Astronomy to Astrobiology*, John Wiley & Sons, New York.
- Smith, D. 1992, *Chem. Rev.*, 92, 1473.
- Smith, D., & Adams, N. G. 1989, *J. Chem. Soc., Faraday Trans. 2*, 85, 1613.
- Snow, T. P. 2001, *Spectrochem. Acta, Part A*, 75, 615.
- Snow, T., 2002, *Diffuse Interstellar Bands* in *Encyclopedia of Astronomy and Astrophysics*, Murdin, P. ed., Bristol Institute of Physics Publishing.
- Snow, T. P., & Bierbaum, V. M. 2008, *Annu. Rev. Anal. Chem.*, 1, 229.
- Snow, T. P. & McCall, B. J. 2006, *Annu. Rev. Astro. Astrophys.*, 44, 367.
- Snow, T. P., Stepanovic, M., Betts, N. B., Eichelberger, B. R., Martinez, O., & Bierbaum, V. M. 2009, *Astrobiology*, 9, 1001.
- Solomon, P. M., & Klemperer, W. 1972, *ApJ*, 178, 389.
- Spitzer, L. 1978, *Physical Processes in the Interstellar Medium*, John Wiley & Sons, New York.
- Swings, P. & Rosenfeld, L. 1937, *ApJ* 86, 483.
- Tielens, A. G. G. M., 2005, *The Physics and Chemistry of the Interstellar Medium*, Cambridge University Press, Cambridge, U.K.
- Tielens, A. G. G. M., & Snow, T. P. eds. 1995, *The Diffuse Interstellar Bands*, Kluwer Academic Publishers, Dordrecht.
- UMIST 2010, *The UMIST Database for Astrochemistry*, <http://www.udfa.net/>.
- Wakelam, V., Herbst, E., & Selsis, F. 2006, *A&A*, 451, 551.
- Wall, W. F., Carraminana, A., Carrasco, L., & Goldsmith, P. F. eds., 1999, *Millimeter-wave Astronomy: Molecular Chemistry & Physics in Space*, Kluwer Academic Publishers, Dordrecht.

Watson, W. D. 1973, ApJ, 183, L17.

Watson, W. D. 1976, Rev. Mod. Phys. 48, 513.

Watson, W. D. 1977, Acc. Chem. Res., 10, 221.

Woodall, J., Agúndez, M., Markwick-Kemper, A. J., & Millar, T. J. 2007, A&A, 466, 1197.

Woon, D. E. 2010, [www.astrochymist.org](http://www.astrochymist.org).

Yang, Z., Eichelberger, B., Carpenter, M. Y., Martinez Jr., O., Snow, T. P., & Bierbaum, V. M. 2010, ApJ, 723, 1325.

Yang, Z., Martinez Jr., O., Carpenter, M. Y., Snow, T. P., & Bierbaum, V. M., in preparation

## Chapter 2

### Experimental Methods

#### 2.1 Introduction

Gas-phase studies of ion-neutral reactions have prompted the development of a variety of experimental techniques. In particular, the flowing afterglow-selected ion flow tube (FA-SIFT) lends itself exceptionally well to these studies, especially due to its flexibility in a variety of experiments. Details of its capabilities and adaptability to a variety of ionization techniques and neutral atom sources are described below.

#### 2.2 Flowing Afterglow-Selected Ion Flow Tube

Kinetic experiments between ions and neutral reagents were performed on the FA-SIFT. Basic information about the instrument has been described elsewhere (Bierbaum 2003; Van Doren 1987, Van Doren et al. 1987). However, the details relevant to this thesis are discussed here.

A schematic of the FA-SIFT in its current configuration is shown in Figure 2.1. The instrument consists of an ion-production source region, an ion-selection region, a reaction region, and a detection region. Ions are produced in the source region using a variety of techniques that are described below. Ions are then gently extracted and guided into a SIFT quadrupole ion selection region using electrostatic lenses. The quadrupole transmits ions of a particular mass to charge ratio ( $m/z$ ); these ions are then focused to a Venturi inlet, which injects the ions into the reaction flow tube region. The ions undergo reactions with neutrals, and parent and product ions

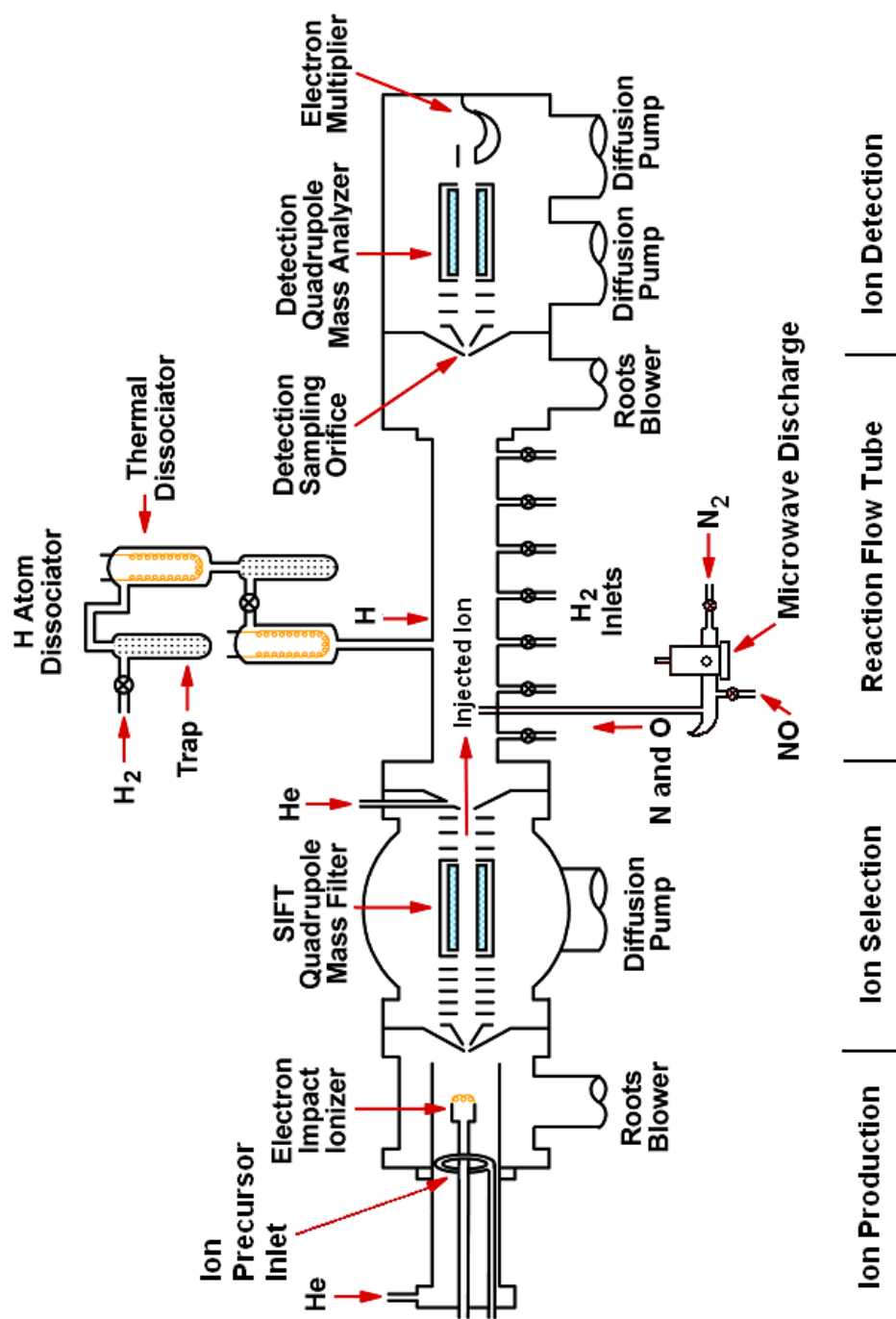


Figure 2.1 Flowing Afterglow-Selected Ion Flow Tube.

are then sampled into the detection region. Here the ions are focused into a second quadrupole coupled to an electron multiplier and a mass spectrum is produced. The falloff of reactant ions is monitored as a function of reaction time or neutral concentration for rate constant determinations and products are monitored to determine branching ratios. Figure 2.2 shows a SIFTed spectrum of the reactant  $C^+$ . Figure 2.3 shows the spectrum produced after a reactive neutral reagent ( $CH_4$ ) is introduced to the reaction flow tube. The reactant ion is depleted and product ions appear.

### 2.3 Ionization and SIFT Regions

The FA-SIFT is compatible with a variety of ionization schemes. Ion sources used in this work include electron ionization, chemical ionization, and cold cathode discharge. These methods are capable of both anion and cation production and can be coupled together for a multistage synthesis.

Ions are created in the source region as described below. The region consists of a flowing afterglow tube which houses the ionization device. Typically, helium ( $\sim 300$  mTorr) serves both as a carrier gas and as an ionization medium. A variety of inlets along the source region allow for the introduction of multiple reagents and ion precursors. Ions are then extracted into the SIFT quadrupole region through a nosecone lens with a 2 mm orifice. The regions about the nosecone are differentially pumped. The bulk helium and neutrals are evacuated from the source flow tube by a Stokes Roots blower ( $190 \text{ L s}^{-1}$ ).

The quadrupole region is evacuated by two diffusion pumps, a 10-inch pump ( $2000 \text{ L s}^{-1}$  air) evacuating the lensing region and an additional 4-inch pump ( $700 \text{ L s}^{-1}$  air) evacuating the quad housing. The quad region is maintained at  $< 10^{-6}$  Torr during operation. A series of six

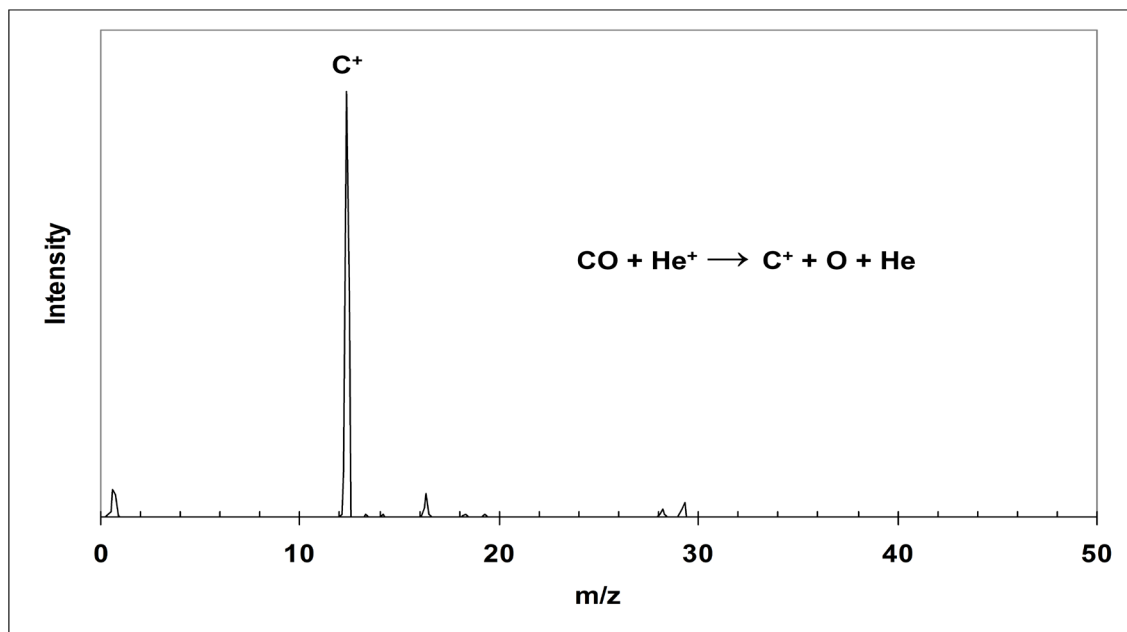


Figure 2.2 Mass spectrum of SIFTed cation  $\text{C}^+$ .

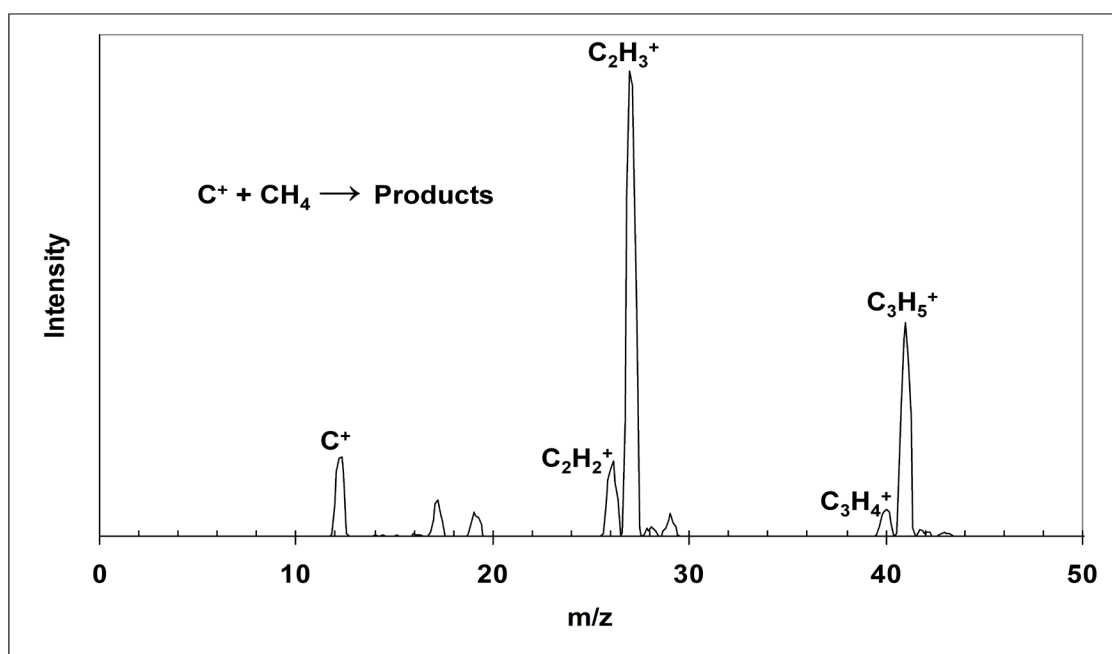


Figure 2.3 Mass spectrum showing reactant-ion depletion and the formation of primary and secondary product ions.

lenses focus the extracted ions into the SIFT quadrupole. The polarities on the extracting and focusing lenses are chosen to transmit the ions of desired polarity. Potentials on the lenses are individually optimized to attain a maximum ion current while minimizing energy imparted to the ions. The SIFT quadrupole is composed of 5/8-inch rods and has a maximum mass range of ~500 amu. The SIFT quadrupole can, with the pole DC off, transmit all ions of a single polarity produced in the source region. Typically, however, the quadrupole mass filter is used to transmit only those ions of a particular mass-to-charge ratio. Additional lensing after the SIFT quadrupole guides the ions to a Venturi inlet, where the ions are injected from a low pressure regime into the higher-pressure reaction flow tube.

### 2.3.1 Electron and Chemical Ionization

Electron and chemical ionization methods typically rely on a filament that emits a current of electrons. The electrons are then accelerated to a specific energy. The University of Colorado FA-SIFT uses a rhenium filament across which a voltage is applied (5 V, 2.5 A). This voltage produces an electron-emission current of ~25 mA that is stabilized using a feedback circuit. A potential bias typically accelerates the electrons to 70 eV, maximizing the interaction cross-section with reagents. A helium carrier gas (~270 mTorr) buffers this region, and its interaction with the electrons generates a plasma. Two ring inlets in addition to a series of downstream-fixed inlets are used to introduce the reagents for gas-phase ion synthesis. Axial movability of the ionizer and the ring inlets allow for optimization of ionization conditions. Reagents can be ionized directly by electrons, as in the case of H<sup>-</sup> production:



Alternatively, electron ionization can be used to initiate chemical ionization, as is the case in the production of  $C^+$ . Here, helium first interacts with the electrons to form  $He^+$ .



$He^+$  then interacts with carbon monoxide, CO, producing  $C^+$  via chemical ionization according to



A schematic of this method is given in Figure 2.4. Further reactions can be carried out to generate the desired reactant ion.

### 2.3.2 Cold-Cathode Discharge

Work involving heteroatomic carbon chain anions used a cold-cathode discharge method of ionization (Leopold et al. 1987). A schematic of the method is shown in Figure 2.5. For our purposes, a graphite rod was biased to the source flow tube at  $\sim -4$  kV ( $\sim 10$  mA DC), producing a discharge. Helium still serves as a carrier gas. However, a separate gas is introduced as a discharge medium. Argon is used to produce bare carbon-chain anions, while nitrogen is used to produce nitrogen-containing carbon-chain anions. Liquid water flows through a hollow sleeve portion of a stainless steel rod supporting the graphite, maintaining a stable discharge by conductively cooling the graphite rod. The hollow stainless support rod is isolated from the source flow tube by a quartz sleeve. A larger quartz sleeve isolates a barrel-type connector joining the graphite and stainless rods.

The exact mechanism of ionization is not clear. However, it is likely that the bias and subsequent discharge lead to carbon sputtering from the surface, resulting in the formation of the bare carbon-chain anions of interest. The addition of nitrogen not only serves as the discharge

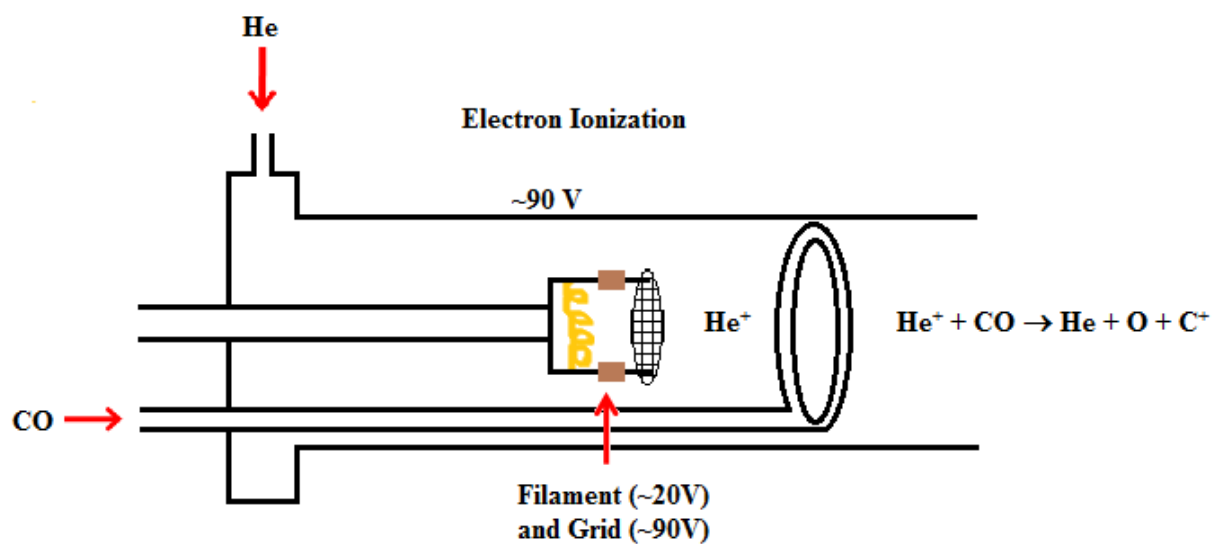


Figure 2.4 Schematic representation of electron impact for  $C^+$  production.

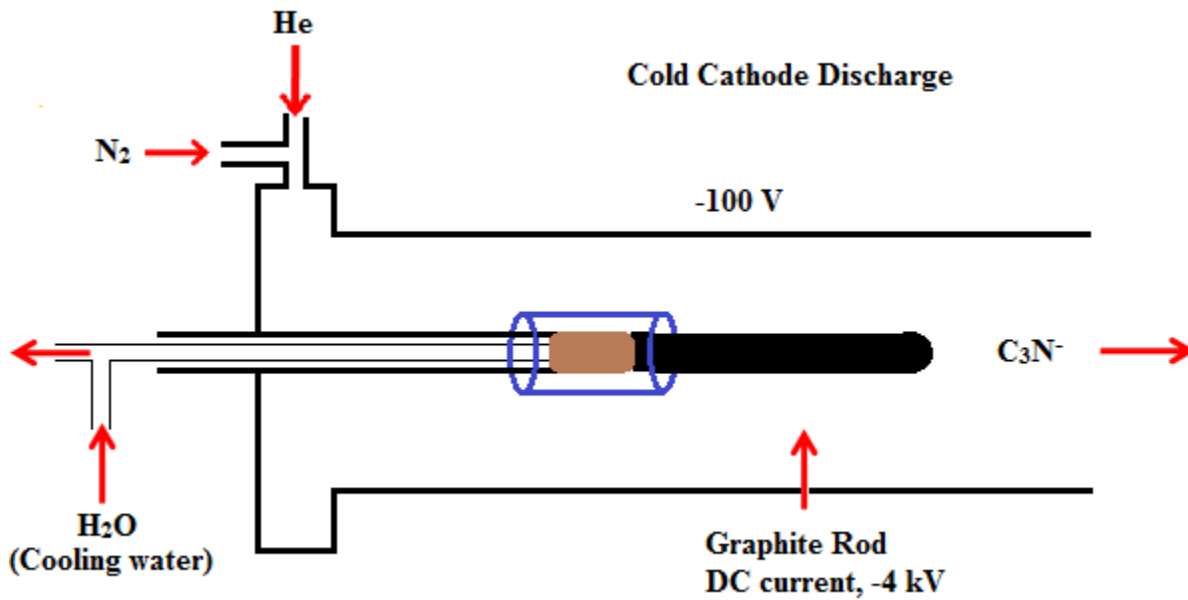


Figure 2.5 Schematic representation of cold-cathode discharge ionization.

medium, but also results in chemical ionization leading to the formation of  $C_xN_y^-$  anions (in our observations  $x=1-6$  and  $y=1-3$ ).

## 2.4 Reaction Flow Tube and Neutral Atom Sources

The reaction flow tube consists of an entry region and a reaction region. Upon injection from the Venturi inlet, ions are collisionally cooled and entrained by a flow of helium buffer gas within the entry region (approximately 30 cm in length). The helium has a constant flow of  $\sim 200$   $\text{std cm}^3 \text{ s}^{-1}$  maintained by a mass flow controller, resulting in a flow-tube pressure of  $\sim 0.5$  Torr. The reaction region (77 cm in length with an inner diameter of 7.3 cm) has 7 equally spaced inlets 11 cm apart. The reaction region terminates at a nosecone lens element. The inlets are connected to a manifold for the introduction of neutral molecular species. There are two additional inlets, one for the introduction of hydrogen atoms (71.5 cm from the downstream nosecone) and N or O atoms (70 cm from the downstream nosecone). Bulk helium and remaining neutrals are pumped away at the end of the reaction flow tube by a Roots blower pump ( $779 \text{ L s}^{-1}$ ).

The abundance of neutral-atomic species is high in the interstellar medium. Therefore, the ability to generate atomic species in the FA-SIFT, especially H, N, and O atoms, allows ion-neutral experiments with relevance to the ISM. Neutral atomic species present their own complexities, since these species are extremely reactive and unstable. Their concentrations can often be a challenge to determine. Nonetheless, these challenges can be overcome, as outlined below.

### 2.4.1 Hydrogen Atoms

Hydrogen atoms are generated by using a hydrogen-dissociator device, as shown in Figure 2.1. Ultrahigh purity hydrogen gas ( $\sim 8 \text{ std cm}^3 \text{ s}^{-1}$ , Airgas Inc., 99.999%) is flowed through molecular sieve traps immersed in liquid nitrogen to remove impurities. Immediately downstream from each molecular sieve is a coiled tungsten filament. Variable transformers apply voltages across the filaments, which resistively heat the filaments and thermally dissociate  $\text{H}_2$  into H atoms. Although two filaments are used in tandem, a lower voltage is applied to the upstream filament, serving only to condition it, keeping it oxide free and ready to use should the second filament become unusable. A measured voltage is applied to the second filament. The resulting H atoms are subsequently introduced into the reaction flow tube via Teflon tubing to minimize surface recombination. Because dissociation and transfer are only about 1% efficient, it is imperative that ions of interest do not react with molecular hydrogen.

H atom concentration is determined using calibration reactions. Calibrant ions of a particular polarity are chosen to coincide with the polarity of the reactant ion being studied. With respect to anions, reactions of H atoms with chloride ( $\text{Cl}^-$ ) and hydroxide ( $\text{OH}^-$ ) have been studied extensively; their reaction rate constants have consequently been measured to a significant accuracy. Values used for the experiments in this thesis are  $9.6 \times 10^{-9} \text{ cm}^3 \text{ s}^{-1}$  for  $\text{Cl}^-$  with H atom and  $1.40 \times 10^{-9} \text{ cm}^3 \text{ s}^{-1}$  for  $\text{OH}^-$  with H atom, each of which has an associated error of 20% (Fehsenfeld et al. 1973; Ferguson et al. 1969). In a single experiment, a series of two data points registers the falloff of either  $\text{Cl}^-$  or  $\text{OH}^-$  calibrant at two different voltage applications.

Applied voltages are chosen to lie close to the extremes of reactivity. Typically the lower voltage produces a concentration of H atom that will result in a 10% decrease in calibrant ion signal, while the higher voltage will result in a 90% decrease. Flows of H-atom are also adjusted to ensure adequate signal falloff of the reactant anions  $A^-$ . Typically, voltages between 25 and 60 volts are used. H atoms are also introduced into the flow tube for approximately  $\frac{1}{2}$  hour before quantitative measurements to ensure that conditions stabilize. Stability is verified by assuring that the reactant-ion signal returns to its former value after the introduction of hydrogen atoms for 5–10 minutes, the time-span of a single run of rate measurements.

#### 2.4.2 Nitrogen and Oxygen Atoms

In addition to H atoms, the FA-SIFT (Figure 2.1) allows us to study reactions with N and O atoms. These atoms can be produced using an Evenson cavity coupled to a microwave generator (Fehsenfeld et al. 1965). Figure 2.6 shows a schematic of N and O generation. Molecular nitrogen is introduced into the microwave discharge cavity ( $\sim 30$  W forward power) where it is dissociated to two N atoms and introduced into the reaction flow tube. O atoms are formed by introducing NO immediately after the discharge cavity where it interacts with the N atoms produced from the  $N_2$  dissociation via the quantitative reaction  $N + NO \rightarrow N_2 + O$ . O atoms are then subsequently introduced directly into the reaction flow tube. Addition of NO also serves as a titration in determining N and O atom concentrations. To illustrate the titration, Figure 2.7 shows a sample plot of the natural log of the reactant-ion concentration,  $\ln[I^\pm]$ , vs the NO flow in molecules per second. The plot shows a decrease in  $\ln[I^\pm]$  as the discharge is turned on, initiating N-atom flow. As one begins to add NO, N atoms are converted to  $N_2$  and O atom. During this stage, both N and O atoms are present. This continues until the titration end point, where all N atoms have been converted to  $N_2$  and O. The NO flow at this point indicates the

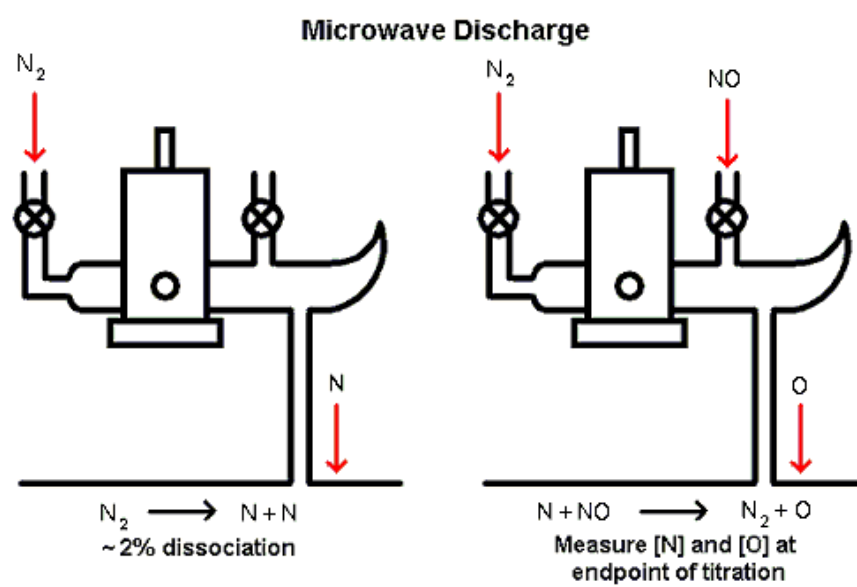


**Figure 2.6** Schematic showing generation of N and O atoms using microwave discharge.

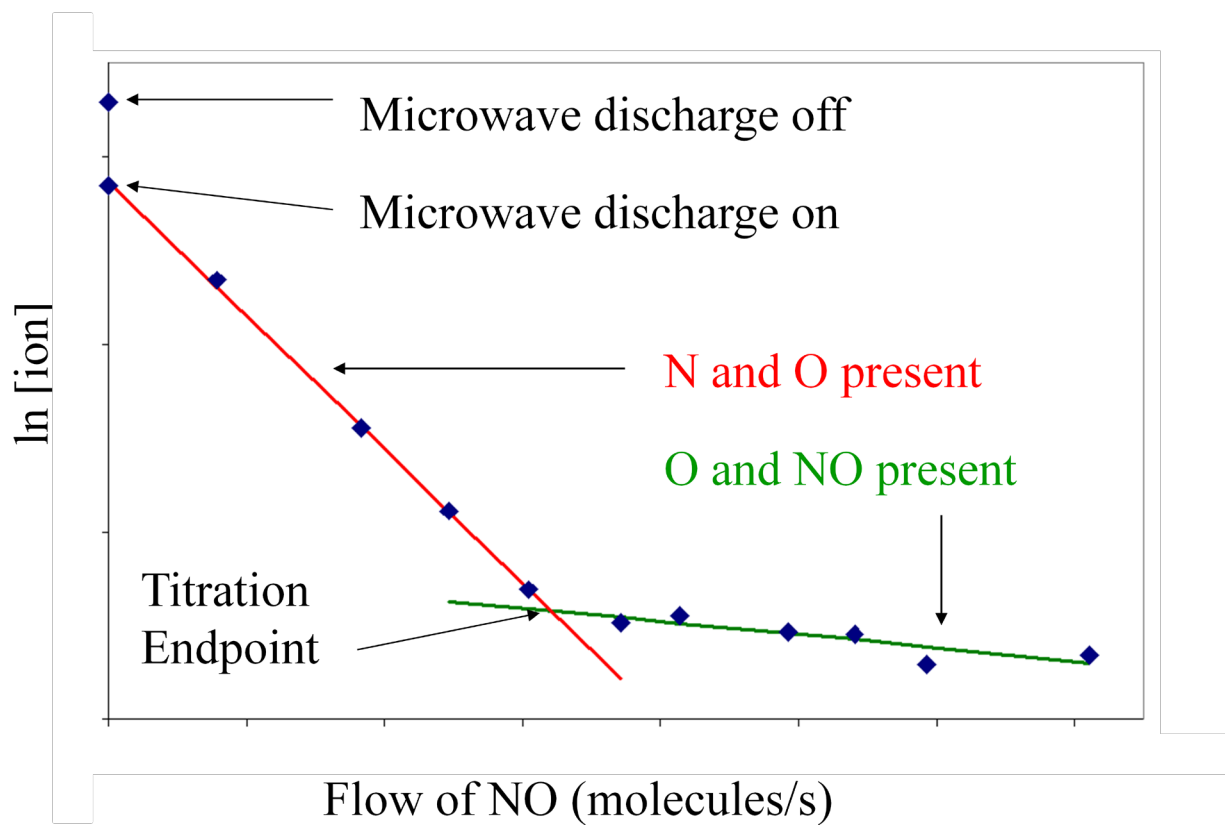


**Figure 2.7** Titration plot for determination of N and O atom concentrations.

maximum O-atom flow and the N-atom flow prior to NO addition. Beyond this point, the flow consists only of O and NO. This titration method is applicable when the reaction rate constant of the reactant ion differs for the N and O atom reactions.

## 2.5 Detection Region

The detection quadrupole region is evacuated by two diffusion pumps, a 6-inch pump ( $2400 \text{ L s}^{-1}$  air) which evacuates the lensing region and an additional 4-inch pump ( $1200 \text{ L s}^{-1}$  air) which evacuates the quadrupole and multiplier. The diffusion pumps are equipped with molecular sieve traps and have, in effect, a lower pumping capacity. A pressure differential exists across the nose cone element, with  $\sim 0.5$  Torr on the reaction-flow-tube side and  $\sim 10^{-5}$  Torr in the detection region, effectively preventing reactions at its threshold. Reactant and product ions are sampled via a 0.5 mm aperture in the nosecone element. A series of five electrostatic lenses focus the ions into a detection quadrupole.

The quadrupole is constructed of 5/8-inch rods and has a mass range of  $\sim 1000$  amu. The quadrupole is coupled to an electron multiplier with a gain of  $10^8$ . Pulsed signal from the multiplier is processed by a discriminator/amplifier and by the Extrel Merlin data system software package. A spectrum is produced, which shows a decrease in parent ion signal as it reacts with a neutral reagent, and an increase in product ion signal.

## 2.6 Traditional Flowing Afterglow

Experiments involving hydride ion were performed using the traditional flowing-afterglow mode of the instrument. In this mode, helium carrier gas is introduced at the entry region of the reaction flow tube. Ionization takes place by passing the helium over a rhenium filament. Additional ion-synthesis reagents can then be introduced through inlets located

downstream from the filament region. Because of the proximity of the detection region and the high intensity of ions produced in flowing-afterglow mode, a much lower emission current ( $\sim 10 \mu\text{A}$ ) was used as compared to the FA-SIFT method.

## 2.7 Reaction Kinetics

Consider the following bimolecular ion-neutral reaction,



where  $I^\pm$  is either a reactant cation or an anion, B is a neutral reactant, and  $C^\pm$  and D are products.

The second-order rate law describing the change in ion concentration as a function of time can be written as

$$-\frac{d[I^\pm]}{dt} = k_{exp} [I^\pm][B]. \quad (2.5)$$

Here  $k_{exp}$  is the experimental rate constant and  $[I^\pm(t)]$  and  $[B(t)]$  are the ion and reactant neutral concentrations as functions of time. Reactions are carried out under pseudo first-order conditions, where  $[B] \gg [I^\pm]$  ( $\sim 10^{11}$  molecule  $\text{cm}^{-3}$  vs  $10^6$  ions  $\text{cm}^{-3}$ ). The neutral concentration remains essentially unchanged throughout the reaction. Equation (2.5) can be integrated and rearranged to give

$$\ln[I^\pm] = -k_{exp}[B]t + \ln[I^\pm]_0. \quad (2.6)$$

The FA-SIFT is a constant flow system. Therefore, a specific reaction time can be derived by measuring the bulk flow of the helium carrier gas and the distance it carries the ions within the reaction flow tube, as shown by

$$t = \frac{z}{\alpha_v \bar{v}}. \quad (2.7)$$

Ions that come in contact with the flow-tube walls are lost via neutralization. Their loss results in a radial ion-density gradient in which the density is highest at the center of the flow tube. Additionally, flowing helium interacts with the walls of the flow tube. Helium at the wall experiences the highest viscous forces causing a reduced velocity. These forces subside further from the walls, and therefore, the helium velocity is greatest in the center. Coupling of these two factors results in ions having a higher velocity than the bulk flow of the helium. This phenomenon is accounted for with the  $\alpha_v$  factor in equation (2.7), which has been previously measured to be 1.6. Substitution in equation (2.6) gives

$$\ln[I^\pm] = -k_{exp}[B] \frac{z}{\alpha_v \bar{v}} + \ln[I^\pm]_0. \quad (2.8)$$

Recognizing the linear form of equation (2.8), a semilogarithmic plot of the ion concentration vs the reaction distance can be constructed as shown in figure 2.8. The slope of this plot ( $m$ ) can be used to solve for  $k_{exp}$  as shown below:

$$k_{exp} = -m \frac{\alpha_v \bar{v}}{[B]}. \quad (2.9)$$

A similar plot can be made vs the neutral concentration:

$$k_{exp} = -m' \frac{\alpha_v \bar{v}}{z}. \quad (2.10)$$

An experimental measurement of the neutral reactant concentration can be obtained in terms of the neutral flow ( $F_B$ ), the average helium carrier-gas velocity ( $\bar{v}$ ), and the flow tube area ( $A$ ):

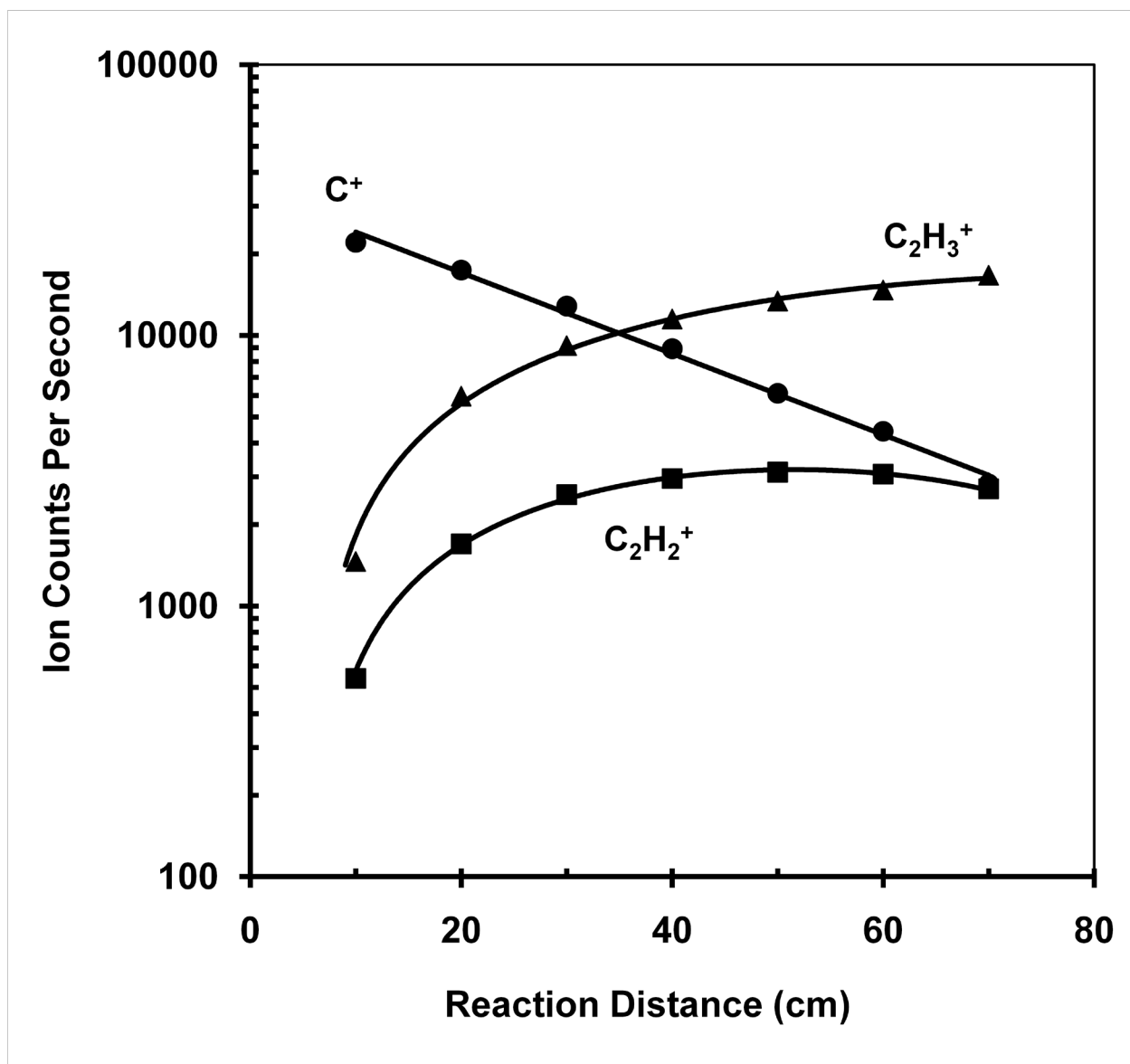


Figure 2.8 Semilogarithmic plot of ion signal vs reaction distance for  $C^+ + CH_4$ .

$$[B] \left( \frac{\text{particle}}{\text{cm}^3} \right) = \frac{F_B \left( \frac{\text{atm} \cdot \text{cm}^3}{\text{s}} \right)}{\bar{v} \left( \frac{\text{cm}}{\text{s}} \right) \cdot A(\text{cm}^2)} \cdot 760 \left( \frac{\text{Torr}}{\text{atm}} \right) \cdot 3.535 \times 10^{16} \left( \frac{\text{particle}}{\text{cm}^3 \cdot \text{Torr}} \right). \quad (2.11)$$

The neutral reactant that is introduced into the reaction flow tube can be isolated to flow through one of two calibrated volumes (2401.3 cm<sup>3</sup> or 2423.4 cm<sup>3</sup>). This flow ( $F_B$ ) can be determined by the change in a monitored pressure, which is measured with a capacitance manometer, for a calibrated volume in a given time.

The equations above require an experimental measurement of the bulk helium-flow velocity. A helium mass-flow controller is used to determine the flow of helium ( $F_{He}$ ), and a capacitance manometer is used to determine helium pressure ( $P_{He}$ ). By including the reaction flow tube area ( $A = 41.854 \text{ cm}^2$ ) and adjusting for experimental temperature, the helium velocity can be determined by

$$\bar{v} \left( \frac{\text{cm}}{\text{s}} \right) = \frac{F_{He} \left( \frac{\text{atm} \cdot \text{cm}^3}{\text{s}} \right)}{P_{He}(\text{Torr}) \cdot A(\text{cm}^2)} \cdot 760 \left( \frac{\text{Torr}}{\text{atm}} \right) \cdot \frac{T(\text{K})}{273.15(\text{K})}. \quad (2.12)$$

Substituting into equation (2.9) and simplifying (constants are combined into  $C = 4.6104 \times 10^{-19}$ ) gives

$$k_{exp} \left( \frac{\text{cm}^3}{\text{particle} \cdot \text{s}} \right) = -m \left( \frac{1}{\text{cm}} \right) \cdot \frac{F_{He}^2 \left( \frac{\text{atm} \cdot \text{cm}^3}{\text{s}} \right)^2 \cdot T^2(\text{K})^2}{P_{He}^2(\text{Torr})^2 \cdot F_B \left( \frac{\text{atm} \cdot \text{cm}^3}{\text{s}} \right) \cdot A(\text{cm}^2)} \cdot C \left( \frac{\text{cm}^3 \cdot \text{Torr}^2}{\text{atm} \cdot \text{particle} \cdot \text{K}^2} \right) \quad (2.13)$$

Similarly, substitution and simplification with equation (2.10) (constants are combined into  $C' = 4.4518$ ) gives

$$k_{exp} \left( \frac{\text{cm}^3}{\text{particle} \cdot \text{s}} \right) = -m' \left( \frac{\text{cm}^3}{\text{particle}} \right) \cdot \frac{F_{He} \left( \frac{\text{atm} \cdot \text{cm}^3}{\text{s}} \right) \cdot T(\text{K})}{P_{He}(\text{Torr}) \cdot z(\text{cm}) \cdot A(\text{cm}^2)} \cdot C' \left( \frac{\text{Torr}}{\text{atm} \cdot \text{K}} \right) \quad (2.14)$$

Equation (2.14) is also used in this thesis to determine a rate constant for an ion-neutral reaction using a calibration, eliminating the need for a neutral flow determination as discussed in section 2.4.1. A ratio of the rate constants for the reactions of both a reactant ion (anion,  $A^-$ , shown here) and a calibrant ( $Cl^-$  with H atom in this case) can be written as

$$\frac{k_{A^-}}{k_{Cl^-}} = \frac{\left(-m' \cdot \frac{F_{He} \cdot T}{P_{He} \cdot z \cdot A} \cdot C'\right)_{A^-}}{\left(-m' \cdot \frac{F_{He} \cdot T}{P_{He} \cdot z \cdot A} \cdot C'\right)_{Cl^-}}. \quad (2.15)$$

Reactions for the reactant and calibrant ions occur under the same conditions (i.e., helium pressure, reaction distance, helium flow, and temperature). These parameters, including the constants comprising  $C'$ , cancel in the above equation, leaving only the ratios of rate constants and the slopes from the logarithmic plots of the ion signal vs neutral flow. Equation (2.4) can be simplified and rearranged to solve for the rate constant under consideration

$$k_{A^-} = \frac{(m')_{A^-}}{(m')_{Cl^-}} k_{Cl^-}. \quad (2.16)$$

For reactions involving the formation of more than one product, e.g.,



it becomes necessary to determine the contribution of each reaction to the products. The initial branching ratios can be determined (free from the effects of differential diffusion or secondary reactions) by plotting the percentage of product ions vs the reaction distance and extrapolating to zero reaction distance, as shown in Figure 2.9. However, care must be taken to account for mass discrimination, i.e., the transfer of different masses through the quadrupole with different

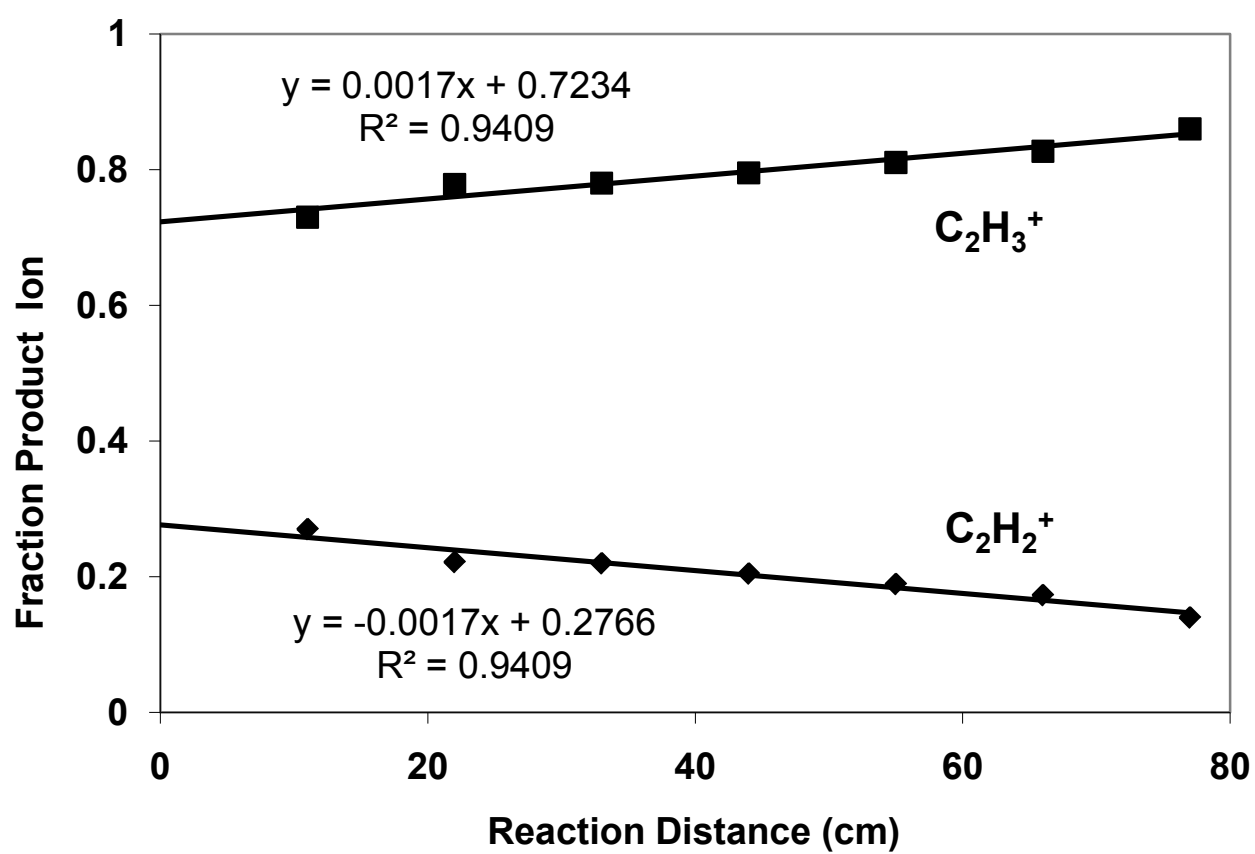


Figure 2.9 Product ion extrapolation plot for reaction of  $C^+ + CH_4$ .

efficiencies. Calibration reactions can be used to account and correct for mass discrimination. Calibration reactions use reactant ions to approximate the same range of ion-product masses from equation (2.17). However, reactions are chosen that proceed only via one channel. A calibration curve can then be constructed using the detection efficiencies for reactant and product ions, and a correction can be made to account for mass discrimination in the experimental work.

Sources of error in the FA-SIFT rate-constant and branching-ratio determinations have been derived and discussed elsewhere (Van Doren 1987). A brief summary follows. Systematic errors include uncertainties in conditions assumed for the instrument's performance. Examples of these errors include incorrect descriptions of instrument conditions such as laminar flow within the reaction flow tube, the subsequent helium velocity profile, and possible variations in  $\alpha_v$  with pressure. Temperatures, pressures, and flows are assumed to be measured at equilibrium, however small variations could be present.

The parameters used in equations (2.13) and (2.14) have their independent errors. Since these parameters are measured, these errors are reduced by calibrating the measurement devices. This includes calibration of flow, pressure, temperature, and voltage measurement devices in addition to volumetric measurements of the calibrated volume used in determining neutral concentration flows. Mass flow controllers and flow meters are calibrated by constructing calibration curves by comparing controller and meter readings to actual measurements of corresponding flows using a precision wet test meter. Pressure, temperature, and voltage measurement devices reference standards. Calibrated volumes used for neutral flow measurements are determined by measuring the pressure ( $P_1$ ) in a known volume ( $V_1$ ) (a 2-liter glass bulb whose volume is exactly determined by transferring water with calibrated pipettes);

the gas in the known volume is then expanded into an unknown total volume ( $V_2$ ) and reading the resulting pressure ( $P_2$ ). The unknown volume is given by  $V_2 = \frac{P_1 \cdot V_1}{P_2}$ .

A conservative estimate of the total systematic error associated with the instrument is ~15% for ion-neutral molecule measurements. In addition to this reported error, a statistical error, reported as a standard deviation of a mean of measurements is reported. Additionally when calibration reactions are used to determine neutral concentrations, as for H atom concentration determinations, the errors in the rate constants of those reactions must also be taken into consideration. A special case for the combination weighting of measurements with their associated errors is presented in chapter 4 as was used for the analysis of the H + H<sup>-</sup> experiments of this thesis.

## 2.8 Collision Rate Constants

Normalization of reaction rate constants into a reaction efficiency allows for their direct comparison. A reaction efficiency is the ratio of the experimentally determined rate constant to a rate constant predicted by collisional models  $\left(\frac{k_{\text{experiment}}}{k_{\text{collision}}}\right)$ . In its simplest form, an ion-neutral collision will occur because of the electrostatic potential between the point charge of an ion and the induced dipole of a neutral species. The magnitude of the induced dipole is governed by the polarizability of the neutral species. This simple view of an ion-neutral reaction was formulated over a century ago by Paul Langevin (1905) to predict reaction rate constants:

$$k_{Lan} = 2\pi \cdot q \left(\frac{\alpha}{\mu}\right)^{\frac{1}{2}}, \quad (2.18)$$

where  $q$  represents the charge of the ion,  $\alpha$  is the polarizability of the neutral, and  $\mu$  is the reduced mass of the ion and neutral.

Subsequent improvements in traditional Langevin theory have accounted for effects from neutrals with permanent dipoles. For these species, parametrized trajectory theory is used. This theory provides a more accurate collisional rate constant than the underestimation provided by Langevin theory. Parametrized trajectory theory was developed by Su and Chesnavich (1982), and corrects Langevin theory by accounting for additional electrostatic attraction between an ion and a neutral having a dipole moment. This rate constant,  $(k_{par})$ , is determined according to

$$(k_{par}) = \begin{cases} 0.4767x + 0.6200 ; & x \geq 2, \\ \frac{(x+0.5090)^2}{10.526} + 0.9754 ; & x \leq 2 \end{cases} \cdot k_{Lan}, \quad (2.19)$$

where

$$x = \frac{\mu_D}{\sqrt{2\alpha k_B T}}, \quad (2.20)$$

$\mu_D$  and  $\alpha$  in equation (2.20) are the dipole moment and polarizability of the neutral,  $k_B$  is the Boltzmann constant, and  $T$  is the reaction temperature. Polarizabilities and dipole moments are taken from either the *NIST Chemistry WebBook* (2010), the experimental thermochemical data portion of the *NIST Computational Chemistry Comparison and Benchmark Database* (CCCBD 2010) or from the *89<sup>th</sup> edition of the CRC Handbook of Chemistry and Physics* (2008).

One additional theory is used for the organic anion and carbon-nitrogen anion chapters of this thesis. Because of the high polarizability of these ions, there is an addition to the potential between an ion and a neutral. A point polarizable ion model is a modification to collisional theory by Eichelberger et al. (2003) that accounts for effects from highly polarizable ions.

## 2.9 Computational Support

Substantial support for mechanistic formulation is often derived from computational work. The *Gaussian 03* (Frisch et al. 2004) suite of programs has been used for some of the reactions of this thesis. *Ab initio* and DFT calculations are used to determine reaction enthalpies. For comparison, additivity methods are also used to calculate reaction enthalpies using values for ionization energies, bond energies, electron affinities, and heats of formation taken from either the *NIST Chemistry WebBook* (2010), the experimental thermochemical data portion of the *NIST Computational Chemistry Comparison and Benchmark Database* (CCCBD 2010) or from the *89<sup>th</sup> edition of the CRC Handbook of Chemistry and Physics* (2008). A variety of levels of theory have been applied to investigate structures and energies of the species under investigation in addition to reaction mechanisms in reactivity. Detailed computational methods are described in the following chapters. Dr. Zhibo Yang collaborated with all of the computational work.

## 2.10 References

- Bierbaum, V. M. 2003, in *Encyclopedia of Mass Spectrometry*, ed. P.B. Armentrout (Amsterdam: Elsevier), 940
- Eichelberger, B. R., Snow, T. P., & Bierbaum, V. M. 2003, *J. Am. Soc. Mass Spectrom*, 14, 501.
- Fehsenfeld, F. C., Evenson, K. M., & Broida, H. P. 1965, *Rev. Sci. Instrum.* 36, 29
- Fehsenfeld, F. C., Howard, C. J., & Ferguson, E. E. 1973, *J. Chem. Phys.*, 58, 5841
- Ferguson, E. E., Fehsenfeld, F. F., & Schmeltekopf, A. L. 1969, *Adv. At. Mol. Phys.*, 5, 1
- Frisch, M. J., Trucks, G. W., Schlegel, H. B., Scuseria, G. E., Robb, M. A., Cheeseman, J. R., Montgomery, Jr., J. A., Vreven, T., Kudin, K. N., Burant, J. C., Millam, J. M., Iyengar, S. S., Tomasi, J., Barone, V., Mennucci, B., Cossi, M., Scalmani, G., Rega, N., Petersson, G. A., Nakatsuji, H., Hada, M., Ehara, M., Toyota, K., Fukuda, R., Hasegawa, J., Ishida, M., Nakajima, T., Honda, Y., Kitao, O., Nakai, H., Klene, M., Li, X., Knox, J. E., Hratchian, H. P., Cross, J. B., Bakken, V., Adamo, C., Jaramillo, J., Gomperts, R., Stratmann, R. E., Yazyev, O., Austin, A. J., Cammi, R., Pomelli, C., Ochterski, J. W., Ayala, P. Y., Morokuma, K., Voth, G. A., Salvador, P., Dannenberg, J. J., Zakrzewski, V. G., Dapprich, S., Daniels, A. D., Strain, M. C., Farkas, O., Malick, D. K., Rabuck, A. D., Raghavachari, K., Foresman, J. B., Ortiz, J. V., Cui, Q., Baboul, A. G., Clifford, S., Cioslowski, J., Stefanov, B. B., Liu, G., Liashenko, A., Piskorz, P., Komaromi, I., Martin, R. L., Fox, D. J., Keith, T., Al-Laham, M. A., Peng, C. Y., Nanayakkara, A., Challacombe, M., Gill, P. M. W., Johnson, B., Chen, W., Wong, M. W., Gonzalez, C., & Pople, J. A., *Gaussian 03*, Revision C.02, Gaussian, Inc., Wallingford CT, 2004.
- Langevin, P. 1905, *Ann. Chim. Phys.*, 5, 245
- Leopold, D. G.; Ho, J., & Lineberger, W. C. 1987, *J. Chem. Phys.* 86, 1715
- Lide, D. R. 2008, *CRC Handbook of Chemistry and Physics* (89<sup>th</sup> ed.; Boca Raton, FL: CRC Press; Taylor & Francis Group)
- Linstrom, P. J., & Mallard, W. G. (ed.) 2010, *NIST Chemistry WebBook*, NIST Standard Reference Database Number 69 (Gaithersburg, MD: NIST) 20899 (<http://webbook.nist.gov>)
- NIST Computational Chemistry Comparison and Benchmark Database* 2010, NIST Standard Reference Database Number 101, Release 15a, April 2010, ed. R. D. Johnson III (<http://cccbdb.nist.gov>)
- Su, T., & Chesnavich, W. J. 1982, *J. Chem. Phys.*, 76, 5183
- Van Doren, J. M. 1987, Ph. D. thesis in Chem. Phys. (Boulder: Univ. Colorado), 341
- Van Doren, J. M., Barlow, S. E., DePuy, C. H., & Bierbaum, V.M. 1987, *Int. J. Mass Spectrom. Ion Processes*, 81, 85

## Chapter 3

### Gas Phase Study of $C^+$ Reactions of Interstellar Relevance

#### 3.1 Introduction

Gas phase ion-neutral reactions are critical processes in a variety of astrophysical environments. Chemical models attempt to predict the effects that these reactions have on the development and evolution of the interstellar medium (ISM). Accurate experimental values of rate constants and product branching ratios for interstellar reactions are essential for accurate theoretical predictions. Markwick-Kemper has modeled a small dark cloud using 2955 reactions and 281 total species to determine how errors in reaction rate constants affect the concentrations of various species in the ISM. His results prioritize which reactions, due to their large uncertainty, most affect the calculated abundance of these species (Markwick-Kemper 2005). Several reactions of  $C^+$  are included in this list because of the importance of this ion in the ISM. Markwick-Kemper used reaction rate coefficients tabulated in the University of Manchester Institute of Science and Technology (UMIST) database (Woodall et al. 2007), many of which have uncertainties in their rate constants of more than a factor of two. In addition, values in a second compilation, the Ohio State database, sometimes differ from those in the UMIST database (Herbst 2007).

In areas of the ISM with extremely low temperatures, chemistry not involving surfaces is dominated by ion-atom or ion-molecule reactions, which require no activation energy. Because of its low ionization energy (11.26 eV), the carbon atom is readily ionized by the ambient radiation (<13.60 eV) in diffuse regions of the ISM. Therefore, the carbon cation exists in most diffuse-atomic, diffuse-molecular, and translucent-cloud regions; it is the dominant form of

carbon in diffuse atomic and molecular regions. In these regions, carbon-cation chemistry primarily involves atomic neutrals. At the boundary between the diffuse-molecular and translucent regions, the local density of carbon changes from cationic to neutral, since there is significant attenuation of ionizing radiation (Snow & McCall 2006). As one crosses into the dense molecular region, there is a shift to high densities of carbon monoxide, CO, which is the major form of carbon and the second most abundant molecule in dense clouds. While the inner molecular regions are shielded from interstellar radiation, carbon cation ( $C^+$ ) is formed by cosmic-ray particles that penetrate into these dense regions. Cosmic-ray ionization of helium initiates the dissociative ionization of CO (i.e.,  $He^+ + CO \rightarrow C^+ + O + He$ ); this process is a primary source of ground-state  $C^+$  in dense clouds (Herbst & Klemperer 1973; Watson 1974).

The reactions of  $C^+$  studied here are most relevant in the denser translucent and molecular cloud regions. Although the concentration of carbon cations is several orders of magnitude smaller in these regions than in diffuse atomic clouds, their existence has a significant impact on local chemistry. Because of its low reactivity with major components of the ISM, including  $H_2$ , CO, and free electrons,  $C^+$  is available for reaction with a variety of polyatomic neutrals that are important in dense cloud chemistry (Herbst & Klemperer 1973). These reactions form other ions and molecules that are often more complex, including multicarbon species. Errors in the rate constants and branching ratios of these reactions can have a serious impact on chemical models of these regions.

We have studied gas-phase reactions of carbon cation with ammonia ( $NH_3$ ), methane ( $CH_4$ ), oxygen ( $O_2$ ), water ( $H_2O$ ), and acetylene ( $C_2H_2$ ). Of the reactions reported in this paper, all but the  $CHN^+$  and  $H_3N^+$  product channels produced by the reaction with ammonia (discussed below) are ranked among the top 100 reactions of Markwick-Kemper's study. The goal of this

research is to increase the accuracy of the data provided to the astronomical community, and to reconcile the discrepancies between the databases and the current literature.

### 3.2. Experimental Methods

Two similar flowing afterglow-selected ion flow tube (FA-SIFT) instruments at the University of Colorado at Boulder were used for these studies. The experimental parameters for both instruments were separately optimized and calibrated, including reaction-flow tube pressure, reaction distance, helium flow rate, and neutral-reactant flow rate; mass discrimination was minimized.

$C^+$  is formed by electron impact ionization on a trace amount of CO (Airgas Inc., 99.5% pure) entrained in a flow of helium. The helium (Airgas Inc., 99.998+%) is purified by flow through a molecular sieve trap immersed in liquid nitrogen. The neutral reactants include  $NH_3$  (Air Products & Chemicals Inc., 99.99+%);  $CH_4$  (Airgas Inc., 99.0%);  $O_2$  (Airgas Inc., 99.994%);  $H_2O$  (in house deionized water); and  $C_2H_2$  (Airgas Inc., 99+%).

A concern in these studies is the possible generation of electronically excited  $C^+$  which would skew the rate constant determinations and product-ion branching-ratio measurements. Ionization energies of  $\sim 70$  eV have been found to produce small amounts of excited-state species (Tichy et al. 1979; Xu et al. 1990). Lower-energy electron ionization ( $\sim 30$  eV) has been shown (Twiddy et al. 1986) to create strong signals of ground-state  $C^+(^2P)$  while minimizing formation of electronically excited metastable  $C^+(^4P)$ . We have therefore used 30 eV electron ionization in these studies. We have confirmed the absence of electronically excited  $C^+$  by the lack of reaction of injected  $C^+$  with CO. Twiddy et al. (1986) have found that  $C^+(^4P)$  reacts with CO with a rate constant of  $k \sim 3 \times 10^{-11} \text{ cm}^3 \text{ s}^{-1}$ . In separate experiments, we have increased the electron

ionization energy to 70 eV and confirmed that the branching ratio for the  $C^+ + O_2$  reaction changes so that  $CO^+$  becomes the dominant product ion.

In our tabulation of results, we have noted prior literature values where higher ionization energies were used and where, therefore, excited  $C^+$  may exist. The tables include all published values for experiments near 300 K.

Collision rate constants were calculated using parameterized trajectory theory for reactants with a dipole moment ( $NH_3$  and  $H_2O$ ) or Langevin theory for reactants without a dipole moment ( $CH_4$ ,  $O_2$ , and  $C_2H_2$ ) (Gioumousis & Stevenson 1958; Su & Chesnavich 1982).

Reaction efficiencies are the ratio of the experimental rate constant to the collision rate constant.

### **3.3. Results and Discussion**

We have found good agreement between the results from our series of experiments on two different FA-SIFT instruments (measured rate constants agree within 10%), thus confirming that calibration of instrumental parameters and systematic error have been correctly addressed. In addition, our measured values are in agreement with some of those previously reported in the literature. However, caution must be used when comparing FA-SIFT measurements to those obtained by other means. For example, measurements using ion cyclotron resonance (ICR) can include electronically excited or nonthermal reactant ions, and therefore often have larger rate constants than measurements where only the ground-state species is present. In traditional FA instruments, ions are formed directly in the reaction flow tube, and therefore these measurements can include contamination from the presence of other species. In addition, many of these reactions have been previously studied at a range of temperatures and kinetic energies. However, past research and theoretical predictions have shown either a slightly negative or no temperature dependence of rate constants for many ion-molecule reactions. The reactions

studied here all proceed at relatively high efficiencies (>63%), and therefore only minor temperature effects are expected.

An experimental complication in the SIFT method is that different mass ions are transmitted with different efficiencies through the detection region. While mass discrimination does not affect the reaction rate-constant measurements, it can lead to erroneous product ion branching-ratio determinations. However, a comparison of ion counts before reaction ( $C^+$  ions only) and after reaction ( $C^+$  and product ions) show constant signals, indicating that mass discrimination effects are not substantial for these studies. An additional difficulty in making accurate branching ratio measurements is the occurrence of secondary reactions. We therefore use a method similar to that of Adams & Smith (1976), in which the percentage of each product ion is plotted as a function of the extent of reaction; Adams & Smith use the neutral reactant flow rate for this latter parameter, whereas we have used the ion-neutral reaction distance.

Extrapolation to zero distance yields the primary-product ion distribution, where secondary reactions and differential ion diffusion have been eliminated. We note that this latter effect is small since the  $C_2H_2^+$  and  $C_2H_3^+$  product ions are expected to have similar diffusion coefficients in He buffer gas. These branching-ratio plots are reasonably fit by linear extrapolation; a full modeling of the kinetics and ion diffusion generally yields similar results. In addition, we evaluate and correct for minor drift in mass position ( $m/z$ ). These branching ratio values are compared to those obtained by taking the percentage of product ion (both primary and secondary reactions) and finding the distance where secondary products extrapolate to zero abundance; the percent of product ions at this distance then determines the primary product branching ratios. The two methods produce results that are in good agreement. Nevertheless, the relatively large error bars on the branching ratios for the reactions of  $C^+ + NH_3$  and  $C^+ + O_2$  reflect the inherent

difficulties in accurately determining quantitative product distributions because of secondary reaction and residual mass discrimination.

With careful calibration of instrumental parameters, a total systematic error of  $\pm 13.4\%$  is attainable (Van Doren 1987). In this work, we report a slightly more conservative systematic error of  $\pm 15\%$ . In Tables 3.1–3.6, the reported error bars for the reaction rate constants and branching ratios represent one standard deviation of the mean, and therefore indicate the precision of these values. The reported experimental rate constants represent an average of 8–15 measurements, and the branching ratios represent an average of 6–14 measurements.

### 3.3.1. $C^+ + NH_3$

The reaction of  $C^+$  with  $NH_3$  is significant in the ISM as a pathway leading to the formation of HNC and HCN in dense interstellar clouds through primary and secondary reaction pathways. These reactions create ions and molecules that may serve as intermediaries for the production of more complicated interstellar species. The reaction of  $C^+$  with  $NH_3$  occurs through the following ion-atom exchange and charge transfer channels:



The  $\Delta H_{\text{rxn}}$  for the  $CH_2N^+$  channel is reported by Tichy et al (1979); the  $\Delta H_{\text{rxn}}$  for the  $HCN^+$  channel is for hydrogen cyanide isomer (HCN) in particular. As shown in Table 3.1, our reported value for the overall rate constant  $[(2.36 \pm 0.15) \times 10^{-9} \text{ cm}^3 \text{ s}^{-1}]$  is in good agreement with previous literature values. The first literature measurement of the reaction  $C^+ + NH_3$  (Schiff et al. 1974) did not show evidence of the  $CHN^+$  formation channel. This is likely due to the secondary reactions of the primary product ions with ammonia as shown below:

**Table 3.1** Reaction rate constants and branching ratios for  $C^+ + NH_3$ .

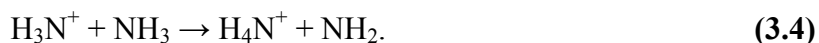
$k$ ( $10^{-9} cm^3 s^{-1}$ )	Products	Branching Ratio	Instrument/Reference
$2.3 \pm 0.2$	$H_3N^+ + C$ $CH_2N^+ + H$ $CHN^+ + H_2$	0.50 0.47 0.03	ICR <sup>a</sup> /Anicich et al. (1976)
$2.0 \pm 30\%$	$H_3N^+ + C$ $CH_2N^+ + H$ $CHN^+ + H_2$	0.70 <0.30 >0	FA/Liddy et al. (1977)
$2.3 \pm 0.2$	$H_3N^+ + C$ $CH_2N^+ + H$	0.95 0.05	FA <sup>b</sup> /Schiff et al. (1974)
2.3	$H_3N^+ + C$ $CH_2N^+ + H$ $CHN^+ + H_2$	Not Reported ~0.5 Not Reported	FA <sup>c</sup> /Schiff & Bohme (1979)
2.3	$H_3N^+ + C$ $CH_2N^+ + H$ $CHN^+ + H_2$	0.23 0.68 0.09	FA-SIFT/Tichy et al. (1979)
$2.3 \pm 20\%$	$H_3N^+ + C$ $CH_2N^+ + H$ $CHN^+ + H_2$	0.22 0.75 0.03	FA-SIFT <sup>d</sup> /Smith & Adams (1977c)
2.1	$H_3N^+ + C$ $CH_2N^+ + H$ $CHN^+ + H_2$	0.32 0.63 0.05	Ohio State Database/ Herbst (2007)
$2.3 \pm 20\%$	$H_3N^+ + C$ $CH_2N^+ + H$ $CHN^+ + H_2$	0.22 0.75 0.03	UMIST Database/Smith & Adams (1977c), Woodall et al. (2007)
$2.36 \pm 0.15$	$H_3N^+ + C$ $CH_2N^+ + H$ $CHN^+ + H_2$	$0.28 \pm 0.12$ $0.67 \pm 0.11$ $0.05 \pm 0.02$	FA-SIFT/This work

<sup>a</sup> Injection energy < 0.1 eV. Product distributions accurate to ~3% of total distribution.

<sup>b</sup> Reactants in thermal equilibrium at 297 K.

<sup>c</sup> Product distribution given only for  $CH_2N^+$ ; reported as  $0.5 \pm 0.2$ .

<sup>d</sup> ~70 eV electron ionization (EI).



While all reported values of branching ratios indicate that formation of  $\text{CHN}^+$  is a minor product, the abundance of the other primary products is not clearly established. Past measurements are in disagreement, with some identifying  $\text{H}_3\text{N}^+$  as the major product and others determining  $\text{CH}_2\text{N}^+$  as the major product. While the two major astronomical databases are in agreement with the identity of the major product,  $\text{CH}_2\text{N}^+$ , their choice of branching ratios differs slightly, as does their choice of rate constants (see Table 3.1). Our results, 28%  $\text{H}_3\text{N}^+$ , 67%  $\text{CH}_2\text{N}^+$ , and 5%  $\text{CHN}^+$ , are consistent with those reported by Smith & Adams (1977c) and by Tichy et al (1979). Note that isomeric structures of the latter two ions are possible but not readily distinguishable by mass spectrometric techniques.

### 3.3.2. $\text{C}^+ + \text{CH}_4$

The reaction of  $\text{C}^+$  with  $\text{CH}_4$  is likely important for the formation of hydrocarbons in interstellar clouds, as first hypothesized by Adams & Smith (1977). Similarly, Schiff & Bohme (1979) reported a viable scheme for hydrocarbon synthesis occurring via condensation of  $\text{C}^+$  with neutrals of the form  $\text{CH}_x$ , as demonstrated by reactions of this type ( $\text{C}^+ + \text{CH}_x$ ). The reaction of  $\text{C}^+$  with  $\text{CH}_4$  occurs through two addition-fragmentation reactions:



Table 3.2 shows that the value for the rate constant of this reaction provided by this study

**Table 3.2** Reaction rate constants and branching ratios for  $C^+ + CH_4$ .

$k$ ( $10^{-9} cm^3 s^{-1}$ )	Products	Branching Ratio	Instrument/Reference
$1.45 \pm 0.12$	$C_2H_2^+ + H_2$ $C_2H_3^+ + H$	0.29 0.71	ICR <sup>a</sup> /Anicich et al. (1976)
1.43	Not Reported	Not Reported	MS <sup>b</sup> /Mackenzie Peers & Milhaud (1974)
1.5	Not Reported	Not Reported	TI <sup>c</sup> /Herod & Harrison (1970)
$0.76 \pm 0.30$	$C_2H_3^+ + H$	Not Reported	HP <sup>d</sup> /Chong & Franklin (1971)
$1.00 \pm 20\%$	Not Reported	Not Reported	FA/Hemsworth et al. (1970)
1.6	$C_2H_2^+ + H_2$ $C_2H_3^+ + H$	Not Reported Not Reported	FA/Schiff & Bohme (1979)
$1.2 \pm 20\%$	$C_2H_2^+ + H_2$ $C_2H_3^+ + H$	0.33 0.67	FA-SIFT/Adams & Smith (1977)
$1.3 \pm 0.4$	$C_2H_2^+ + H_2$ $C_2H_3^+ + H$	0.25 0.75	FA-SIFT <sup>e</sup> /Bohme et al. (1982)
1.2	$C_2H_2^+ + H_2$ $C_2H_3^+ + H$	0.50 0.50	FA-SIFT/Tichy et al. (1979)
1.5	$C_2H_2^+ + H_2$ $C_2H_3^+ + H$	0.33 0.67	Ohio State Database/ Herbst (2007)
1.5	$C_2H_2^+ + H_2$ $C_2H_3^+ + H$	0.25 0.75	UMIST Database <sup>f</sup> /Schiff & Bohme (1979), Woodall et al. (2007)
$1.39 \pm 0.05$	$C_2H_2^+ + H_2$ $C_2H_3^+ + H$	$0.28 \pm 0.02$ $0.72 \pm 0.02$	FA-SIFT/This work

<sup>a</sup> Injection energy <0.1 eV. Product distributions accurate to 3% of total distribution.

<sup>b</sup> Rate constant obtained from a cross-section for disappearance of primary ions in methane with terminal kinetic energy ranging from near thermal to 5 eV; ~100 eV EI; gas temperature of 100° C.

<sup>c</sup> ~30 eV EI. Reactant ion kinetic energies from 0.3 eV to 0.5 eV. Rate constants determined relative to  $CH_4^+ + CH_4$  and therefore reported in a corrected form relative to the methane reaction. Rate constants originally reported as cross sections.

<sup>d</sup> ~150 eV EI. Uncertainty in the rate constant based on uncertainty in the mobility of  $C^+$  in carbon monoxide. Authors report three rate constant values (0.46, 0.81, or  $1.06 \times 10^{-9} cm^3 s^{-1}$ ), based on referenced values and a Langevin equation value for  $C^+$  mobility in carbon monoxide. Value reported here, as in other sources, as  $(0.76 \pm 0.30) \times 10^{-9} cm^3 s^{-1}$ .

<sup>e</sup> Mass discrimination effects cited as negligible for ionic products within a mass range of ~5 amu. Branching ratio error of up to 30% estimated outside this range.

<sup>f</sup> Database cites reference as Schiff, H. I., Mackay, G. I., Vlachos, G. D., & Bohme, D. K. 1980, in IAU Symp. 87, Interstellar Molecules, ed. B. H. Andrews (Dordrecht: Reidel), 307; Schiff, H. I., & Bohme, D. K. 1979, ApJ, 232, 740. However, the first citation gives no data for the  $C^+ + CH_4$  reaction, and the second reference gives its rate as  $1.6 \times 10^{-9} cm^3 s^{-1}$ , not  $1.5 \times 10^{-9} cm^3 s^{-1}$ .

$[(1.39 \pm 0.05) \times 10^{-9} \text{ cm}^3 \text{ s}^{-1}]$  compares reasonably well with earlier literature values.

The products of the primary reactions can further react with neutral methane:



Of the primary product channels reported in the literature, the observation of  $\text{C}_2\text{H}_3^+$  and  $\text{C}_2\text{H}_2^+$  pathways is reported by all but one paper; however, there is some disagreement in the percentages of the two products. The two available databases have chosen the same value of the rate constant, but slightly different branching ratios. Our reported values, 28%  $\text{C}_2\text{H}_2^+$  and 72%  $\text{C}_2\text{H}_3^+$ , are more consistent with data chosen by the UMIST database. Tichy et al. (1979) infer that the reaction of electronically excited  $\text{C}^+$  exclusively forms the  $\text{C}_2\text{H}_2^+$  product; therefore, generation of only ground-state  $\text{C}^+$  is essential for measurement of accurate branching ratios.

### 3.3.3. $\text{C}^+ + \text{O}_2$

The reaction of  $\text{C}^+$  with  $\text{O}_2$  is important in the ISM because of the relatively high abundance of both reactants in many environments. This reaction occurs via two pathways:



Our measurements provide a slightly lower rate constant value  $[(0.796 \pm 0.024) \times 10^{-9} \text{ cm}^3 \text{ s}^{-1}]$ , as shown in Table 3.3, than those chosen for the two databases; however, it is in agreement with the rate constants reported by Tichy et al. (1979) and Burley & Armentrout (1988). A charge-transfer pathway is not observed since this pathway is endothermic by 0.81 eV:



**Table 3.3** Reaction rate constants and branching ratios for  $C^+ + O_2$ .

$k$ ( $10^{-9}cm^3s^{-1}$ )	Products	Branching Ratio	Instrument/Reference
0.90	$O^+ + CO$ $CO^+ + O$	Not Reported Not Reported	MS/Franklin & Munson (1964)
$1.22 \pm 0.10$	$O^+ + CO$ $CO^+ + O$	0.36 0.64	ICR <sup>a</sup> /Anicich et al. (1976)
0.6	$O^+ + CO$ $CO^+ + O$	0.60 0.40	ICR <sup>b</sup> /Rincon et al. (1987)
$0.76 \pm 0.23$	$O^+ + CO$ $CO^+ + O$	0.60 0.40	GIB/Burley & Armentrout (1988)
$1.1 \pm 30\%$	$CO^+ + O$	Not Reported	FA/Fehsenfeld et al. (1966)
$0.90 \pm 0.18$	Not Reported	Not Reported	FA <sup>c</sup> /Rakshit et al. (1978)
$0.99 \pm 20\%$	$O^+ + CO$ $CO^+ + O$	0.62 0.38	FA-SIFT/Adams & Smith (1976)
$0.93 \pm 25\%$	$O^+ + CO$ $CO^+ + O$ $O_2^+ + C$	0.62 <0.38 <0.38	FA-SIFT <sup>d</sup> /Miller et al. (1984)
0.74	$O^+ + CO$ $CO^+ + O$	0.53 0.47	FA-SIFT/Tichy et al. (1979)
1.2	$O^+ + CO$ $CO^+ + O$	0.35 0.65	Ohio State Database/ Herbst (2007)
$1.0 \pm 20\%$	$O^+ + CO$ $CO^+ + O$	0.62 0.38	UMIST Database <sup>e</sup> /Smith & Adams (1977b), Woodall et al. (2007)
$0.796 \pm 0.024$	$O^+ + CO$ $CO^+ + O$	$0.57 \pm 0.12$ $0.43 \pm 0.12$	FA-SIFT/This work

<sup>a</sup> Injection energy <0.1 eV. Product distribution accurate to ~3% of total distribution.

<sup>b</sup> Ground electronic state carbon cation reactant formed by reaction of  $He^+ + CO$ .

<sup>c</sup> Rate constant unchanged at 100 K and 300 K.

<sup>d</sup> Reaction found independent of temperature over the range 90-450 K. Following additional rate constants measured at indicated temperatures (all in units of  $10^{-9} cm^3 s^{-1}$ ); 0.83 (96 K), 0.85 (150 K), 0.88 (200 K), 0.90 (250 K), 0.89 (395 K), and 0.85 (450 K).

<sup>e</sup> Authors' reference contains a previously cited value (Adams & Smith 1976).

While Miller et al. (1984) report this pathway, it is likely that they instead observed secondary reactions of the primary product ions:



The two databases have chosen very different values for the branching ratios of the primary products. Our measurements, 57%  $\text{O}^+$  and 43%  $\text{CO}^+$ , are in closer agreement with the values in the UMIST database and with the results of most researchers. Several papers address the mechanism of the reaction. Rincon et al. (1987) and Burley & Armentrout (1988) discuss the possibility that strong spin-orbit coupling between states correlated to the  $\text{CO}^+$  and  $\text{O}^+$  channels provides for an efficient curve-crossing mechanism that produces  $\text{O}^+$ . Adams & Smith (1976) suggest the formation of a short-lived intermediate complex with exit channels of comparable exothermicity. The slightly greater abundance of  $\text{O}^+$  relative to  $\text{CO}^+$  has also been attributed to the  $\text{CO}^+ + \text{O}$  charge transfer reaction, which Fehsenfeld & Ferguson (1972) have shown to be quite rapid ( $k = 1.4 \times 10^{-9} \text{ cm}^3 \text{ s}^{-1}$ ); thus, charge transfer within the reaction complex is likely.

In their studies of metastable carbon cations, Tichy et al. (1979) find that the  $\text{CO}^+$  channel becomes 100% for reaction of electronically excited  $\text{C}^+$ . We have similarly observed that  $\text{CO}^+$  becomes the dominant product channel when  $\text{C}^+$  is produced using 70 eV rather than 30 eV electrons. In addition, Rincon et al. (1987) report a translational energy dependence of the branching ratio that favors the  $\text{CO}^+$  channel with increased ion kinetic energy.

### 3.3.4. $\text{C}^+ + \text{H}_2\text{O}$

The reaction of  $\text{C}^+$  with  $\text{H}_2\text{O}$  results in hydroxyl (OH) radical abstraction with H atom elimination:



The charge transfer pathway is endothermic by 1.36 eV, and is not observed:



However, Tichy et al. (1979) infer that this channel becomes the sole pathway for the reaction of electronically excited  $\text{C}^+$ . A secondary reaction occurs with water:



While the Ohio State and UMIST databases account for and agree on branching ratios for the formation of the  $\text{HCO}^+$  and  $\text{HOC}^+$  isomers, our studies cannot readily distinguish these ions. However, since the formation of  $\text{HCO}^+$  requires carbon insertion into the O–H bond, the formation of  $\text{HOC}^+$  by direct attack at the oxygen is more likely (Ishikawa et al. 2001).

Table 3.4 shows that our rate constant measurement [ $(2.09 \pm 0.17) \times 10^{-9} \text{ cm}^3 \text{ s}^{-1}$ ] results in a lower value than currently recommended by either of the databases. Our value includes measurements from both FA-SIFT instruments and represents an average of 10 determinations that are in good agreement with one another. The lower rate constant value obtained in this work may result from careful exclusion of electronically excited  $\text{C}^+$ .

### 3.3.5. $\text{C}^+ + \text{C}_2\text{H}_2$

Acetylene formation in the ISM can arise through the neutralization of the primary ions from the  $\text{C}^+$  reaction with  $\text{CH}_4$ . Schiff & Bohme (1979) have suggested that reactions of this type ( $\text{C}_n\text{H}_x^+ + \text{C}_2\text{H}_2$ ) are important in the buildup of hydrocarbon frames, resulting in the addition of two carbon atoms at a time. Reaction of  $\text{C}_2\text{H}_2$  with  $\text{C}^+$  occurs through a single observed pathway (Anicich et al. 1986):



Bohme et al. (1982) suggest that the product ion has carbene character, and that both linear and nonlinear resonance-stabilized structures are thermodynamically possible.

**Table 3.4** Reaction rate constants and branching ratios for  $C^+ + H_2O$ .

$k$ ( $10^{-9} cm^3 s^{-1}$ )	Products	Branching Ratio	Instrument/Reference
$2.7 \pm 0.5$	$HOC^+ + H$	Not Reported	ICR <sup>a</sup> /Anicich et al. (1986)
$2.03 \pm 30\%$	$HOC^+ + H$	Not Reported	FA/Bolden & Twiddy (1972)
$2.5 \pm 30\%$	$HOC^+ + H$	Not Reported	FA-SIFT <sup>b</sup> /Smith & Adams (1977b)
2.4	$HOC^+ + H$	Not Reported	FA-SIFT/Tichy et al. (1979)
2.7	$HCO^+ + H$ $HOC^+ + H$	0.33 0.67	Ohio State Database/ Herbst (2007)
$2.7 \pm 0.5$	$HCO^+ + H$ $HOC^+ + H$	0.33 0.67	UMIST Database <sup>c</sup> /Anicich et al. (1976), Woodall et al. (2007)
$2.09 \pm 0.17$	$HOC^+ + H$	Not Reported	FA-SIFT/ This work

<sup>a</sup> Injection energy <0.1 eV.

<sup>b</sup> ~70 eV EI.

<sup>c</sup> Source for the  $HCO^+/HOC^+$  branching ratio is not cited.

The following secondary reactions of the primary product ion have been observed:



However, since only one primary product is formed, the secondary reactions do not influence the branching ratio measurement.

Values for the rate constant of this reaction are summarized in Table 3.5. Our rate constant value  $[(1.78 \pm 0.15) \times 10^{-9} \text{ cm}^3 \text{ s}^{-1}]$  falls within the error bars of the Bohme et al. (1982) measurement, but appears significantly lower than prior literature values. Commercially available cylinders of acetylene generally contain a trace amount of acetone to prevent polymerization of the acetylene. Acetone is extremely reactive with  $\text{C}^+$  [SIFT measurement by Bohme et al. 1982;  $k = (2.2 \pm 0.7) \times 10^{-9} \text{ cm}^3 \text{ s}^{-1}$ ; 47% efficient] and its presence will therefore lead to an artificially faster reaction rate measurement. We employed two different, relatively new cylinders of acetylene, where the vapor pressure of acetone should be a minor contributor to the total pressure and flow of acetylene. As a precautionary measure, acetylene was passed through a coiled trap immersed in an ice-salt slush bath ( $-6 \text{ }^\circ\text{C}$ ) to reduce impurities. In addition, we did not observe the formation of  $\text{C}_3\text{H}_6\text{O}^+$  and  $\text{C}_2\text{H}_3\text{O}^+$ , which are products of the reaction of  $\text{C}^+$  with acetone. Thus, our lower rate constant value may be due to the absence of trace acetone impurities, as well as the absence of electronically excited  $\text{C}^+$  reactant ions. Our measured rate constant slightly exceeds the Langevin value, which suggests that even larger rate constants are not likely correct.

### 3.4. Conclusions

The chemistry of the ISM involves a rich network of ions and neutral species. Errors in reaction rate constants and branching ratios in interstellar models can propagate uncertainties in

**Table 3.5** Reaction rate constants and branching ratios for  $C^+ + C_2H_2$ 

$k$ ( $10^{-9}cm^3s^{-1}$ )	Products	Instrument/Reference
2.8	$C_3H^+ + H$	ICR <sup>a</sup> /Anicich et al. (1986)
2.7	$C_3H^+ + H$	FA/Schiff & Bohme (1979)
$2.2 \pm 0.7$	$C_3H^+ + H$	FA-SIFT/Bohme et al. (1982)
2.7	$C_3H^+ + H$	Ohio State Database/ Herbst (2007)
$2.2 \pm 0.7$	$C_3H^+ + H$	UMIST Database/Bohme et al. (1982), Woodall et al. (2007)
$1.78 \pm 0.15$	$C_3H^+ + H$	FA-SIFT/ This work

<sup>a</sup>  $\leq 30$  eV EI. ICR experiments at 298 K.

concentrations of interstellar species. This work addresses five reactions for which improvements in kinetic data have been identified as critical for increased accuracy of model calculations. Table 3.6 summarizes our recommended rate constants and branching ratios for the reactions of  $C^+$  with  $NH_3$ ,  $CH_4$ ,  $O_2$ ,  $H_2O$ , and  $C_2H_2$ , for inclusion in astrochemical models; the calculated reaction efficiencies are also indicated. These experiments used two calibrated and optimized FA-SIFT instruments, in which ground-state  $C^+$  was cleanly generated; in addition, we systematically addressed reactant purity, mass discrimination, and secondary reactions. We report these final numbers with two significant figures to properly reflect the combined reproducibility and systematic error. Further studies of these reactions as a function of temperature would be valuable for more accurate astrochemical modeling.

**Table 3.6** Recommended reaction rate constants and branching ratios for reactions of  $C^+$  with  $NH_3$ ,  $CH_4$ ,  $O_2$ ,  $H_2O$ , and  $C_2H_2$

Reaction	$k$ ( $10^{-9}cm^3s^{-1}$ )	Reaction Efficiency	Products	Branching Ratio
$C^+ + NH_3$	$2.4 \pm 0.2$	0.79	$H_3N^+ + C$	$0.28 \pm 0.12$
			$CH_2N^+ + H$	$0.67 \pm 0.11$
			$CHN^+ + H_2$	$0.05 \pm 0.02$
$C^+ + CH_4$	$1.4 \pm 0.1$	0.97	$C_2H_2^+ + H_2$	$0.28 \pm 0.02$
			$C_2H_3^+ + H$	$0.72 \pm 0.02$
$C^+ + O_2$	$0.80 \pm 0.03$	0.73	$O^+ + CO$	$0.57 \pm 0.12$
			$CO^+ + O$	$0.43 \pm 0.12$
$C^+ + H_2O$	$2.1 \pm 0.2$	0.63	$HOC^+ + H$	1.0
$C^+ + C_2H_2$	$1.8 \pm 0.2$	1.1	$C_3H^+ + H$	1.0

### 3.5 References

- Adams, N. G., & Smith, D. 1976, *J. Phys. B*, 9, 1439
- Adams, N. G., & Smith, D. 1977, *Chem. Phys. Lett.*, 47, 383
- Anicich, V. G., Huntress, W. T., & Futrell, J. H. 1976, *Chem. Phys. Lett.*, 40, 233
- Anicich, V. G., Huntress, W. T., & McEwan, M. J. 1986, *J. Phys. Chem.*, 90, 2446
- Bohme, D. K., Rakshit, A. B., & Schiff, H. I. 1982, *Chem. Phys. Lett.*, 93, 592
- Bolden, R. C., & Twiddy, N. D. 1972, *Faraday Discussions of the Chemical Society*, 53, 192
- Burley, J. D., & Armentrout, P. B. 1988, *Int. J. Mass Spectrom. Ion Proc.*, 84, 157
- Chong, S.-L., & Franklin, J. L. 1971, *J. Chem. Phys.*, 54, 1487
- Fehsenfeld, F. C., & Ferguson, E. E. 1972, *J. Chem. Phys.*, 56, 3066
- Fehsenfeld, F. C., Schmeltekopf, A. L., & Ferguson, E. E. 1966, *J. Chem. Phys.*, 45, 23
- Franklin, J. L., & Munson, M. S. B. 1964, in *Proc. Tenth Symp. (International) on Combustion*, ed. W. G. Berl (Pittsburgh: Combustion Inst.), 1488
- Gioumousis, G., & Stevenson, D. P. 1958, *J. Chem. Phys.*, 29, 294
- Hemsworth, R. S., Bolden, R. C., Shaw, M. J., & Twiddy, N. D. 1970, *Chem. Phys. Lett.*, 5, 237
- Herbst, E. 2007, Ohio State Chemical Database, available at (<http://www.physics.ohio-state.edu/~eric>), listed under "gas phase model"
- Herbst, E., & Klemperer, W. 1973, *ApJ*, 185, 505
- Herod, A. A., & Harrison, A. G. 1970, *Int. J. Mass Spectrom. Ion Proc.*, 4, 415
- Ishikawa, Y., Binning, R. C., & Ikegami, T. 2001, *Chem. Phys. Lett.*, 343, 413
- Liddy, J. P., Freeman, C. G., & McEwan, M. J. 1977, *MNRAS*, 180, 683
- Mackenzie Peers, A., & Milhaud, J. 1974, *Int. J. Mass Spectrom. Ion Proc.*, 15, 145
- Markwick-Kemper, A. J. 2005, in *Proc. IAU Symp. 231, Astrochemistry: Recent Successes and Current Challenges*, ed. D. C. Lis, G. A. Blake, & E. Herbst (Cambridge: Cambridge Univ. Press), 204

- Miller, T. M., Wetterskog, R. E., & Paulson, J. F. 1984, *J. Chem. Phys.*, 80, 4922
- Rakshit, A. B., Stock, H. M. P., Wareing, D. P., & Twiddy, N. D. 1978, *J. Phys. B*, 11, 4237
- Rincon, M., Pearson, J., & Bowers, M. T. 1987, *Int. J. Mass Spectrom. Ion Proc.*, 80, 133
- Schiff, H. I., & Bohme, D. K. 1979, *ApJ*, 232, 740
- Schiff, H. I., Hemsworth, R. S., Payzant, J. D., & Bohme, D. K. 1974, *ApJ*, 191, L49
- Smith, D., & Adams, N. G. 1977b, *Int. J. Mass Spectrom. Ion Proc.*, 23, 123
- Smith, D., & Adams, N. G. 1977c, *Chem. Phys. Lett.*, 47, 145
- Snow, T. P., & McCall, B. J. 2006, *ARA&A*, 44, 367
- Su, T., & Chesnavich, W. J. 1982, *J. Chem. Phys.*, 76, 5183
- Tichy, M., Rakshit, A. B., Lister, D. G., Twiddy, N. D., Adams, N.G., & Smith, D. 1979, *Int. J. Mass Spectrom. Ion Proc.*, 29, 231
- Twiddy, N. D., Mohebati, A., & Tichy, M. 1986, *Int. J. Mass Spectrom. Ion Proc.*, 74, 251
- Van Doren, J. M. 1987, in Ph.D. thesis *Chem. Phys.* (Boulder: Univ. Colorado), 341
- Watson, W. D. 1974, *ApJ*, 188, 35
- Woodall, J., Agúndez, M., Markwick-Kemper, A. J., & Millar, T. J. 2007, *A&A*, 466, 1197;  
<http://www.udfa.net>
- Xu, Y., Moran, T. F., & Thomas, E. W. 1990, *Phys. Rev. A*, 41, 1408

## Chapter 4

### Study of the Associative Detachment Reaction of Hydride Ion with Hydrogen Atom

#### 4.1. Introduction

In the early Universe, cloud condensation and the formation of protogalaxies and primary stars were contingent on sufficient cooling of primordial gases. Although atomic processes can lower temperatures only to  $\sim 10^4$  K, molecules would enable efficient cooling and protogalactic collapse. Molecular hydrogen,  $\text{H}_2$ , is the only molecular species with sufficient concentration to have enabled cooling during this epoch. Processes involved in molecular hydrogen formation and destruction are, therefore, important to models describing the seeding of stars and the forming of protogalaxies. The physics and chemistry in the early Universe, as well as the role of  $\text{H}_2$  in structure formation, have been the focus of extensive discussion in the literature (Lepp & Shull 1984; Abel et al. 1997; Galli & Palla 1998; Lepp et al. 2002; Glover & Abel 2008 and references therein; Bromm 2010). According to the comprehensive study by Glover et al. (2006), the critical gas-phase reaction in forming  $\text{H}_2$  (before dust grains were present to catalyze the process) is the associative detachment reaction of hydride ions with hydrogen atoms,



Despite the importance of this reaction, experimental determinations of the rate constant have had large uncertainties. In the earliest measurement, Schmeltekopf et al. (1967) used a newly constructed flowing-afterglow instrument in which  $\text{H}_2$  was passed through a microwave discharge, and the resulting H-atom concentration was measured mass spectrometrically using a chemical titration with nitrogen dioxide. They reported a rate constant value of  $1.3 \times 10^{-9} \text{ cm}^3 \text{ s}^{-1}$ , which is reliable to within a factor of two. Six years later, these researchers (Fehsenfeld et al. 1973) utilized thermal dissociation of  $\text{H}_2$  to generate hydrogen atoms, since this method

produces fewer excited reactive species; moreover, in contrast to discharge methods, which require an impurity to operate properly, high purity H<sub>2</sub> was used. Fehsenfeld et al. (1973) used a comparison with previously determined, but unspecified, absolute measurements to report a rate constant value of  $1.8 \times 10^{-9} \text{ cm}^3 \text{ s}^{-1}$ , again reliable within a factor of two. In the intervening four decades, this important reaction has not been revisited experimentally. However, Glover et al. (2006) have shown the dramatic impact of the uncertainty in this rate constant on cosmological models; predictions of the time scale for protogalaxy formation from hot, highly ionized gas within a Hubble time become inconclusive. Thus the propagation of errors in the associative detachment reaction rate constant poses a serious problem to our understanding of the evolution of the early Universe.

For this reason, we have re-evaluated the rate constant for the H<sup>-</sup> + H reaction. As described below, we have used the thermal dissociation of H<sub>2</sub> to generate H atoms, and we have employed exceptionally well-characterized calibration reactions to determine the absolute concentration of H atoms.

## 4.2 Experimental Methods

A flowing afterglow-selected ion flow tube (FA-SIFT) instrument was used for these studies. For the experiments, helium buffer gas (99.99%) is passed through a molecular sieve trap immersed in liquid nitrogen, and admitted to the reaction flow tube at a pressure of  $\sim 0.4$  Torr and a flow rate of  $\sim 200 \text{ std cm}^3 \text{ s}^{-1}$ . Trace amounts of ammonia gas (NH<sub>3</sub>, Air Products and Chemicals Inc., 99.99%) are added to the upstream region of this reaction flow tube, and H<sup>-</sup> ions are formed by electron-impact ionization (70 eV electron energy) via the dissociative-attachment process



Amide ions ( $\text{NH}_2^-$ ) were also formed; therefore, a small flow of molecular hydrogen ( $\text{H}_2$ ) was added to convert  $\text{NH}_2^-$  to  $\text{H}^-$  by the reaction



(Otto et al 2008). The only other ions in the initial mass spectrum are hydroxide ions,  $\text{OH}^-$ , formed by trace impurities of oxygen ( $\text{O}_2$ ) or water vapor ( $\text{H}_2\text{O}$ ); these ions do not complicate the kinetic analysis for reaction of  $\text{H}^-$  with H, and in fact, as discussed below, provide an internal calibration of the H-atom concentration.

Low ionization emission currents ( $\sim 1 \mu\text{A}$ ) were used to maintain low ion densities; this approach insures that free diffusion conditions prevail throughout the experiment and that changes in diffusive loss do not occur when negative ions are converted to electrons in the associative detachment process. Sulfur hexafluoride ( $\text{SF}_6$ ) can sometimes be used to scavenge free electrons and prevent changes in diffusive loss at high ion densities; however, this approach is not possible in these experiments, since  $\text{SF}_6$  rapidly destroys  $\text{H}^-$  ions by reactive processes.

We note that attempts to generate  $\text{H}^-$  ions in the source flow tube, followed by mass selection and injection into the reaction flow tube, were not successful; efficient scattering of  $\text{H}^-$  ions by helium in the injection process at the Venturi inlet may be the cause of this difficulty. The reactant H atoms are formed via thermal dissociation. A flow of  $\text{H}_2$  gas ( $\sim 8 \text{ std cm}^3 \text{ s}^{-1}$ , Airgas Inc., 99.999%) is passed through a molecular sieve trap immersed in liquid nitrogen, over a heated tungsten filament (Trainor et al. 1973), and through a second trap and filament assembly. Teflon tubing (0.25 inch ID), used to minimize recombination, then transfers the H atoms from the thermal dissociator into the reaction flow tube; the inlet is positioned 35 cm downstream of the ionizer to allow development of the laminar profile and collisional relaxation of ions. The inlet position is also 70 cm upstream of the ion sampling orifice to allow adequate

reaction time. Dissociation of H<sub>2</sub> is proportional to the voltage applied across the filament (Barkholtz et al. 2001).

The concentration of hydrogen atoms was determined by monitoring the loss of chloride ions (Cl<sup>-</sup>) or hydroxide ions (OH<sup>-</sup>) in the associative-detachment reactions with hydrogen atoms. The rate constant for the reaction



has been reported in three studies from the NOAA laboratory in Boulder (Ferguson et al. 1969; Fehsenfeld et al. 1973; Howard et al. 1974), all of which were in excellent agreement. The third study was exceptionally comprehensive and reported a rate constant of  $9.6 \times 10^{-10} \text{ cm}^3 \text{ s}^{-1}$ . These experiments were carried out both in He and O<sub>2</sub> buffer gases, at pressures between 0.108 and 0.498 Torr, at velocities between 6000 and 8300 cm s<sup>-1</sup>, with reaction distances of 40.0 and 81.4 cm. The NOAA laboratory authors used sulfur hexafluoride to scavenge electrons, and isothermal calorimetry was used to determine absolute H atom concentrations that were generated by thermal dissociation. The scatter of nine measurements was about 10%, and the total error in the rate constant was reported as  $\pm 20\%$ . Thus this reaction serves as an excellent calibration for the hydrogen-atom concentration. The rate constant for the reaction



has been reported (Howard et al. 1974) to be  $1.4 \times 10^{-9} \text{ cm}^3 \text{ s}^{-1}$  with an accuracy of  $\pm 30\%$ . Two previous measurements were in good agreement (Ferguson et al. 1969; Fehsenfeld et al. 1973).

For our experiments, Cl<sup>-</sup> ions were made in the source flow tube via electron impact on trace amounts of carbon tetrachloride (CCl<sub>4</sub>) entrained in He buffer gas (0.27 Torr); OH<sup>-</sup> ions were generated by adding a mixture of CH<sub>4</sub> (0.04 Torr) and N<sub>2</sub>O (0.02 Torr), to the buffer gas. The desired ions, either Cl<sup>-</sup> or OH<sup>-</sup>, were mass selected and injected into the reaction flow tube

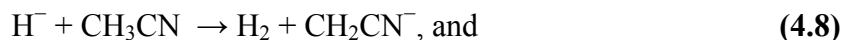
for reaction with H atoms. Alternatively, OH<sup>-</sup> ions were present in the reaction flow tube when H<sup>-</sup> ions were produced; the loss of H<sup>-</sup> and OH<sup>-</sup> could be monitored simultaneously upon addition of H atoms.

### 4.3. Discussion

A major challenge in these studies was tuning the detection quadrupole mass filter to transmit extremely low-mass ions; proper tuning of the instrument was achieved with assistance from the staff at Extrel Corporation. A second prerequisite was insuring that the signal intensity near  $m/z$  1 is due to H<sup>-</sup> ions, rather than to the “on blast,” which is the transmission of all ions when the quadrupole mass filter is set near zero. This issue was explored with ion chemistry. Upon addition of water vapor to the reaction flow tube, the peaks identified as H<sup>-</sup> and NH<sub>2</sub><sup>-</sup> decreased in intensity because of the proton transfer reactions,



The peak identified as the OH<sup>-</sup> product increased in intensity. In contrast, the peak identified as the “on blast” remained relatively constant, since the number density of total ions did not change, although their identities were altered. Similarly, upon addition of acetonitrile (CH<sub>3</sub>CN), the peaks identified as H<sup>-</sup> and NH<sub>2</sub><sup>-</sup> decreased in intensity because of proton transfer, i.e.,



The “on blast” remained constant. Thus we are confident that we are generating and detecting H<sup>-</sup> ions.

For our study of the reactivity of H<sup>-</sup> + H, 64 measurements were made relative to the reactivity of Cl<sup>-</sup> ions, while 30 measurements were made relative to the reactivity of OH<sup>-</sup>.

Individual measurements are shown in an appendix to this chapter as raw data.  $\text{H}^-$  ions were generated in the reaction flow tube, and their intensity was monitored as the voltage across the tungsten filament in the thermal dissociator, and therefore the H atom concentration, was increased. Data were recorded for two to ten different voltages.  $\text{Cl}^-$  ions were then formed in the source flow tube and injected into the reaction flow tube; their intensity was monitored under identical conditions. Since pseudo-first-order conditions exist, the following equations can be written, where  $k_{\text{Cl}^-}$  is the bimolecular rate constant for  $\text{Cl}^- + \text{H}$ ,  $k_{\text{H}^-}$  is the bimolecular rate constant for  $\text{H}^- + \text{H}$ ,  $t$  represents the reaction time, square brackets indicate concentrations, and the subscript zero indicates initial conditions:

$$\frac{[\text{Cl}^-]}{[\text{Cl}^-]_0} = \exp\{-(k_{\text{Cl}^-}) \cdot [\text{H}]t\}, \quad (4.10)$$

$$\frac{[\text{H}^-]}{[\text{H}^-]_0} = \exp\{-(k_{\text{H}^-}) \cdot [\text{H}]t\}. \quad (4.11)$$

Our raw data give the value of  $\frac{[\text{Cl}^-]}{[\text{Cl}^-]_0}$ , and since  $k_{\text{Cl}^-}$  is known, the value of  $[\text{H}]t$  is readily determined. From this value and the experimental ratio  $\frac{[\text{H}^-]}{[\text{H}^-]_0}$ , the desired rate constant for the reaction  $\text{H}^- + \text{H}$  is measured. We note that  $t$  depends on the pressure and flow of helium, and these values were varied by about 10%; however,  $[\text{H}]$  was varied more significantly, so that the product  $[\text{H}]t$  spanned a factor of seven. The average of the 64 measurements of  $k_{\text{H}^-}$  is  $2.11 (\pm 0.32) \times 10^{-9} \text{ cm}^3 \text{ s}^{-1}$ , where the error bars represent  $1\sigma$  of the measurements. No trends of  $k_{\text{H}^-}$  with experimental parameters were observed. However, reproducibility of results was enhanced by allowing hydrogen atoms to flow for about an hour before accumulating data and rapidly interspersing calibration and hydride experiments.

Studies using the reactivity of hydroxide ions as a calibration reaction were carried out in a similar manner; in addition, for some experiments, hydroxide and hydride ions were

cogenerated and monitored simultaneously as discussed above. The average of the 30 measurements of  $k_{H^-}$  is  $1.74 (\pm 0.23) \times 10^{-9} \text{ cm}^3 \text{ s}^{-1}$ , where the error bars represent  $1\sigma$  of the measurements. Again, there was no variation with experimental conditions.

The rate constant values determined from the  $\text{Cl}^-$  and  $\text{OH}^-$  calibrations have been weighted and combined according to

$$\bar{k}_{H^-} = k_{H^-, \text{Cl}^-} \cdot \left(\frac{64}{94}\right) + k_{H^-, \text{OH}^-} \cdot \left(\frac{30}{94}\right) \quad (4.12)$$

to give a recommended value of  $\bar{k}_{H^-} = 2.0 \times 10^{-9} \text{ cm}^3 \text{ s}^{-1}$  (The symbol  $k_{H^-, \text{Cl}^-}$  represents the rate constant for Equation (4.1) using Equation (4.4) as the calibration reaction.). The uncertainties and the number of measurements were weighted according to a pooled standard deviation:

$$\sigma_{Exp} = \sqrt{\frac{(64-1)\sigma_{H^-, \text{Cl}^-}^2 + (30-1)\sigma_{H^-, \text{OH}^-}^2}{64+30-2}}. \quad (4.13)$$

Combining the absolute error of the calibration reactions with the reproducibility of our measurements according to

$$\sigma_{Tot} = \sqrt{\sigma_{Exp}^2 + \sigma_{\text{Cl}^- \text{-cal}}^2 \left(\frac{64}{94}\right) + \sigma_{\text{OH}^- \text{-cal}}^2 \left(\frac{30}{94}\right)} \quad (4.14)$$

gives a total absolute error of  $\pm 30\%$ . We report the recommended value of  $k_{H^-} = 2.0 (\pm 0.6) \times 10^{-9} \text{ cm}^3 \text{ s}^{-1}$ . This value is compared to previous experimental determinations in Table 4.1, and to the calculated Langevin collision rate constant determined by the theory of Gioumousis & Stevenson (1958).

The classical Langevin limit calculated here and elsewhere (Sakimoto 1989),  $2.69 \times 10^{-9} \text{ cm}^3 \text{ s}^{-1}$ , describes the collision rate constant caused by a charge-induced dipole interaction between an ion and a neutral species. Of the two potential energy surfaces ( $^2\Sigma_u^+$  and  $^2\Sigma_g^+$ ) for the

**Table 4.1** Rate constants for the reaction of  $\text{H}^- + \text{H} \rightarrow \text{H}_2 + \text{e}^-$ .

Rate Constant ( $10^{-9} \text{ cm}^3 \text{ s}^{-1}$ )	Reference
<b>Experimental Values</b>	
$2.0 \pm 0.6$	This work
$1.3 \pm \text{factor of } 2$	Schmeltekopf et al. <sup>21</sup>
$1.8 \pm \text{factor of } 2$	Fehsenfeld et al. <sup>8</sup>
<b>Theoretical Values</b>	
2.69 (Langevin limit)	Sakimoto <sup>8</sup>
1.35 (Langevin limit)	Čížek et al. <sup>6</sup>
1.9	Dalgarno & Browne <sup>7</sup>
2.0	Browne & Dalgarno <sup>5</sup>
1.89	Bieniek & Dalgarno <sup>3</sup>
2.03	Launay et al. <sup>16</sup>
3.8	Čížek et al. <sup>6</sup>

reaction  $\text{H}^- + \text{H}$ , the  $^2\Sigma_g^+$  potential energy surface, which describes the reaction



has a barrier at low temperatures. Reactions occurring at our experimental temperature do not possess the energy necessary to proceed to the products of reaction (4.15). This is evident in the extremely small rate constants shown by Dalgarno & Browne (1967) for low temperatures in the range of our experiment. The low-energy thermal collisions at room temperature do not contribute to the reaction because of the repulsive nature of the  $^2\Sigma_g^+$  potential (Glover et al. 2006); therefore, the reaction rate constant is likely to be no more than half of the Langevin collision-rate constant ( $1.35 \times 10^{-9} \text{ cm}^3 \text{ s}^{-1}$ ), which is smaller than our experimental result. However, more sophisticated potential energy functions and different theoretical approaches are needed to properly describe the interaction between  $\text{H}^-$  ions and H atoms during the reaction (Browne & Dalgarno 1969; Bienek & Dalgarno 1979, Sakimoto 1989; Launay et al. 1991). Dalgarno and co-workers have studied the  $\text{H}^- + \text{H}$  associative detachment reaction with a variety of potentials and have found values for the reaction rate constant of  $2.0 \times 10^{-9} \text{ cm}^3 \text{ s}^{-1}$  (Browne & Dalgarno 1969) and  $1.89 \times 10^{-9} \text{ cm}^3 \text{ s}^{-1}$  (Bienek & Dalgarno 1979), which are very similar to our experimental value at room temperature. Similarly, a study by Launay et al. (1991) gives a value ( $2.03 \times 10^{-9} \text{ cm}^3 \text{ s}^{-1}$ ) consistent with our result at room temperature, as does the radiative dissociation method ( $1.9 \times 10^{-9} \text{ cm}^3 \text{ s}^{-1}$ ) of Dalgarno & Browne (1967). In contrast, Čížek et al. (1998) calculate a reaction rate constant ( $3.8 \times 10^{-9} \text{ cm}^3 \text{ s}^{-1}$ ) at 300 K that exceeds our experimental value by a factor of 2. Several computational studies have addressed the temperature dependence of this reaction (Glover et al. 2006). A recent study by Kreckel et al. (2010) suggests substantial temperature dependence for the  $\text{H}^- + \text{H}$  atom associative detachment-rate constant. Their reported rate constant is twice that of this study; the origin of the

discrepancy between the value of Kreckel et al. and our work is not understood. A number of additional studies, both experimental and theoretical, are underway. These studies will also attempt to determine the meaning of an experimental rate constant that is significantly higher than that predicted by simple collisional models.

#### **4.4. Implications of Our Results**

We have measured the rate constant for the associative detachment reaction of  $\text{H}^- + \text{H}$  at 300 K as  $2.0 (\pm 0.6) \times 10^{-9} \text{ cm}^3 \text{ s}^{-1}$ . This measurement represents a refinement of the absolute value and a reduction in the uncertainty compared to previous literature values from a factor of 2 to  $\pm 30\%$ . The reduced error bar will enable a more accurate modeling and understanding of cooling and protogalaxy formation in the early Universe.

Our revised rate constant indicates that  $\text{H}_2$  was formed at an earlier epoch than was previously thought. As emphasized by Glover et al. (2006), cooling to collapse a protogalactic halo must occur prior to heating by gravitational disruption because of collision with another protogalactic halo and must thus occur within a Hubble time. This cooling of the primordial gas clouds prompts collapse and formation of a protogalaxy, and  $\text{H}_2$  quadrupole emission is thought to be the dominant cooling mechanism. Therefore, earlier  $\text{H}_2$  formation implies earlier star formation and thus earlier heavy element creation in the interiors of massive stars.

## 4.5 References

- Abel, T., Anninos, P., Zhang, Y., & Norman, M. L. 1997, *New Astron.*, 2, 181
- Barckholtz, C., Snow, T. P., & Bierbaum, V. M. 2001, *ApJ*, 547, L171
- Bieniek, R. J., & Dalgarno, A. 1979, *ApJ*, 228, 635
- Bromm, V. 2010, *Science* 329, 45
- Browne, J. C., & Dalgarno, A. 1969, *J. Phys. B: At. Mol. Phys.*, 2, 885
- Čížek, M., Horáček, J., & Domcke, W. 1998, *J. Phys. B: At. Mol. Opt. Phys.*, 31, 2571
- Dalgarno, A., & Browne, J. C. 1967, *ApJ*, 149, 231
- Fehsenfeld, F. C., Howard, C. J., & Ferguson, E. E. 1973, *J. Chem. Phys.*, 58, 5841
- Ferguson, E. E., Fehsenfeld, F. C., & Schmeltekopf, A. L. 1969, *Adv. At. Mol. Phys.*, 5, 1
- Galli, D., & Palla, F. 1998, *A&A*, 335, 403
- Gioumousis, G., & Stevenson, D. P. 1958, *J. Chem. Phys.*, 29, 294
- Glover, S. C., Savin, D. W., & Jappsen, A.-K. 2006, *ApJ*, 640, 553
- Glover, S. C. O., & Abel, T. 2008, *MNRAS*, 388, 1627
- Howard, C. J., Fehsenfeld, F. C., & McFarland, M. 1974, *J. Chem. Phys.*, 60, 5086
- Kreckel, H., Bruhns, H., Čížek, M., Glover, S. C. O., Miller, K. A., Urbain, X., & Savin, D. W. 2010, *Science* 329, 69
- Launay, J. M., Le Dourneuf, M., & Zeippen, C. J. 1991, *A&A*, 252, 842
- Lepp, S., & Shull, J. M. 1984, *ApJ*, 280, 465
- Lepp, S., Stancil, P. C., & Dalgarno, A. 2002, *J. Phys. B: At. Mol. Opt. Phys.*, 35, R57
- Otto, R., Mikosch, J., Trippel, S., Weidemüller, M., & Wester, R. 2008, *Phys. Rev. Lett.*, 101, 063201
- Sakimoto, K. 1989, *Chem. Phys. Lett.*, 164, 294
- Schmeltekopf, A. L., Fehsenfeld, F. C., & Ferguson, E. E. 1967, *ApJ*, 148, L155

Trainor, D. W., Ham, D. O., & Kaufman, F. 1973, J. Chem. Phys., 58, 4599

## 4.6 Appendix

**Table 4.2** Experimental data for  $\text{H}^- + \text{H}$  reaction using  $\text{Cl}^- / \text{H}$  atom multipoint concentration calibration.

Rate Constant ( $10^{-9} \text{ cm}^3 \text{ s}^{-1}$ )	$[\text{H}]t$ ( $10^9 \text{ particle s cm}^{-3}$ )	He Flow (Standard Liters per Minute)	Date
2.202	2.165		
2.197	2.831	12.09	1-9-2009
2.795			
2.775	3.316	13.04	
2.374	2.938		2-5-2009
2.492	2.367	12.09	
2.263	1.887	10.8	
1.798			
1.849	2.075		3-6-2009
1.798		12.09	
2.043	2.016		
2.486	1.457		
2.132	1.575	12.5	
1.294			
1.390	1.800		3-12-2009
1.414		10.89	
1.572	1.688		
2.533	1.575		
2.780	1.605		
2.107		11.08	
2.220	1.884		
1.784			
1.962	2.154		
1.506			5-5-2009
2.319			
2.551	1.605	12.09	
1.958			
2.707			
2.972	1.390		
2.281			

**Table 4.3** Experimental data for  $\text{H}^- + \text{H}$  reaction using  $\text{Cl}^- / \text{H}$  atom two-point concentration calibration.

Rate Constant ( $10^{-9} \text{ cm}^3 \text{ s}^{-1}$ )	$[\text{H}]t$ ( $10^9 \text{ particle s cm}^{-3}$ )	He Flow (Standard Liters per Minute)	Date
2.118			
2.076			
2.089	0.867	12.09	5-11-09
2.132			
2.088			
2.134			
1.932			
1.943			
1.905	1.118		
1.879			
1.890			
1.954		12.09	5-19-09
1.947			
1.911			
1.952	0.897		
1.952			
2.052			
2.009			
2.129			
2.197			
2.165	0.536	12.09	
2.249			
2.224			
2.281			5-21-2009
2.437			
2.381			
2.419	0.487	11.09	
2.362			
2.476			
2.448			

**Table 4.4** Experimental data for  $\text{H}^- + \text{H}$  reaction using  $\text{OH}^- / \text{H}$  atom multipoint concentration calibration.

Rate Constant ( $10^{-9} \text{ cm}^3 \text{ s}^{-1}$ )	$[\text{H}]t$ ( $10^9 \text{ particle s cm}^{-3}$ )	He Flow (Standard Liters per Minute)	Date
2.205	1.422	11.18	
1.734			
1.710	1.154		3-12-2009
1.733		12.1	
1.726	1.383		
1.408	1.484		
1.454	1.393		
1.439	1.269	12.1	
1.406	1.017		3-20-2009
1.647	1.129		
1.342	1.812	11.08	
1.306	1.937		
1.598			
1.682	1.491		
1.796		11.13	
1.926	1.235		
1.577			
1.622	1.385		
1.723			4-2-2009
1.755			
1.799	1.548	12.09	
1.901			
1.973			
2.046	1.426		
2.184			
2.023	1.359		
1.916		12.09	
1.911			4-15-2009
1.811	1.258		
1.813	1.580	11.09	

## Chapter 5

### H<sup>-</sup> Reactivity Overview

#### 5.1 Introduction

The anion of the hydrogen atom, though seemingly simple, has drawn much attention because of its involvement in many reactions important to our understanding of cosmology and astrophysics. Hydride (H<sup>-</sup>) has been implicated in the formation of molecular hydrogen (H<sub>2</sub>), the first coolant available to the Universe for seeding star and galaxy formation after the Big Bang (cf. Glover et al. 2006). Our experimental studies recently contributed to early Universe models by remeasuring and refining an older measurement of the reaction rate constant for the associative-detachment (AD) reaction  $\text{H} + \text{H}^- \rightarrow \text{H}_2 + e^-$  (Fehsenfeld et al. 1973; Schmeltekopf et al. 1967; Martinez et al. 2009).

Although detection of H<sup>-</sup> in astrophysical environments remains elusive (Ross et al. 2008), a firm acceptance of its presence exists. The H<sup>-</sup> ion has been correlated to the opacity of the Sun and other late-type stars (Wildt 1939; Chandrasekhar 1944; Münch 1945; Chandrasekhar & Breen 1946). Additionally, there is support for the prediction of H<sup>-</sup> in regions of the interstellar medium, such as in the transition zones of planetary nebulae (Black 1978), where populations of neutral hydrogen and free electrons suggest the existence of H<sup>-</sup>, or in photodissociation regions and dark clouds. Field (2000) proposed a model suggesting H<sup>-</sup> may also be involved in H<sub>2</sub> formation, again via an AD process similar to the one that was important in the early Universe. However, in this case, H<sup>-</sup> production occurs on the surface of dust grains with weakly bound surface electrons rather than by direct electron capture by H atoms.

A variety of the regions that likely contain H<sup>-</sup> overlap molecular regions at their boundaries. A range of chemical processes can be expected in such regions because of the

reactivity of the  $\text{H}^-$  anion. Thus, an understanding of this reactivity should reveal the degree to which  $\text{H}^-$  drives astrophysical processes. For this study, we chose acetylene ( $\text{C}_2\text{H}_2$ ), water ( $\text{H}_2\text{O}$ ), acetonitrile ( $\text{CH}_3\text{CN}$ ), methanol ( $\text{CH}_3\text{OH}$ ), acetone [ $(\text{CH}_3)_2\text{CO}$ ], acetaldehyde ( $\text{CH}_3\text{CHO}$ ), nitrous oxide ( $\text{N}_2\text{O}$ ), carbon dioxide ( $\text{CO}_2$ ), oxygen ( $\text{O}_2$ ), carbon monoxide ( $\text{CO}$ ), methyl chloride ( $\text{CH}_3\text{Cl}$ ), *tert*-butyl chloride [ $(\text{CH}_3)_3\text{CCl}$ ], diethyl ether [ $(\text{CH}_3\text{CH}_2)_2\text{O}$ ], benzene ( $\text{C}_6\text{H}_6$ ) and deuterium ( $\text{D}_2$ ). We used these representatives from prototypical groups of compounds to map the chemistry of  $\text{H}^-$ . Eleven of the compounds studied ( $\text{C}_2\text{H}_2$ ,  $\text{H}_2\text{O}$ ,  $\text{CH}_3\text{CN}$ ,  $\text{CH}_3\text{OH}$ ,  $(\text{CH}_3)_2\text{CO}$ ,  $\text{CH}_3\text{CHO}$ ,  $\text{N}_2\text{O}$ ,  $\text{CO}_2$ ,  $\text{O}_2$ ,  $\text{CO}$ , and  $\text{C}_6\text{H}_6$ ) have been detected in the interstellar medium (ISM).

Rate constants for  $\text{H}^-$  with several neutral molecules ( $\text{C}_2\text{H}_2$ ,  $\text{H}_2\text{O}$ ,  $\text{CH}_3\text{CN}$ ,  $\text{N}_2\text{O}$ ,  $\text{O}_2$ ,  $\text{CO}$ ,  $\text{CH}_3\text{Cl}$ , and  $\text{C}_6\text{H}_6$ ) were initially determined decades ago to test ion-molecule collision models. For references, see the footnotes to Table 5.1. Only the rate constant for  $\text{H}^- + \text{H}_2\text{O}$  has been studied by more than one laboratory. In this work, we increase the number and source of existing measurements and contribute seven previously unmeasured reaction-rate constants of  $\text{H}^-$  with  $\text{CH}_3\text{OH}$ ,  $(\text{CH}_3)_2\text{CO}$ ,  $\text{CH}_3\text{CHO}$ ,  $\text{CO}_2$ ,  $(\text{CH}_3)_3\text{CCl}$ ,  $(\text{CH}_3\text{CH}_2)_2\text{O}$ , and  $\text{D}_2$ . A majority of these reactions exhibit proton-transfer mechanisms, illustrating the basicity of the  $\text{H}^-$  ion. In contrast, reactions with nonacidic neutrals occur by AD, atom transfer, addition, substitution, or elimination channels. Reaction efficiencies are strongly correlated with the potential energy surface along the reaction coordinate. *Ab initio* calculations provide insight into the reaction mechanisms and their relation to reaction efficiencies.

## 5.2 Experimental Methods

Experiments were carried out using a flowing-afterglow instrument.  $\text{H}^-$  is formed by electron ionization (70 eV ionization energy) on a trace amount of ammonia gas ( $\text{NH}_3$ , Air

**Table 5.1** Hydride / Neutral Molecule Reactions.

Neutral Reactant	Product	$k_{\text{exp}}^{\text{a}}$ ( $10^{-9}\text{cm}^3\text{s}^{-1}$ )	$k_{\text{col}}^{\text{b}}$ ( $10^{-9}\text{cm}^3\text{s}^{-1}$ )	Efficiency ( $k_{\text{exp}}/k_{\text{col}}$ )	Literature Values ( $10^{-9}\text{cm}^3\text{s}^{-1}$ )	$\Delta H_{\text{exp}}^{\text{c}}$ ( $\text{kcal mol}^{-1}$ )	$\Delta H_{\text{theo}}^{\text{d}}$ (0 K) ( $\text{kcal mol}^{-1}$ )	$\Delta H_{\text{theo}}^{\text{d, e}}$ (298 K) ( $\text{kcal mol}^{-1}$ )
<b>Proton Abstraction Reactions</b>								
C <sub>2</sub> H <sub>2</sub>	C <sub>2</sub> H <sup>-</sup> + H <sub>2</sub>	3.1 ± 0.3	4.44	0.70	4.42 <sup>f</sup> ± 25%	-21.6	-26.2	-24.1
H <sub>2</sub> O <sup>g</sup>	OH <sup>-</sup> + H <sub>2</sub>	4.8 ± 1.1	9.18	0.61	3.8 <sup>h</sup> ± 30%, 3.7 <sup>i</sup> ± 25%	-10.3	-14.3	-12.5
CH <sub>3</sub> CN	CH <sub>2</sub> CN <sup>-</sup> + H <sub>2</sub>	11 ± 1	18.5	0.57	13 <sup>j</sup> ± 2 (± 25%)	-26.3	-27.2	-25.1
CH <sub>3</sub> OH	CH <sub>3</sub> O <sup>-</sup> + H <sub>2</sub>	6.1 ± 0.8	9.3	0.66	N/A	-18.6	-21.3	-19.5
(CH <sub>3</sub> ) <sub>2</sub> CO	CH <sub>3</sub> COCH <sub>2</sub> <sup>-</sup> + H <sub>2</sub>	7.0 ± 0.8	14.9	0.47	N/A	-31.8	-33.1	-31.5
CH <sub>3</sub> CHO	CH <sub>2</sub> CHO <sup>-</sup> + H <sub>2</sub>	6.4 ± 1.1	13.9	0.51	N/A	-34.9	-35.9	-34.0
<b>Atom Abstraction / Addition Reactions</b>								
N <sub>2</sub> O	OH <sup>-</sup> + N <sub>2</sub>	1.0 ± 0.1	4.27	0.23	1.1 <sup>k</sup> ± 0.3	-87.7	-89.2	-87.4
CO <sub>2</sub>	HCO <sub>2</sub> <sup>-</sup>	0.09 ± 0.02	4.03	0.022	N/A	-50.9	-52.2	-52.0
<b>Associative Detachment Reactions</b>								
O <sub>2</sub>	HO <sub>2</sub> + e <sup>-</sup>	1.4 ± 0.1	2.97	0.46	1.2 <sup>k</sup> (±20%)	-34.2	-30.3 <sup>l</sup>	-29.4 <sup>l</sup>
CO	CHO + e <sup>-</sup>	0.020 ± 0.008	3.76	0.007	≈0.05 <sup>k</sup>	2.1	-1.2	-0.9
<b>S<sub>N</sub>2 / E2 Reactions</b>								
CH <sub>3</sub> Cl	Cl <sup>-</sup> + CH <sub>4</sub>	2.5 ± 0.1	10.7	0.23	3.0 <sup>m</sup> ± 0.2 (±20%)	-85.0	-91.4	-91.5
(CH <sub>3</sub> ) <sub>3</sub> CCl	Cl <sup>-</sup> + H <sub>2</sub> + (CH <sub>3</sub> ) <sub>2</sub> CCH <sub>2</sub>	4.0 ± 0.5	13.4	0.32	N/A	-76.2	-77.5	-78
<b>No Reaction</b>								
(CH <sub>3</sub> CH <sub>2</sub> ) <sub>2</sub> O	H <sub>2</sub> + C <sub>2</sub> H <sub>5</sub> O <sup>-</sup> + C <sub>2</sub> H <sub>4</sub>	N/A	7.2	N/A	N/A	-5.2	-6.2	-3.5
C <sub>6</sub> H <sub>6</sub>	C <sub>6</sub> H <sub>5</sub> <sup>-</sup> + H <sub>2</sub>	Slow	7.55	N/A	>0.05 <sup>n</sup>	1.1	-2.5	-0.5
D <sub>2</sub>	D <sup>-</sup> + HD	<0.01	2.33	N/A	N/A	0.9	1.1	1.1

<sup>a</sup> Error represents 1σ of the mean of the experimental measurements. There is an additional systematic error of ± 20%.

<sup>b</sup>  $k_{\text{col}}$  is determined according to Langevin theory for reactions involving neutral species having no dipole moment and parameterized trajectory theory for those reactions involving neutral species with dipole moments.

<sup>c</sup> Values determined using additivity methods with experimental values for ionization energies, bond energies, electron affinities, and heats of formation taken from Linstrom & Mallard (2010).

<sup>d</sup> MP2(full)/aug-cc-pVDZ theory level including zero-point energy corrections.

<sup>e</sup> Including thermal energy corrections at 298 K.

<sup>f</sup> Mackay et al (1977).

<sup>g</sup> Stockdale et al. (1969) reported an unreasonably high value of  $540 \pm 160 \times 10^{-9} \text{cm}^3 \text{s}^{-1}$ .

<sup>h</sup> Melton & Neece (1971).

<sup>i</sup> Betowski et al. (1975).

<sup>j</sup> Mackay et al. (1976)

<sup>k</sup> Dunkin et al. (1970).

<sup>l</sup> CCSD(T)/aug-cc-pVTZ//MP2(full)/aug-cc-pVDZ theory level including zero-point energy corrections.

<sup>m</sup> Tanaka et al. (1976).

<sup>n</sup> Bohme & Young (1971).

Products and Chemicals Inc., 99.99%) via the dissociative attachment process  $\text{NH}_3 + e^- \rightarrow \text{H}^- + \text{NH}_2$  (cf. Martinez et al. 2009). Ions are formed in low density using a 1–2  $\mu\text{A}$  emission current to ensure the existence of free diffusion. Sufficient concentration of  $\text{NH}_3$  is used to ensure that  $\text{H}^-$  formation (ionization) was complete before the reaction region. Additionally, ions are thermalized by  $\sim 10^4$  collisions with the helium carrier gas (pressure = 0.5 Torr; flow = 220 std  $\text{cm}^3 \text{s}^{-1}$ ). The reaction region is a flow tube ( $41.85 \text{ cm}^2$ ) with seven inlets at fixed distances for the addition of neutral reagents. A measured amount of reactant is added, then the decrease of the reactant-ion signal is monitored as a function of reaction distance by a quadrupole mass filter coupled to an electron multiplier. Reactions are carried out under pseudo first order conditions, and standard kinetic analysis is used to determine rate constants. Neutral reagents and purities are  $\text{C}_2\text{H}_2$  ( $\geq 99.6\%$ ),  $\text{H}_2\text{O}$  (deionized),  $\text{CH}_3\text{CN}$  (99.8%),  $\text{CH}_3\text{OH}$  ( $\geq 99.9\%$ ),  $(\text{CH}_3)_2\text{CO}$  ( $\geq 99.5\%$ ),  $\text{CH}_3\text{CHO}$  ( $\geq 99.5\%$ ),  $\text{N}_2\text{O}$  (99.0%),  $\text{CO}_2$  ( $\geq 99\%$ ),  $\text{O}_2$  ( $\geq 99.994\%$ ),  $\text{CO}$  (99.5%),  $\text{CH}_3\text{Cl}$  (99.5%),  $(\text{CH}_3)_3\text{CCl}$  ( $\geq 99.5\%$ ),  $(\text{CH}_3\text{CH}_2)_2\text{O}$  (99.9%),  $\text{C}_6\text{H}_6$  ( $\geq 99.9\%$ ), and  $\text{D}_2$  ( $\geq 99.8\%$ ).

### 5.3 Results and Discussion

Table 5.1 summarizes our results for all reactions, including reaction-rate constants, collision-rate constants, efficiencies, prior literature values, and exothermicities. We observe a wide range of rate constants and their resulting efficiencies. Here, theoretical calculations allow us to explore reaction mechanisms and identify those that are viable. In this work, we report a systematic error of  $\pm 20\%$ , based on the accuracy of the measurements used in determining our rate constants. These reaction rate constants are reported with error bars representing  $1\sigma$  of the mean, an indication of the precision of our measurements. Our reported rate-constant values in the text are followed by the total number of rate constant measurements for each reaction.

We report efficiency as  $k_{\text{exp}}/k_{\text{col}}$ , where  $k_{\text{col}}$  is the collision rate constant determined by Langevin theory (Gioumousis & Stevenson 1958) for reactions involving neutral species without a dipole moment ( $\text{C}_2\text{H}_2$ ,  $(\text{CH}_3\text{CH}_2)_2\text{O}$ ,  $\text{CO}_2$ ,  $\text{O}_2$ ,  $\text{C}_6\text{H}_6$ , and  $\text{D}_2$ ) and by parameterized trajectory theory (Su & Chesnavich 1982) for those reactions involving neutral species with dipole moments ( $\text{H}_2\text{O}$ ,  $\text{CH}_3\text{CN}$ ,  $\text{CH}_3\text{OH}$ ,  $(\text{CH}_3)_2\text{CO}$ ,  $\text{N}_2\text{O}$ ,  $\text{CH}_3\text{CHO}$ ,  $\text{CO}$ ,  $\text{CH}_3\text{Cl}$  and  $(\text{CH}_3)_3\text{CCl}$ ). Values for dipole moments and polarizabilities were taken either from the experimental thermochemical data portion of the *NIST Computational Chemistry Comparison and Benchmark Database* (CCCBD 2010) or from the 89th edition of the *CRC Handbook of Chemistry and Physics* (Lide 2008).

We determine enthalpies of reaction, reported in Table 5.1 as  $\Delta H_{\text{exp}}$ , using additivity methods with values for ionization energies, bond energies, electron affinities, and heats of formation taken from the *NIST Chemistry WebBook* (Linstrom & Mallard 2010) and the *CRC Handbook of Chemistry and Physics* (Lide 2008). For comparison, enthalpies were also determined using *ab initio* calculations; these values are reported at both absolute zero and 298 K. Structures and energies of anions and neutral species were determined using *Gaussian 03* (Frisch et al. 2004) at the MP2(full)/aug-cc-pVDZ level of theory.<sup>10</sup> Enthalpies resulting from additivity methods and calculated enthalpy determinations are in excellent agreement.

Experimental difficulties arise when we quantitatively compare ion intensities to determine product branching ratios. Mass discrimination (the transmission of different-mass ions with different efficiencies through the detection region) manifests to a significant degree with hydride studies because of the sizable range of masses of ions monitored simultaneously. Moreover, secondary ion chemistry can occur. Although mass discrimination can make it a challenge to account for 100% conversion of a reactant ion into products, one can make

reasonable assumptions to understand the reaction pathways involved. Where applicable, we have noted other possible channels of a reaction based on calculated reaction enthalpies and *ab initio* calculations. However, we do not present quantitative branching ratio determinations.

For discussion, reactions have been categorized into five groups based on their reaction mechanism. These mechanisms include proton abstraction, atom abstraction or addition reactions, AD, substitution ( $S_N2$ )/elimination (E2), and a final group where reactions were not observed.

### 5.3.1 Proton Abstraction

The neutral reagents  $C_2H_2$ ,  $H_2O$ ,  $CH_3CN$ ,  $CH_3OH$ ,  $(CH_3)_2CO$ , and  $CH_3CHO$  react with  $H^-$  to form  $H_2$  via  $RH + H^- \rightarrow R^- + H_2$ . Such proton abstraction reactions have relatively large rate constants ranging from 3.1 to  $11 \times 10^{-9} \text{ cm}^3 \text{ s}^{-1}$ . Similarly, reaction efficiencies, while not at 100%, are generally higher than for other reactions in this study.

Mackay et al. (1977) measured the rate constant for the proton transfer reaction of  $H^-$  with  $C_2H_2$  with a flowing-afterglow instrument in a manner similar to ours and reported  $k = 4.42 \pm 25\% \times 10^{-9} \text{ cm}^3 \text{ s}^{-1}$ . In comparison, our measured rate constant is  $3.1 \pm 0.3 \times 10^{-9} \text{ cm}^3 \text{ s}^{-1}$  (15 measurements). Because of the rapid reaction between  $H^-$  and  $(CH_3)_2CO$ , as shown below, we worked to eliminate contamination from this reaction in the rate-constant measurement of  $H^-$  with  $C_2H_2$ . Based on calculations and careful experiments, we conclude that an insignificant amount of  $(CH_3)_2CO$  is present at reaction. Our rate-constant measurements overlap with the previously measured rate constant of Mackay et al. within our combined error bars.

The reaction of  $H^-$  with  $H_2O$  is the only reaction in this study for which more than one rate constant measurement has been reported. Betowski et al. (1975) determined a rate constant of  $3.7 \pm 25\% \times 10^{-9} \text{ cm}^3 \text{ s}^{-1}$  from four experimental measurements for the reaction  $H^- + H_2O \rightarrow$

$\text{OH}^- + \text{H}_2$  at 297 K using the flowing-afterglow technique. Melton & Neece (1971) carried out an energy-variable study for this reaction ranging from 0 to 10 eV and reported a value of  $3.8 \pm 30\% \times 10^{-9} \text{ cm}^3 \text{ s}^{-1}$  (0 eV) using a mass spectrometric technique. An earlier measurement from Stockdale et al. (1968, 1969) for the same reaction was reported as  $5.4 \pm 1.6 \times 10^{-7} \text{ cm}^3 \text{ s}^{-1}$ . Rate constants by Stockdale et al. were measured using a pulsed source time-of-flight mass spectrometer, and their reported rate constant measurement at 0 eV ion energy [i.e.,  $E_{\text{lab}}(\text{H}^-)$ ] exceeds the collision rate constant by a factor of 60 and is therefore not physically reasonable. Our determination of this reaction rate constant is  $4.8 \pm 1.1 \times 10^{-9} \text{ cm}^3 \text{ s}^{-1}$  (19 measurements). The experimental conditions of our study are most similar to those of Betowski et al., who produced ions using a similar method (i.e., electron ionization on a precursor). The ions were subsequently thermalized via collisions with carrier gas molecules.

Mackay et al. (1976) reported a rate constant of  $13 \pm 2 \times 10^{-9} \text{ cm}^3 \text{ s}^{-1}$  (mean value and precision of eight measurements, with an overall accuracy of  $\pm 25\%$ ) for the reaction of  $\text{H}^-$  with  $\text{CH}_3\text{CN}$ . The measurement was made using a flowing-afterglow instrument under conditions similar to ours. Our reported measurement,  $11 \pm 1 \times 10^{-9} \text{ cm}^3 \text{ s}^{-1}$  (10 measurements), is within the error bars of the former measurement, when systematic errors are included. As with the data of Mackay et al., we saw no evidence of nucleophilic displacement,  $\text{H}^- + \text{CH}_3\text{CN} \rightarrow \text{CN}^- + \text{CH}_4$ , even though additivity methods indicate that the reaction is exothermic,  $\Delta H = -53.0 \text{ kcal mol}^{-1}$ . In fact, calculations indicate that nucleophilic displacement by the hydride anion has a transition-state barrier above the total energy of the reactants of  $15.1 \text{ kcal mol}^{-1}$ .

We report a rate constant for the proton transfer reaction of  $\text{CH}_3\text{OH}$  with  $\text{H}^-$  as  $6.1 \pm 0.8 \times 10^{-9} \text{ cm}^3 \text{ s}^{-1}$  (12 measurements). Although a substitution mechanism for the  $\text{CH}_3\text{OH} / \text{H}^-$  reaction producing  $\text{OH}^-$  and  $\text{CH}_4$  is more exothermic ( $\Delta H = -37.0 \text{ kcal mol}^{-1}$  versus  $-18.6 \text{ kcal}$

$\text{mol}^{-1}$  for the proton-transfer mechanism), calculations predict a high transition-state energy barrier of  $13.2 \text{ kcal mol}^{-1}$  along the reaction coordinate that effectively prohibits this reaction.

Our measured rate constant for the reaction of  $\text{H}^-$  with  $(\text{CH}_3)_2\text{CO}$ ,  $7.0 \pm 0.8 \times 10^{-9} \text{ cm}^3 \text{ s}^{-1}$  (10 measurements), indicates a rather rapid reaction. Our measurement for the rate constant of  $\text{H}^-$  with  $\text{CH}_3\text{CHO}$  is  $6.4 \pm 1.1 \times 10^{-9} \text{ cm}^3 \text{ s}^{-1}$  (nine measurements). There are no previous studies of these reactions.

### 5.3.2 Atom Abstraction/Addition

Reaction rate constants and efficiencies for the reactions of  $\text{H}^-$  with  $\text{N}_2\text{O}$  and  $\text{CO}_2$  are markedly different than those of proton-transfer reactions, as shown in Table 5.1. The reaction coordinate plot of  $\text{H}^-$  with  $\text{N}_2\text{O}$  is shown in Figure 5.1, with all energies relative to the total energy of the reactants. The most viable pathway, an attack of  $\text{H}^-$  on the terminal nitrogen atom, leads to the formation of an association intermediate that is more stable than the reactants by  $-45.7 \text{ kcal mol}^{-1}$ . From the intermediate, an AD path is endothermic by  $17.1 \text{ kcal mol}^{-1}$  and does not occur; however, the reactants can proceed through a transition state at  $-20.6 \text{ kcal mol}^{-1}$  along the dissociation path and on to a dissociation intermediate ( $93.0 \text{ kcal mol}^{-1}$  lower in energy than reactants). Similarly, a direct attack on the oxygen atom leads to an association intermediate then a transition state that is  $-4.2 \text{ kcal mol}^{-1}$  and  $-0.2 \text{ kcal mol}^{-1}$  lower in energy than the reactants, respectively. This transition state then proceeds to the dissociation intermediate described above. Dunkin et al. (1970) measured the reactivity of  $\text{H}^-$  with  $\text{N}_2\text{O}$  and reported a rate constant of  $1.1 \pm 0.3 \times 10^{-9} \text{ cm}^3 \text{ s}^{-1}$ , in agreement with our measurement of  $1.0 \pm 0.1 \times 10^{-9} \text{ cm}^3 \text{ s}^{-1}$  (seven measurements).

For the reaction of  $\text{H}^-$  with  $\text{CO}_2$ , four channels were investigated. Figure 5.2(a) shows the hydrogen atom attacking an O atom in  $\text{CO}_2$ . The AD and oxygen abstraction channels that

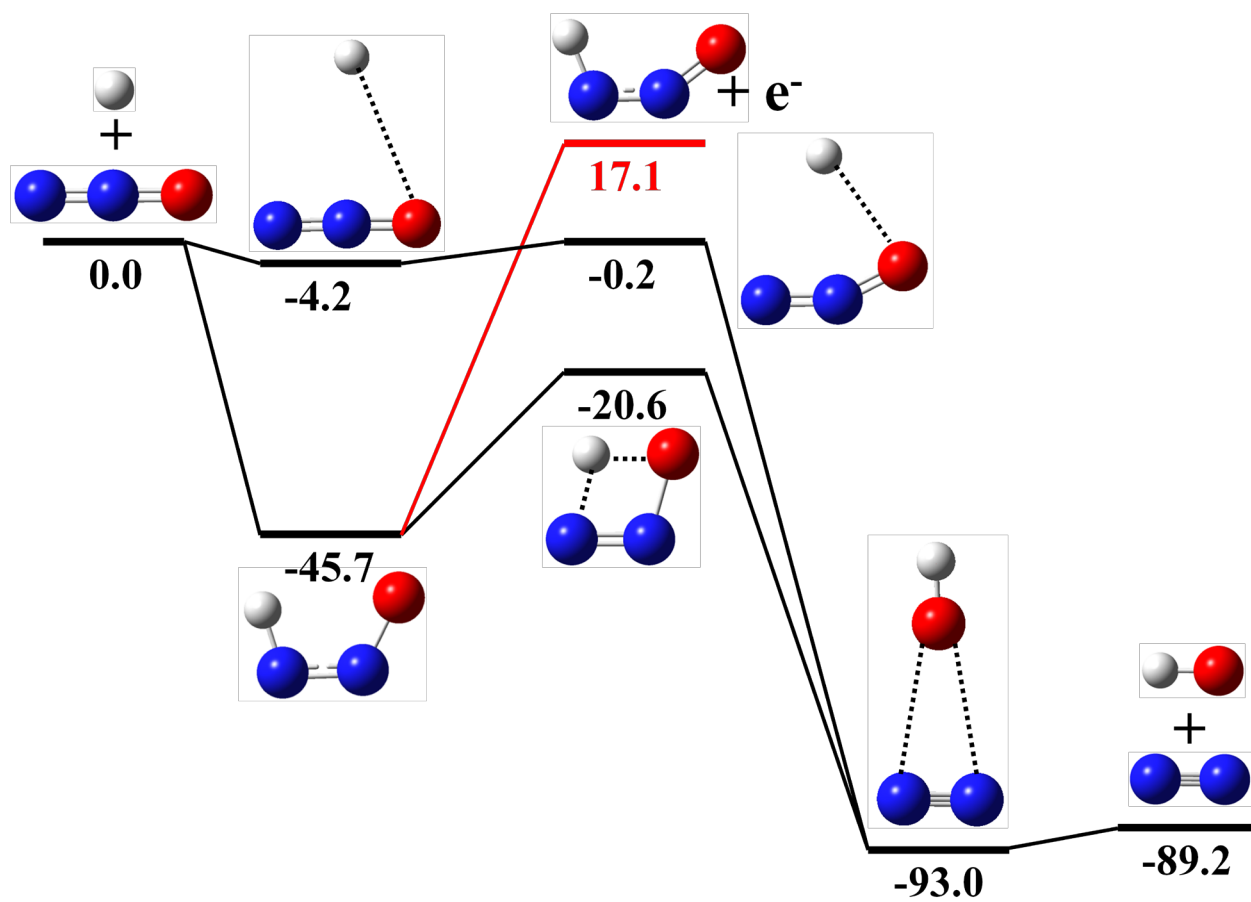
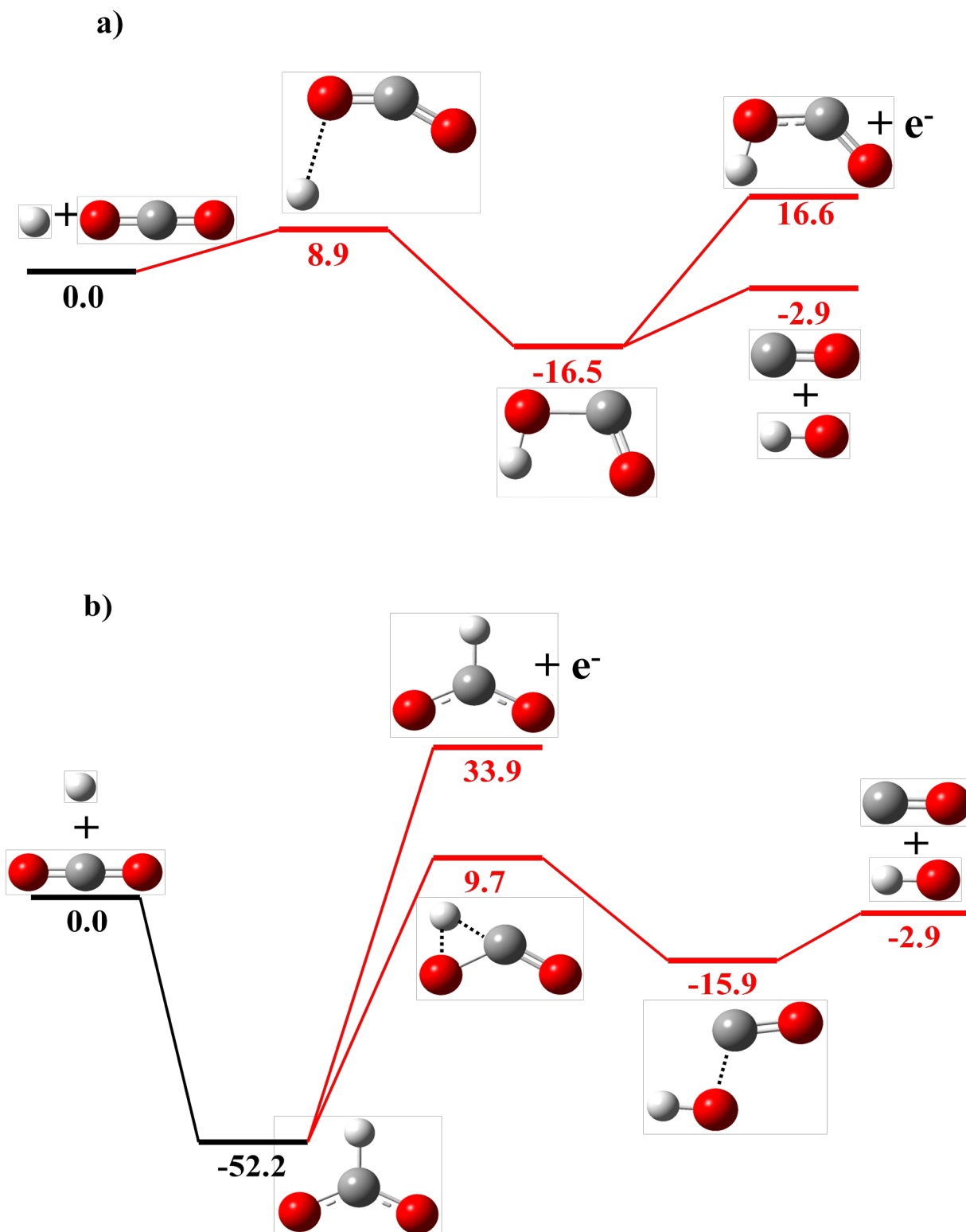


**Figure 5.1**  $\text{H}^- + \text{N}_2\text{O}$  reaction coordinate plot. Energies obtained from calculations performed at the MP2(full)/aug-cc-pVDZ level of theory ( $\text{kcal mol}^{-1}$ ).



could result from this attack are hampered by a transition state that is  $8.9 \text{ kcal mol}^{-1}$  above the energy of the reactants. Alternately, Figure 5.2(b) shows the H atom attacking the C atom of the  $\text{CO}_2$  and forming a reactant intermediate  $-52.2 \text{ kcal mol}^{-1}$  lower in energy than the reactants.

The AD channel producing the neutral product with the H bound to the C does not occur; the reaction is endothermic with the products  $33.9 \text{ kcal mol}^{-1}$  above the reactants. The atom-transfer reaction forming CO and  $\text{HO}^-$  from the reactant intermediate has a transition-state barrier of  $9.7 \text{ kcal mol}^{-1}$  higher in energy than the reactants and also does not occur. Reaction of  $\text{H}^-$  with  $\text{CO}_2$  is slow. Our measured rate constant is  $0.09 \pm 0.02 \times 10^{-9} \text{ cm}^3 \text{ s}^{-1}$  (six measurements). Evidence of trace formation of the  $\text{HCO}_2^-$  species described in Figure 5.2(b) is seen, indicating the process is third order (He reaction flow tube pressure = 0.450 Torr). Reaction in the interstellar medium, however, may occur by radiative association.

### 5.3.3 Associative Detachment

$\text{H}^-$  reacts with  $\text{O}_2$  and CO via AD reactions. Similar to the proton-transfer reactions discussed previously, these reactions proceed without barriers along the approach of reactants. A large difference is evident, however, when we compare efficiencies and rate constants for these reactions, as shown in Table 5.1. The differences are attributed to relative enthalpies; whereas the AD channel for the  $\text{O}_2$  reaction is exothermic ( $\Delta H = -34.2 \text{ kcal mol}^{-1}$ ), the CO reaction is essentially thermoneutral ( $2.1 \text{ kcal mol}^{-1}$ ). Additionally, we found that MP2 enthalpy calculations underestimate values for this channel by  $\sim 9 \text{ kcal mol}^{-1}$  relative to the experimental values. Better agreement was found using the CCSD(T)/aug-cc-pVTZ//MP2(full)/aug-cc-pVDZ level of theory.

Dunkin et al. (1970), in clarifying the electron affinity of  $\text{O}_2$ , measured a rate constant of  $1.2 \pm 20\% \times 10^{-9} \text{ cm}^3 \text{ s}^{-1}$  for the  $\text{H}^- + \text{O}_2$  reaction. Our study of the AD reaction used a flowing-

afterglow apparatus with conditions similar to theirs. Our value,  $1.4 \pm 0.1 \times 10^{-9} \text{ cm}^3 \text{ s}^{-1}$  (eight measurements), is in good agreement with their published value.

Dunkin et al. also determined the reaction products and considered formation of  $\text{O}_2^- + \text{H}$ ,  $\text{OH}^- + \text{O}$ , and  $\text{O}^- + \text{OH}$ .  $\text{OH}^-$  formation seemed plausible since this reaction is exothermic by  $8.6 \text{ kcal mol}^{-1}$ .  $\text{O}^-$  formation, however, is thermoneutral ( $0.4 \text{ kcal mol}^{-1}$ ) and cannot compete with AD. Charge transfer is endothermic by  $7.0 \text{ kcal mol}^{-1}$  and should therefore not occur. A careful experimental search for these alternative products turned out negative, implying that if these reactions occur, they have less than 1% of the AD rate. Similarly, our studies show clear evidence of the AD channel. However, the presence of background  $\text{OH}^-$  in our spectra prevents quantitative branching-ratio determination for relatively minor channels.

Our determination of the rate constant for hydride reacting with CO is  $2.0 \pm 0.8 \times 10^{-11} \text{ cm}^3 \text{ s}^{-1}$  (eight measurements), and AD is the only channel. Our result is smaller than the previously published value of  $\sim 5.0 \times 10^{-11} \text{ cm}^3 \text{ s}^{-1}$ . However, the large error bars reflect considerable variation in our measurements. Influence of the thermoneutrality of the reaction of  $\text{H}^-$  with CO manifests itself in the low reaction-rate constant.

#### 5.3.4 $\text{S}_{\text{N}}2/\text{E}2$ Reactions

$\text{H}^-$  reaction with  $\text{CH}_3\text{Cl}$  proceeds via a substitution mechanism, and reaction with  $(\text{CH}_3)_3\text{CCl}$  proceeds via an elimination mechanism. The lower reaction efficiencies relative to the proton-transfer reactions discussed earlier are due to transition states along the reaction coordinates. Transition states higher in energy than either a reactive intermediate or a dissociative intermediate effectively serve as “barriers” that must be overcome along the energy pathway of the reaction coordinate. The reaction coordinate plot for  $\text{H}^- + \text{CH}_3\text{Cl}$  is shown in Figure 5.3. Here, we consider proton-abstraction and substitution channels for this reaction.

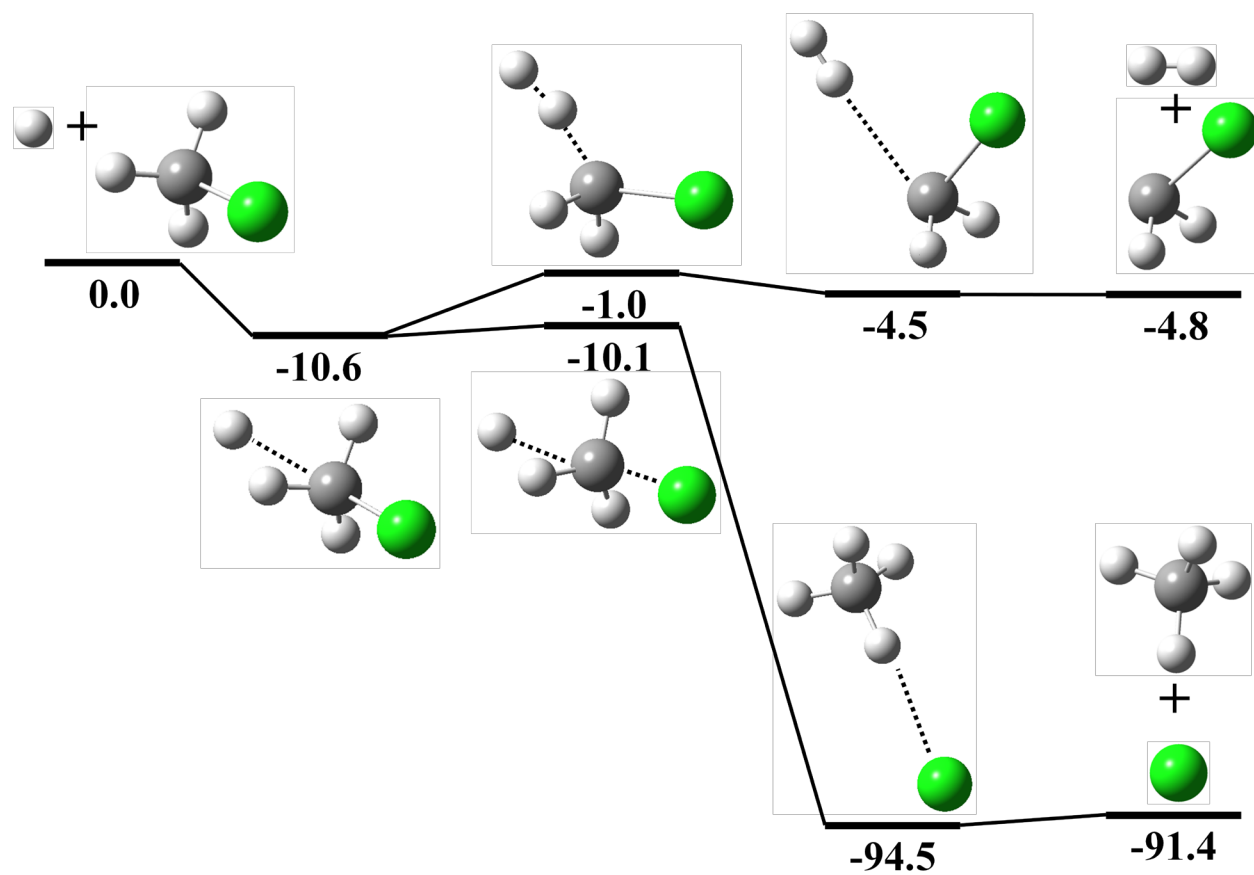


**Figure 5.3**  $\text{H}^- + \text{CH}_3\text{Cl}$  reaction coordinate plot. Energies obtained from calculations performed at the MP2(full)/aug-cc-pVDZ level of theory ( $\text{kcal mol}^{-1}$ ).

While both channels have transition-state barriers, the substitution channel has a lower barrier in addition to being more exothermic overall ( $\Delta H = -91.4 \text{ kcal mol}^{-1}$  for the substitution versus  $-4.8 \text{ kcal mol}^{-1}$  for the proton abstraction with respect to reactants). Additionally, we saw no evidence of the weakly bound  $\text{CH}_3^-$  anion. Similarly, we considered a substitution mechanism for the  $(\text{CH}_3)_3\text{CCl}$  reaction. We cannot distinguish between competing mechanisms for the  $(\text{CH}_3)_3\text{CCl}$  reaction since  $\text{Cl}^-$  is produced by both reactions. However, calculations predict the substitution reaction to have a higher transition-state energy barrier than the elimination reaction ( $\Delta H = 10.7 \text{ kcal mol}^{-1}$  versus  $-8.4 \text{ kcal mol}^{-1}$  at 298 K relative to reactant species). Therefore, we expect the substitution channel to have no contribution.

Prior measurement of the rate constant for the  $\text{CH}_3\text{Cl}$  reaction was reported as  $3.0 \pm 0.2 \times 10^{-9} \text{ cm}^3 \text{ s}^{-1}$  (mean value and precision of two measurements, with an overall accuracy of  $\pm 20\%$ ) by Tanaka et al. (1976). Our determination for the  $\text{CH}_3\text{Cl}$   $\text{S}_{\text{N}}2$  reaction is  $2.5 \pm 0.1 \times 10^{-9} \text{ cm}^3 \text{ s}^{-1}$  (seven measurements) and  $4.0 \pm 0.5 \times 10^{-9} \text{ cm}^3 \text{ s}^{-1}$  (nine measurements) for the  $(\text{CH}_3)_3\text{CCl}$   $\text{E}2$  reaction.

### 5.3.5 Unreactive Neutral Reagents

Some reactions in this study ( $\text{H}^-$  with  $(\text{CH}_3\text{CH}_2)_2\text{O}$ ,  $\text{C}_6\text{H}_6$ , and  $\text{D}_2$ ) exhibited little or no reactivity. We saw no decrease of reactant ion or formation of product ions in the reaction of  $\text{H}^-$  with  $(\text{CH}_3\text{CH}_2)_2\text{O}$ . Typically, strong bases have been found to react prominently with ethers by elimination mechanisms (DePuy & Bierbaum). However, calculations suggest that the elimination channel for the reaction of  $\text{H}^-$  with diethyl ether does not occur because of a barrier  $5.4 \text{ kcal mol}^{-1}$  higher in energy than the reactants along the reaction coordinate.

In reacting  $\text{H}^-$  with  $\text{C}_6\text{H}_6$ , we noted a decrease in signal and made several attempts to measure a rate constant. In 14 attempts over the course of three days using two different high-

purity C<sub>6</sub>H<sub>6</sub> samples, we were left with an unreasonably low precision ( $2 \pm 2 \times 10^{-11} \text{ cm}^3 \text{ s}^{-1}$ ). Experimental and calculated enthalpies suggest that the reaction is thermoneutral, a possible cause of our problem. The presence of a relatively stable adduct could account for a slight decrease in the reactant ion signal. Bohme & Young (1971) studied the reaction of H<sup>-</sup> with C<sub>6</sub>H<sub>6</sub> in a series of bracketing experiments to determine electron affinities from thermal proton-transfer reactions. Their study was performed using a flowing-afterglow instrument, and generated H<sup>-</sup> via electron ionization on NH<sub>3</sub> in He. Their rate determination,  $\geq 5 \times 10^{-11} \text{ cm}^3 \text{ s}^{-1}$ , resulted only in limiting values.

We observe only slight falloff in H<sup>-</sup> signal intensity with the addition of D<sub>2</sub> (up to  $\sim 2 \times 10^{12} \text{ cm}^{-3}$ ). The reaction, however, is thermoneutral, and hence, we see similar behavior to that in the reaction with C<sub>6</sub>H<sub>6</sub>. Based on our observation, we set a limit to the reaction rate constant of  $< 1 \times 10^{-11} \text{ cm}^3 \text{ s}^{-1}$ . However, our observations do show D<sup>-</sup> production as H<sup>-</sup> is depleted.

#### 5.4. Conclusions

Table 5.1 is a compilation of our results that provide an increase in the accuracy of existing rate constants and a contribution of new rate constants. This study represents a chemical mapping of hydride reactivity with neutral species, many of which have been detected in the ISM. Experimental observations and contributions from *ab initio* calculations have accounted for a variety of reaction mechanisms and a range of reaction efficiencies.

## 5.5 References

- Betowski, D., Payzant, J. D., Mackay, G. I., & Bohme, D. K. 1975, *Chem. Phys. Lett.*, 31, 321
- Black, J. H. 1978, *ApJ*, 222, 125
- Bohme, D. K., & Young, L. B. 1971, *Can. J. Chem.*, 49, 2918
- Chandrasekhar, S. 1944, *ApJ*, 100, 176
- Chandrasekhar, S., & Breen, F. H. 1946, *ApJ*, 104, 430
- DePuy, C. H., & Bierbaum, V. M. 1981, *J. Am. Chem. Soc.*, 103, 5034
- Dunkin, D. B., Fehsenfeld, F. C., & Ferguson, E. E. 1970, *J. Chem. Phys.*, 53, 987
- Fehsenfeld, F. C., Howard, C. J., & Ferguson, E. E. 1973, *J. Chem. Phys.*, 58, 5841
- Field, D. 2000, *A&A*, 362, 774
- Frisch, M. J., Trucks, G. W., Schlegel, H. B., Scuseria, G. E., Robb, M. A., Cheeseman, J. R., Montgomery, Jr., J. A., Vreven, T., Kudin, K. N., Burant, J. C., Millam, J. M., Iyengar, S. S., Tomasi, J., Barone, V., Mennucci, B., Cossi, M., Scalmani, G., Rega, N., Petersson, G. A., Nakatsuji, H., Hada, M., Ehara, M., Toyota, K., Fukuda, R., Hasegawa, J., Ishida, M., Nakajima, T., Honda, Y., Kitao, O., Nakai, H., Klene, M., Li, X., Knox, J. E., Hratchian, H. P., Cross, J. B., Bakken, V., Adamo, C., Jaramillo, J., Gomperts, R., Stratmann, R. E., Yazyev, O., Austin, A. J., Cammi, R., Pomelli, C., Ochterski, J. W., Ayala, P. Y., Morokuma, K., Voth, G. A., Salvador, P., Dannenberg, J. J., Zakrzewski, V. G., Dapprich, S., Daniels, A. D., Strain, M. C., Farkas, O., Malick, D. K., Rabuck, A. D., Raghavachari, K., Foresman, J. B., Ortiz, J. V., Cui, Q., Baboul, A. G., Clifford, S., Cioslowski, J., Stefanov, B. B., Liu, G., Liashenko, A., Piskorz, P., Komaromi, I., Martin, R. L., Fox, D. J., Keith, T., Al-Laham, M. A., Peng, C. Y., Nanayakkara, A., Challacombe, M., Gill, P. M. W., Johnson, B., Chen, W., Wong, M. W., Gonzalez, C., & Pople, J. A., *Gaussian 03*, Revision C.02, Gaussian, Inc., Wallingford CT, 2004.
- Gioumousis, G., & Stevenson, D. P. 1958, *J. Chem. Phys.*, 29, 294
- Glover, S. C., Savin, D. W., & Jappson, A. -K. 2006, *ApJ*, 640, 553
- Lide, D. R. 2008, *CRC Handbook of Chemistry and Physics* (89th ed.; Boca Raton, FL: CRC Press; Taylor & Francis Group)
- Linstrom, P. J., & Mallard, W. G. (ed.) 2010, *NIST ChemistryWebBook*, NIST Standard Reference Database Number 69 (Gaithersburg, MD: NIST) 20899 (<http://webbook.nist.gov>)
- Mackay, G. I., Betowski, L. D., Payzant, J. D., Schiff, H. I., & Bohme, D. K. 1976, *J. Phys. Chem.*, 80, 2919

Mackay, G. I., Tanaka, K., & Bohme, D. K. 1977, *Int. J. Mass Spectrom. Ion Proc.*, 24, 125

Martinez, O., Yang, Z., Betts, N. B., Snow, T. P., & Bierbaum, V.M. 2009, *ApJ*, 705, L172

Melton, C. E., & Neece, G. A. 1971, *J. Am. Chem. Soc.*, 93, 6757

Münch, D. 1945, *ApJ*, 102, 385

*NIST Computational Chemistry Comparison and Benchmark Database (CCCBD) 2010*, NIST Standard Reference Database Number 101, Release 15a, April 2010, ed. R. D. Johnson III (<http://cccbdb.nist.gov/>)

Ross, T., Baker, E. J., Snow, T. P., Destree, J. D., Rachford, B. L., Drosback, M. M., & Jensen, A. G. 2008, *ApJ*, 684, 358

Schmeltekopf, A. L., Fehsenfeld, F. C., & Ferguson, E. E. 1967, *ApJ*, 148, L155

Stockdale, J. A. D., Compton, R. N., & Reinhardt, P. W. 1969, *Phys. Rev.*, 184, 81

Stockdale, J. A. D., Compton, R. N., & Reinhardt, P.W. 1968, *Phys. Rev. Lett.*, 21, 664

Su, T., & Chesnavich, W. J. 1982, *J. Chem. Phys.*, 76, 5183

Tanaka, K., Mackay, G. I., Payzant, J. D., & Bohme, D. K. 1976, *Can. J. Chem.*, 54, 1643

Wildt, R. 1939, *ApJ*, 90, 611

## Chapter 6

### Experimental and Theoretical Studies of Reactions Between H Atoms and Carbanions of Interstellar Relevance

#### 6.1. Introduction

The interstellar medium (ISM) is extremely heterogeneous. It is composed of atoms, molecules, ions, and dust grains. More than 160 molecular species have now been detected in the ISM, indicating that a rich and complex chemistry occurs. The recent detection of negative ions in circumstellar envelopes and the denser regions of the ISM has expanded the realm of astrochemistry research (McCarthy et al. 2006; Brünken et al. 2007; Cernicharo et al. 2007 & 2008; Remijan et al. 2007; Thaddeus et al. 2007, Agúndez et al. 2010). This important discovery suggests that anions are involved in the chemical reactions within the ISM; therefore, laboratory studies of reactions of anions with abundant species, such as atomic and molecular hydrogen, are crucial for characterizing the negative ion chemistry in the ISM.

With respect to the recent discovery of the anions  $\text{HC}_4^-$ ,  $\text{HC}_6^-$ , and  $\text{HC}_8^-$  (Brünken et al. 2007; Remijan et al. 2007; Cernicharo et al. 2008), we have previously reported the reactions of closed- and open-shell carbon chain anions,  $\text{HC}_n^-$  ( $n = 2, 4, 6, \text{ and } 7$ ) and  $\text{C}_n^-$  ( $n = 2, 4\text{--}10$ ), with H atoms (Barckholtz et al. 2001). Reactions between cations and H atoms exhibit a variety of pathways, including association, hydrogen abstraction, electron transfer, etc. In contrast, the reactions between anions and H atoms exhibit associative detachment (AD), as well as simple association for larger  $\text{C}_n^-$  ( $n = 7\text{--}10$ ) anions (Barckholtz et al. 2001; Snow et al. 2008).

In addition to the reaction channels, reaction efficiencies are important characteristics of the anion-atom reactions. For example, we have recently studied the gas phase reactions of ISM-

related anions with N and O atoms (Yang et al. 2010a, 2010b). The efficiencies of these reactions are mainly determined by the portion of collisions undergoing spin-conserved barrierless reaction channels; the accessibility to these pathways is correlated to many factors including the electronic structure of the reactants (open- or closed-shell), the potential energy curve of the approaching reactants, and the spin-conversion efficiency.

In reactions between closed-shell anions and H atoms, spin effects are not critical because of the single reaction pathway. However, the general reaction mechanism and efficiency trends of these reactions are not well understood, and more detailed studies are essential. In the current work, experimental and theoretical studies were carried out for three categories of closed-shell anions that are classified by their structural similarities and reaction sites, as detailed later in the text. These anions include the deprotonated species of group I: nitriles ( $\text{CH}_2\text{CN}^-$ ,  $\text{CH}_3\text{CHCN}^-$ , and  $(\text{CH}_3)_2\text{CCN}^-$ ); group II: acetaldehyde ( $\text{HC}(\text{O})\text{CH}_2^-$ ), acetone ( $\text{CH}_3\text{C}(\text{O})\text{CH}_2^-$ ), and ethyl acetate ( $\text{CH}_3\text{CH}_2\text{OC}(\text{O})\text{CH}_2^-$ ); and group III: methanol ( $\text{CH}_3\text{O}^-$ ) and acetic acid ( $\text{CH}_3\text{CO}_2^-$ ). The experimental results of glycine anion ( $\text{NH}_2\text{CH}_2\text{CO}_2^-$ ) were adopted from our previously published work (Snow et al. 2009). A series of *ab initio* theoretical calculations were carried out at several levels of theory to explore the reaction mechanisms and investigate the factors influencing the reaction efficiencies.

Hydrogen atom is the most abundant atomic species in the ISM, and the rate constants of reactions involving H atom are important for astrochemical modeling. The reactions of H atom with neutral and cationic species have been extensively studied, whereas anion-H atom reactions are still not well-understood. However, these AD reactions can be critical in determining the ionization balance between anions and free electrons (Snow et al. 2006, 2008; Walsh et al.

2009). The neutral molecules of the corresponding anions investigated here have been detected in the ISM. The discovery of glycine, however, is still controversial (Kuan et al. 2003; Snyder et al. 2005; Cunningham et al. 2007; Jones et al. 2007). Therefore, the current study of anion-H atom reactions can enhance our understanding of the mechanisms and reactivities of negative ion chemistry in the ISM.

## 6.2. Experimental Methods

Ions were generated using electron-impact and chemical-ionization methods in a source flow tube. A small flow of nitrous oxide ( $\text{N}_2\text{O}$ ) entrained in helium buffer gas was passed over a rhenium filament to generate  $\text{O}^-$ , which reacts further with methane ( $\text{CH}_4$ ) to form hydroxide ( $\text{OH}^-$ ). The desired organic anion was then produced by reacting  $\text{OH}^-$  with the corresponding neutral precursor (HA):  $\text{OH}^- + \text{HA} \rightarrow \text{H}_2\text{O} + \text{A}^-$ . The reactant hydrogen atoms are formed via thermal dissociation (Martinez et al. 2009; Trainor et al. 1973). The concentration of H atoms was determined by monitoring the loss of chloride ions ( $\text{Cl}^-$ ) in the AD reaction with H atoms (Ferguson et al. 1969; Fehsenfeld et al. 1973; Howard et al. 1974).

Our reaction rate-constant values are reported with error bars representing one standard deviation of the mean of 5 to 14 measurements of the anion-H atom reactions. This error is combined with uncertainty in the H-atom concentration measurement and systematic errors. The total error is estimated as  $\pm 50\%$ .

## 6.3. Theoretical Calculations

To obtain the structures and energies of the anions and neutral species involved in the current study, theoretical calculations were carried out using the *Gaussian 03* suite of programs

(Frisch et al. 2004). Geometry optimization and frequency analyses were calculated at the MP2(full)/aug-cc-pVDZ level of theory. A single point energy was calculated at the (RO)MP2(full)/aug-cc-pVTZ level of theory for the optimized structures, where the restricted open-shell method (ROMP2(full)) was applied to the open-shell species to minimize the influence of spin contamination on the energies. Zero point energy (ZPE) and thermal energy (298 K) corrections were included using the same level of theory for geometry optimization. The computational results were used to construct the reaction coordinate plots of four selected systems and to calculate the enthalpies of all reactions involved in the current study. Natural bond orbital (NBO) analyses were carried out at the MP2(full)/aug-cc-pVTZ level of theory for some species of interest to estimate the partial charge on the reactive site of these anions. In some cases, relaxed potential energy scans were performed at the B3LYP/6-31+G(d,p) level of theory to obtain semiquantitative profiles of the energy changes along the reaction coordinates of interest.

## 6.4 Results and Discussion

The reactant anions were allowed to react with H atoms. The reactions proceeded by AD, in which the H atom bonds to the anion, and an electron is ejected without further rearrangement ( $A^- + H \rightarrow AH + e^-$ ). Rate constants and efficiencies for reactions of the carbanions with H atoms are summarized in Table 6.1. Reaction efficiencies are reported as the ratio of experimental rate constant ( $k_{\text{exp}}$ ) to  $k_{\text{PPI}}$ , a point-polarizable-ion (PPI) model adjustment to traditional Langevin theory as detailed elsewhere (Eichelberger et al. 2003).

The experimental reaction enthalpies were derived from Hess' law, as summarized in Table 6.1. The enthalpy of reaction 6.1 is accurately known, and  $\Delta H_2$ , the enthalpy of

**Table 6.1** Reactions between anions and H atoms.

Anion	$k_{\text{exp}}^{\text{a}}$ ( $10^{-9} \text{ cm}^3 \text{ s}^{-1}$ )	Efficiency <sup>b</sup> ( $k_{\text{exp}}/k_{\text{PPI}}$ )	$\Delta H_{\text{theo}}^{\text{c}}$ (0 K) (kcal mol <sup>-1</sup> )	$\Delta H_{\text{theo}}^{\text{c,d}}$ (298 K) (kcal mol <sup>-1</sup> )	$\Delta H_{\text{exp}}^{\text{e}}$ (kcal mol <sup>-1</sup> )
<b>Group I</b>					
CH <sub>2</sub> CN <sup>-</sup>	1.02 ± 0.03	0.44	-58.4	-58.4	-59.3 ± 2.1
CH <sub>3</sub> CHCN <sup>-</sup>	1.39 ± 0.05	0.59	-61.3	-61.3	-61.4 ± 2.1
(CH <sub>3</sub> ) <sub>2</sub> CCN <sup>-</sup>	1.82 ± 0.13	0.76	-61.7	-61.7	-61.5 ± 2.2
<b>Group II</b>					
HC(O)CH <sub>2</sub> <sup>-</sup>	1.12 ± 0.05	0.49	-50.0	-49.8	-52.2 ± 2.2
CH <sub>3</sub> C(O)CH <sub>2</sub> <sup>-</sup>	1.14 ± 0.04	0.49	-52.5	-52.0	-55.2 ± 2.0
CH <sub>3</sub> CH <sub>2</sub> OC(O)CH <sub>2</sub> <sup>-</sup>	0.97 ± 0.07	0.41	-56.3	-56.1	-58.1 ± 4.1
<b>Group III</b>					
CH <sub>3</sub> O <sup>-</sup>	1.63 ± 0.04	0.72	-65.4	-65.1	-68.4 ± 1.0
CH <sub>3</sub> CO <sub>2</sub> <sup>-</sup>	0.48 ± 0.06	0.21	-31.4 (-33.2)	-31.3 (-33.1)	-34.5 ± 2.2
NH <sub>2</sub> CH <sub>2</sub> CO <sub>2</sub> <sup>-</sup>	0.20 ± 0.06 <sup>f</sup>	0.09	-25.9 (-23.0)	-25.7 (-22.8)	-28.0 ± 2.1

<sup>a</sup> The error bars represent one standard deviation of the mean of 5 to 14 measurements of the anion-H atom reactions. This error is combined with the uncertainty in the H-atom concentration measurement and systematic errors. Total error is estimated as ± 50%.

<sup>b</sup>  $k_{\text{PPI}}$  is the theoretical reaction rate constant obtained from the point-polarizable ion model (Eichelberger et al. 2003).

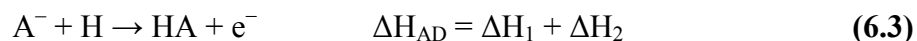
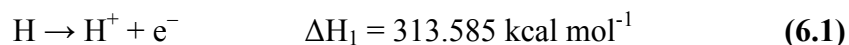
<sup>c</sup> Relative energies calculated at the (RO)MP2(full)/aug-cc-pVTZ//MP2(full)/aug-cc-pVDZ level of theory including zero-point energy corrections. Values in parentheses were obtained from the CCSD(T)/aug-cc-pVTZ//MP2(full)/aug-cc-pVDZ level of theory including zero-point energy corrections.

<sup>d</sup> Including thermal energy corrections at 298 K.

<sup>e</sup> Values determined using additivity methods with experimental values for ionization energies, bond energies, electron affinities, and heats of formation taken from Linstrom (2009).

<sup>f</sup> Results adopted from previous publication (Snow et al. 2009).

deprotonation of the neutral species, was obtained from the *NIST Chemistry WebBook* (Linstrom et al. 2009). The reaction enthalpy for AD ( $\Delta H_{AD}$ ) can be derived by combining reactions 6.1 and 6.2:



In general, very good agreement between the calculated reaction enthalpies and experimental values was obtained. Except for  $(\text{CH}_3)_2\text{CCN}^-$ , where the calculated value is slightly above the experimental result by  $0.2 \text{ kcal mol}^{-1}$ , the calculations underestimate the exothermicities by  $0.1\text{--}3.3 \text{ kcal mol}^{-1}$ . The correlation between the measured reaction efficiency and the experimental exothermicity for each of the nine systems is represented in Figure 6.1. The logarithm of the reaction efficiency has an approximately linear relationship to the exothermicity; similar correlations have been reported in the literature for other gas phase ion-molecule reactions (Ren et al. 2007; Villano et al. 2009; Wu et al. 2009). However, some exceptions are observed in this study. For example, in the reactions of increasing size of the nitrile anions ( $\text{CH}_2\text{CN}^-$ ,  $\text{CH}_3\text{CHCN}^-$ , and  $(\text{CH}_3)_2\text{CCN}^-$ ) in group I, the exothermicity increases very slightly. The corresponding reaction efficiencies increase more substantially. As another example, for the reactions of group II species,  $\text{CH}_3\text{CH}_2\text{OC}(\text{O})\text{CH}_2^-$  has a higher exothermicity than  $\text{HC}(\text{O})\text{CH}_2^-$  and  $\text{CH}_3\text{C}(\text{O})\text{CH}_2^-$ , but its reaction efficiency is the lowest among these three anions. Therefore, exothermicity provides only a semiquantitative interpretation of the reaction

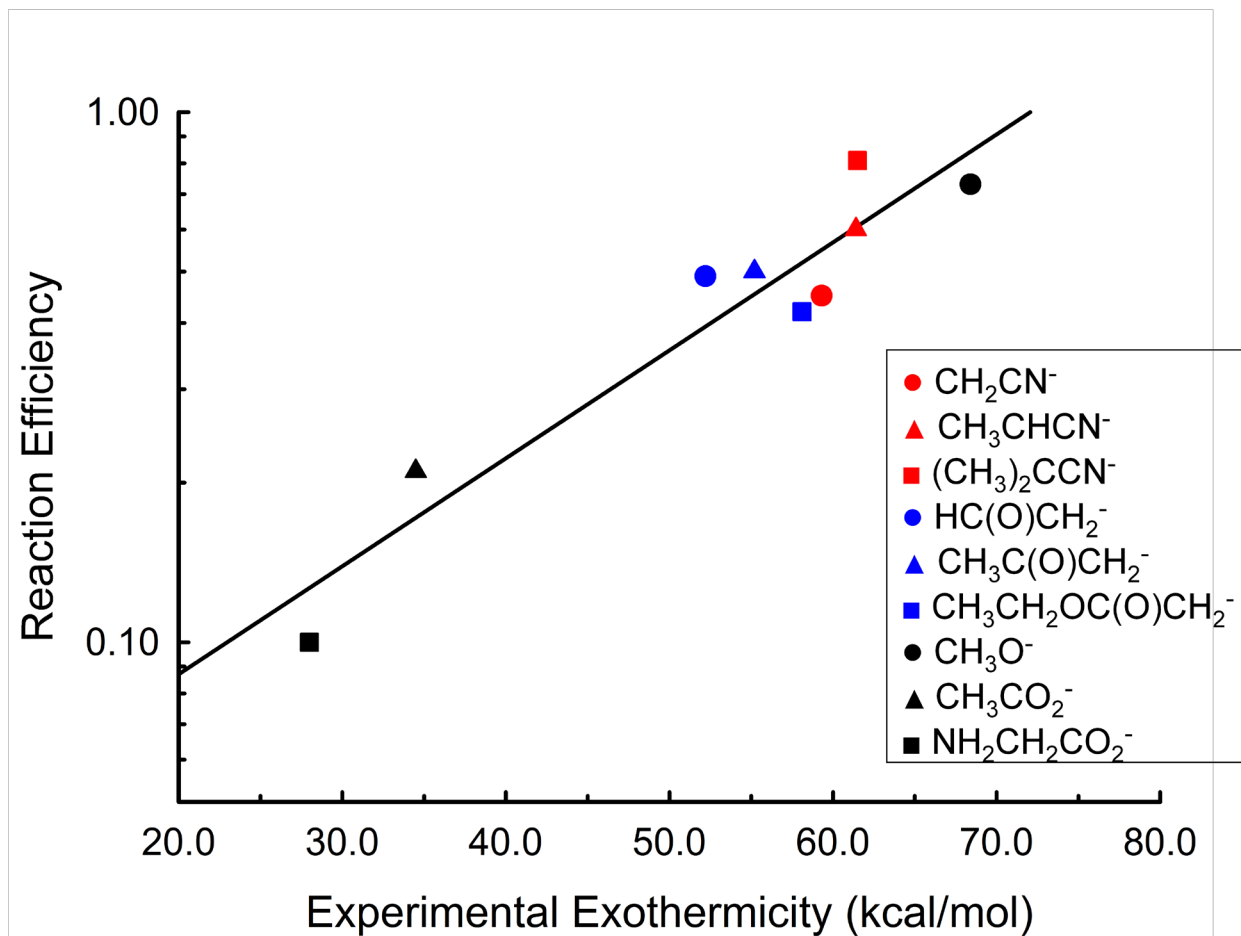
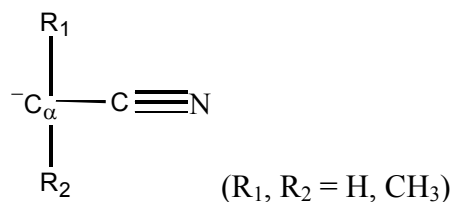


**Figure 6.1** The correlation between the logarithm of the reaction efficiency and experimental exothermicity. Symbols indicate the anions, and the line indicates the linear regression of all points. Experimental exothermicities were derived from Hess' law, as described in the text.

efficiency for the systems investigated here. More detailed studies are necessary for a complete understanding of anion-H atom reactions.

#### 6.4.1 Reactions of group I: deprotonated nitriles [ $\text{CH}_2\text{CN}^-$ , $\text{CH}_3\text{CHCN}^-$ , and $(\text{CH}_3)_2\text{CCN}^-$ ]

The reactions of deprotonated nitriles (Scheme 6.1, where  $\text{R}_1 = \text{R}_2 = \text{H}$  for  $\text{CH}_2\text{CN}^-$ ;  $\text{R}_1 = \text{H}$  and  $\text{R}_2 = \text{CH}_3$  for  $\text{CH}_3\text{CHCN}^-$ ;  $\text{R}_1 = \text{R}_2 = \text{CH}_3$  for  $(\text{CH}_3)_2\text{CCN}^-$ ) with H atoms occur by AD: H atom bonds to the  $\text{C}_\alpha$  carbon of the anions, and detachment of an electron produces neutral nitriles.



**Scheme 6.1**

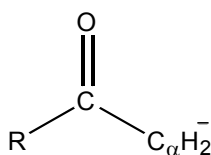
Theoretical calculations were carried out at the (RO)MP2(full)/aug-cc-pVTZ//MP2(full)/aug-cc-pVDZ level of theory to investigate the proposed reaction mechanisms and calculate the reaction exothermicities. As summarized in Table 6.1, the calculated exothermicities are in good agreement with the experimental results for all three nitrile anions.

The reaction efficiencies of nitrile anions increase in the order  $\text{CH}_2\text{CN}^-$  (0.44) <  $\text{CH}_3\text{CHCN}^-$  (0.59) <  $(\text{CH}_3)_2\text{CCN}^-$  (0.76), whereas the corresponding reaction exothermicities increase only slightly in the order  $\text{CH}_2\text{CN}^-$  ( $59.3 \pm 2.1 \text{ kcal mol}^{-1}$ ) <  $\text{CH}_3\text{CHCN}^-$  ( $61.4 \pm 2.1 \text{ kcal mol}^{-1}$ ) <  $(\text{CH}_3)_2\text{CCN}^-$  ( $61.5 \pm 2.2 \text{ kcal mol}^{-1}$ ), indicating that in this system, the reaction efficiency is not exclusively determined by the reaction exothermicity. Instead, the reaction efficiency trend can be rationalized by the decreased electron density on the  $\text{C}_\alpha$  carbon due to

charge redistribution that is induced by the methyl ( $-\text{CH}_3$ ) substituent. For the anion-H atom reaction, the collision rate constant is mainly determined by the long-range charge-induced dipole interaction. However, upon the formation of a new C–H bond at short distances, the electrostatic repulsion between the negatively charged  $\text{C}_\alpha$  carbon on the anion and the unpaired electron on the H atom may result in decreased affinity between them, thus leading to a lower reaction efficiency. Because carbon has a higher electronegativity than hydrogen, and methyl is more polarizable than hydrogen atom, the substitution of  $-\text{CH}_3$  for  $-\text{H}$  in the anions allows transfer of some of the negative charge on the  $\text{C}_\alpha$  carbon to the  $-\text{CH}_3$  group. Therefore, the reduced negative charge density on the  $\text{C}_\alpha$  carbon allows higher affinity for the H atom during the new C–H bond formation. This explanation is supported by the NBO computational results obtained at the MP2(full)/aug-cc-pVTZ level of theory: the reaction efficiency increases as the  $\text{C}_\alpha$  carbon negative charge decreases in the order of  $\text{CH}_2\text{CN}^-$  (-0.984 e) >  $\text{CH}_3\text{CHCN}^-$  (-0.741 e) >  $(\text{CH}_3)_2\text{CCN}^-$  (-0.549 e).

#### 6.4.2 Reactions of group II: deprotonated acetaldehyde ( $\text{HC}(\text{O})\text{CH}_2^-$ ), acetone ( $\text{CH}_3\text{C}(\text{O})\text{CH}_2^-$ ), and ethyl acetate ( $\text{CH}_3\text{CH}_2\text{OC}(\text{O})\text{CH}_2^-$ )

These anions are classified together because of the similarity of their structures, as shown in scheme 6.2.



**Scheme 6.2**

Here R = H, CH<sub>3</sub>, and CH<sub>3</sub>CH<sub>2</sub>O for HC(O)CH<sub>2</sub><sup>-</sup>, CH<sub>3</sub>C(O)CH<sub>2</sub><sup>-</sup>, and CH<sub>3</sub>CH<sub>2</sub>OC(O)CH<sub>2</sub><sup>-</sup>, respectively. The reactions of these anions occur by AD: H atom bonds to the C<sub>α</sub> carbon on the anions to produce the corresponding neutral species via electron detachment. Theoretical calculations were carried out to investigate the reaction mechanisms proposed. As shown in Table 6.1, calculated exothermicities are in good agreement with the experimental results, and the reaction exothermicity slightly increases as the size of the substituent group increases.

In this system the reaction efficiencies are not directly correlated to the exothermicities: the reaction efficiencies of these three species exhibit a trend as CH<sub>3</sub>CH<sub>2</sub>OC(O)CH<sub>2</sub><sup>-</sup> (0.41) < CH<sub>3</sub>C(O)CH<sub>2</sub><sup>-</sup> (0.49) = HC(O)CH<sub>2</sub><sup>-</sup> (0.49). In contrast, their exothermicities decrease in the order of CH<sub>3</sub>CH<sub>2</sub>OC(O)CH<sub>2</sub><sup>-</sup> (58.1 ± 4.1 kcal mol<sup>-1</sup>) > CH<sub>3</sub>C(O)CH<sub>2</sub><sup>-</sup> (55.2 ± 2.0 kcal mol<sup>-1</sup>) > HC(O)CH<sub>2</sub><sup>-</sup> (52.2 ± 2.2 kcal mol<sup>-1</sup>). The reaction efficiencies are inversely correlated to the partial negative charges on the C<sub>α</sub> carbon that are obtained from NBO analyses:

CH<sub>3</sub>CH<sub>2</sub>OC(O)CH<sub>2</sub><sup>-</sup> (-0.827 e) > CH<sub>3</sub>C(O)CH<sub>2</sub><sup>-</sup> (-0.790 e) ≈ HC(O)CH<sub>2</sub><sup>-</sup> (-0.789 e). In agreement with the trends for the group I anions, this result implies that the interaction between the negatively charged C<sub>α</sub> carbon on the anion and the unpaired electron on the H atom plays an important role in determining the efficiency of forming a new C–H bond.

### 6.4.3 Reactions of group III: deprotonated methanol (CH<sub>3</sub>O<sup>-</sup>), acetic acid (CH<sub>3</sub>CO<sub>2</sub><sup>-</sup>), and glycine (NH<sub>2</sub>CH<sub>2</sub>CO<sub>2</sub><sup>-</sup>)

The experimental results for NH<sub>2</sub>CH<sub>2</sub>CO<sub>2</sub><sup>-</sup> were adopted from our previous work (Snow et al. 2009). All three reactions proceed through AD, in which H atom bonds to the negatively charged O atom in the anions. However, significantly different reaction efficiencies were observed for CH<sub>3</sub>O<sup>-</sup>, CH<sub>3</sub>CO<sub>2</sub><sup>-</sup>, and NH<sub>2</sub>CH<sub>2</sub>CO<sub>2</sub><sup>-</sup>: CH<sub>3</sub>O<sup>-</sup> (0.72) > CH<sub>3</sub>CO<sub>2</sub><sup>-</sup> (0.21) >

$\text{NH}_2\text{CH}_2\text{CO}_2^-$  (0.09). This trend is generally correlated to the reaction exothermicities that decrease as  $\text{CH}_3\text{O}^-$  ( $68.4 \pm 1.0 \text{ kcal mol}^{-1}$ )  $>$   $\text{CH}_3\text{CO}_2^-$  ( $34.5 \pm 2.2 \text{ kcal mol}^{-1}$ )  $>$   $\text{NH}_2\text{CH}_2\text{CO}_2^-$  ( $28.0 \pm 2.1 \text{ kcal mol}^{-1}$ ). The reaction efficiencies of the acetate anions are very low despite their moderate reaction exothermicities. Other factors are likely influencing the reaction efficiencies.

In order to investigate the potential energy curve along the approach of the reactants, relaxed potential energy scans were performed at the B3LYP/6-31+G(d,p) level of theory. The association of  $\text{CH}_3\text{O}^-$  with H atom proceeds through an attractive potential energy curve to form a transient species ( $\text{CH}_3\text{OH}^{\bullet-}$ ) as shown in Figure 6.2. This species can form neutral  $\text{CH}_3\text{OH}$  by electron detachment. Because of the high exothermicity and the barrierless potential energy curve along the approach of the reactants, this reaction has fairly high efficiency (0.72). In contrast, the potential energy curve describing the association of  $\text{CH}_3\text{CO}_2^-$  with H atom (Figure 6.3) is attractive at large O $\cdots$ H distances ( $> 1.943 \text{ \AA}$ ) because of the charge-induced dipole interaction. However, closer approach of the reactants results in slightly increased energy until they form a transition state at a distance of  $1.393 \text{ \AA}$ . A complete reaction coordinate was constructed from calculations performed at the higher level of theory (RO)MP2(full)/aug-cc-pVTZ//MP2(full)/aug-cc-pVDZ. Passage through this transition state is the rate-determining step of the reaction, and the calculated energy barrier is  $1.7 \text{ kcal mol}^{-1}$  above the total energy of the reactants. More accurate results were obtained from the CCSD(T)/aug-cc-pVTZ//MP2(full)/aug-cc-pVDZ level of theory. The transition state is slightly below the total energy of the reactants by  $0.9 \text{ kcal mol}^{-1}$ , such that the low reaction efficiency (0.21) is attributed to an energy barrier hindering the access of the reactants.

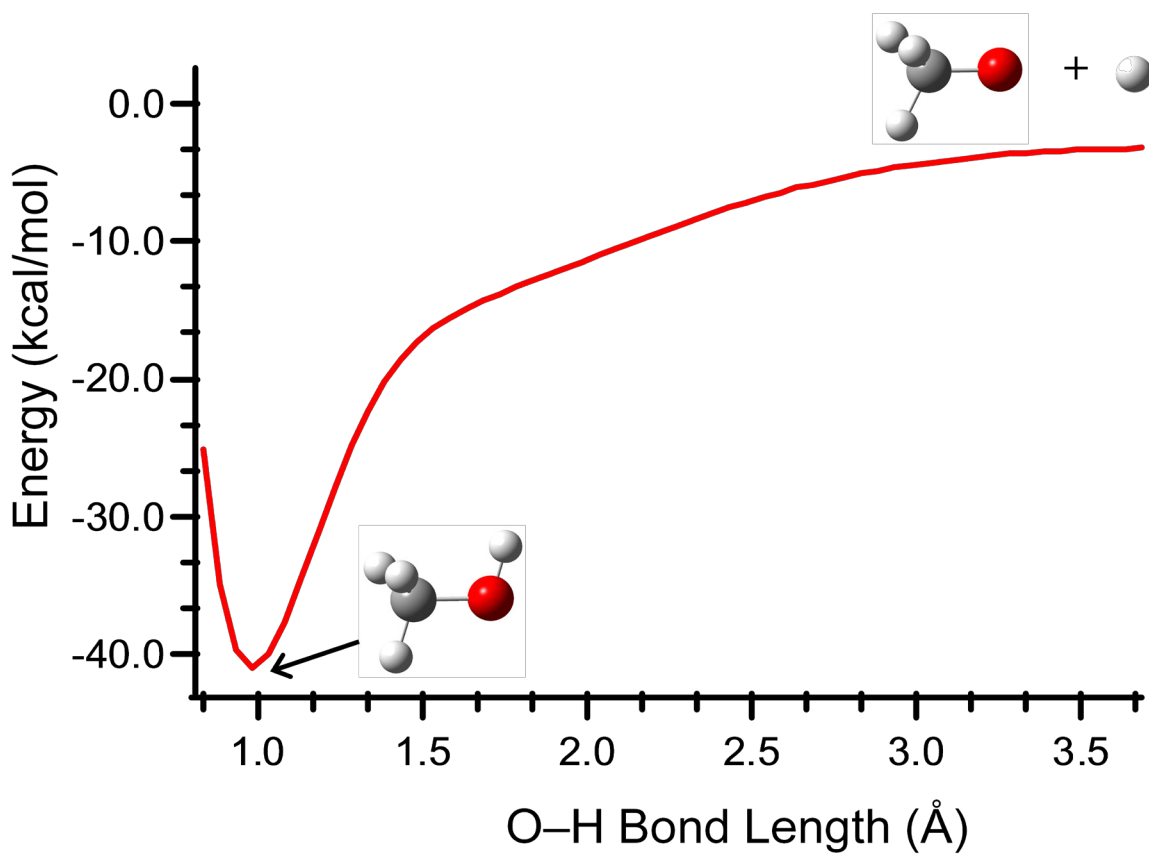


**Figure 6.2** The relaxed potential energy surface scan of the entrance channel of the  $\text{CH}_3\text{O}^- + \text{H}$  reaction at the B3LYP/6-31+G(d,p) level of theory.

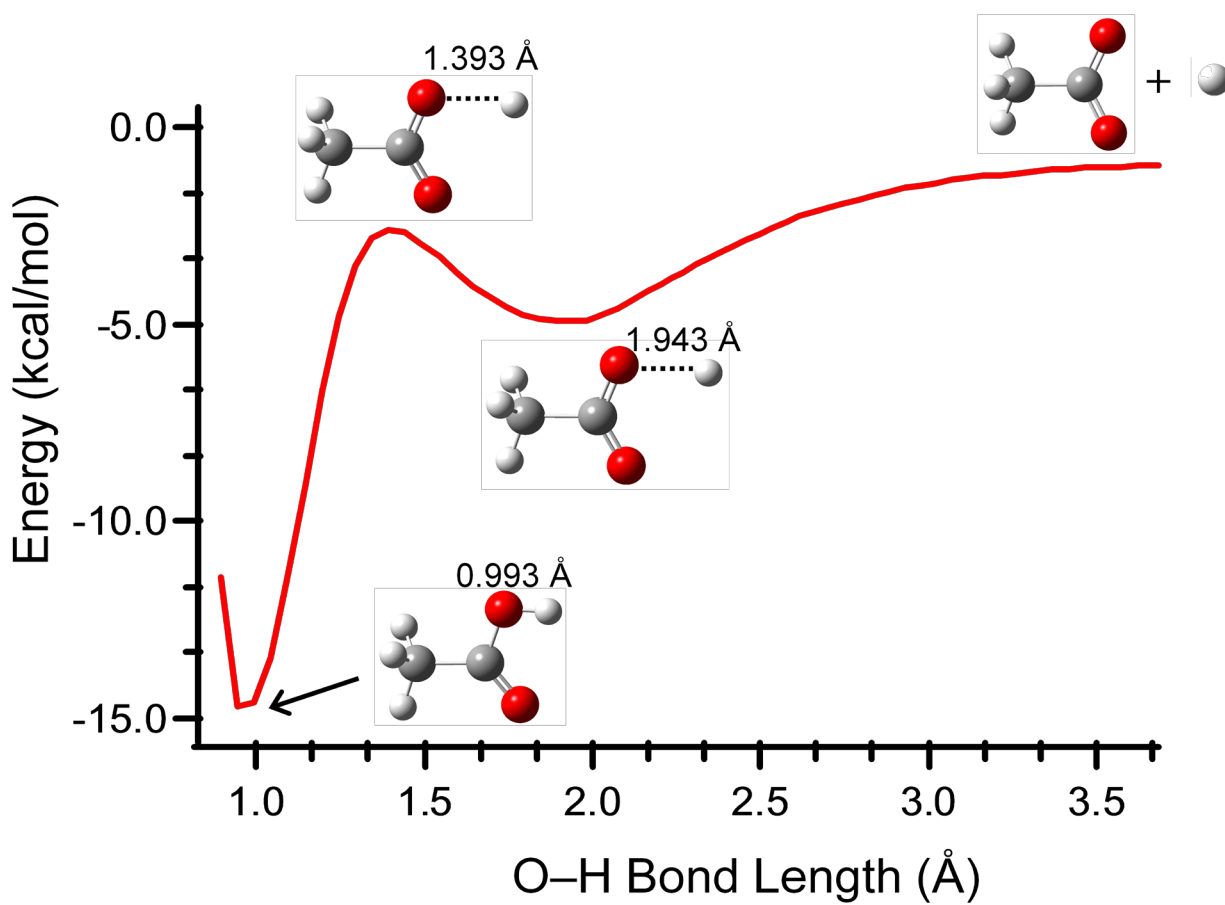


**Figure 6.3** The relaxed potential energy surface scan of the entrance channel of the  $\text{CH}_3\text{CO}_2^- + \text{H}$  reaction at the B3LYP/6-31+G(d,p) level of theory.

The reaction between  $\text{NH}_2\text{CH}_2\text{CO}_2^-$  and H atom exhibits an even lower reaction efficiency (0.09), indicating the existence of a higher energy barrier along the reaction coordinate. The computational results obtained from the (RO)MP2(full)/aug-cc-pVTZ//MP2(full)/aug-cc-pVDZ level of theory show that this energy barrier is slightly above the reactants by  $2.9 \text{ kcal mol}^{-1}$ . In contrast calculations performed at the CCSD(T)/aug-cc-pVTZ//MP2(full)/aug-cc-pVDZ level of theory indicate that this transition state energy is only above the reactants by  $0.3 \text{ kcal mol}^{-1}$ . Although other higher level calculations may provide more reliable results, our current computations are sufficient to indicate that the reaction efficiency of  $\text{CH}_3\text{CO}_2^-$  and  $\text{NH}_2\text{CH}_2\text{CO}_2^-$  with H atom is correlated to the transition-state energy-barrier height. Under our experimental conditions, the reactants have a thermal distribution of kinetic and internal energies, such that only the reactants possessing enough energy can pass over the barrier, and the portion of these reactants is likely correlated to the corresponding reaction efficiency.

To completely explore the potential energy profile along the approach of the reactants, the B3LYP/6-31+G(d,p) relaxed potential energy scans were also carried out for the other seven reactions. The results show that only the reactions of  $\text{CH}_3\text{CO}_2^-$  and  $\text{NH}_2\text{CH}_2\text{CO}_2^-$  exhibit an energy barrier upon association, indicating that the acetate group possesses a unique property in the anion-H atom reaction. In fact, the acetate anions ( $\text{R-CO}_2^-$ ) have a resonance structure stabilizing the negative charge. This resonance stabilization is destroyed as the H atom approaches the carboxylate group; the resulting charge redistribution results in destabilization of the system, and therefore, an energy barrier on the potential energy curve.

#### 6.4.4 Anion-H-atom reaction efficiencies

Our experimental results show that the efficiencies of all anion-H-atom reactions are less than unity. As discussed above, approach of reactants to form the transition species is a critical step during the reactions. For example, the energy barriers along the approach of acetate anions ( $\text{CH}_3\text{CO}_2^-$  and  $\text{NH}_2\text{CH}_2\text{CO}_2^-$ ) and H atoms inhibit the reaction process, even though these reactions have moderate exothermicities. For the barrierless reactions, i.e., group I and II, the partial charge on the  $\text{C}_\alpha$  carbon of the anions affects the efficiency of new  $\text{C}_\alpha\text{-H}$  bond formation and influences the reactivity. In addition, angular momentum conservation is likely to be a factor influencing these reactions. During the anion-H-atom collisions, the two species can form a rapidly rotating complex because of angular momentum conservation (Koizumi et al. 2003 & 2004), then develop a new chemical bond by ejecting an electron to form a neutral product. However, for collisions with high angular momentum, reactants may not associate efficiently because of the very low mass of the H atom, and reactions may not occur.

#### 6.5 Conclusions

The recent detections of anions in the ISM have highlighted the important role they may play in interstellar chemistry. Further observations may continue to reveal additional molecular anions. To further develop an understanding of possible anion chemistry in the ISM, we have explored reactions of possible interstellar candidates ( $\text{CH}_2\text{CN}^-$ ,  $\text{CH}_3\text{CHCN}^-$ ,  $(\text{CH}_3)_2\text{CCN}^-$ ,  $\text{HC(O)CH}_2^-$ ,  $\text{CH}_3\text{C(O)CH}_2^-$ ,  $\text{CH}_3\text{CH}_2\text{OC(O)CH}_2^-$ ,  $\text{CH}_3\text{O}^-$ , and  $\text{CH}_3\text{CO}_2^-$ ) with H atom using experimental and theoretical methods. The sole reaction channel is AD, in which the H atom bonds to the anion and a stable neutral species is formed by the ejection of an electron. In the reactions of group I and II anions, the reaction efficiency increases as the  $\text{C}_\alpha$  partial negative

charge on the anion decreases. This trend is attributed to the reduced electrostatic repulsion between the negative charge on the  $C_{\alpha}$  atom and the unpaired electron on H atom upon formation of the new C–H bond. On the other hand, the anions  $CH_3CO_2^-$  and  $NH_2CH_2CO_2^-$  exhibit fairly low reaction efficiencies in spite of their moderate reaction exothermicities. This phenomenon is explained by the unique energy barrier along the approach of the reactants, which does not exist for other species (as shown by the calculations).

Our current results indicate that the reaction efficiencies of anions with H atoms are largely determined by their reaction exothermicity. In addition, the charge density on the reactive site of the anion, the characteristics of the reaction coordinate curve, and angular-momentum conservation of the anion-H-atom collision may play important roles in some systems. This study of anion-H atom reactions enhances our understanding from both experimental and theoretical perspectives, enriching our knowledge of negative ion chemistry in the interstellar medium.

## 6.6 References

- Agúndez, M., Cernicharo, J., Guélin, M., Kahane, C., Roueff, E., Klos, J., Aoiz, F. J., Lique, F., Marcelino, N., Goicoechea, J. R., González García, M., Gottlieb, C. A., McCarthy, M. C., & Thaddeus, P. 2010, *A&A* 517:L2.
- Barkholtz, C., Snow, T. P., & Bierbaum, V. M. 2001, *ApJ*, 547, L171.
- Brünken, S., Gupta, H., Gottlieb, C. A., McCarthy, M. C.; & Thaddeus, P. 2007, *ApJ*, 664, L43.
- Cernicharo, J., Guélin, M., Agúndez, M., Kawaguchi, K., McCarthy, M., & Thaddeus, P. 2007, *A&A*, 467, L37.
- Cernicharo, J., Guélin, M., Agúndez, M., McCarthy, M. C., & Thaddeus, P. 2008, *ApJ*, 688, L83.
- Cunningham, M. R., Jones, P. A., Godfrey, P. D., Cragg, D. M., Bains, I., Burton, M. G., Calisse, P., Crighton, N. H. M., Curran, S. J., Davis, T. M., Dempsey, J. T., Fulton, B., Hidas, M. G., Hill, T., Kedziora-Chudczer, L., Minier, V., Pracy, M. B., Purcell, C., Shobbrook, J., & Travouillon, T., 2007, *MNRAS*, 376, 1201.
- Eichelberger, B. R., Snow, T. P., & Bierbaum, V. M. 2003, *J. Am. Soc. Mass Spectrom.*, 14, 501.
- Fehsenfeld, F. C., Howard, C. J., & Ferguson, E. E. 1973, *J. Chem. Phys.*, 58, 5841.
- Ferguson, E. E., Fehsenfeld, F. C., & Schmeltekopf, A. L. 1969, *Adv. At. Mol. Phys.*, 5, 1.
- Frisch, M. J., Trucks, G. W., Schlegel, H. B., Scuseria, G. E., Robb, M. A., Cheeseman, J. R., Montgomery, Jr., J. A., Vreven, T., Kudin, K. N., Burant, J. C., Millam, J. M., Iyengar, S. S., Tomasi, J., Barone, V., Mennucci, B., Cossi, M., Scalmani, G., Rega, N., Petersson, G. A., Nakatsuji, H., Hada, M., Ehara, M., Toyota, K., Fukuda, R., Hasegawa, J., Ishida, M., Nakajima, T., Honda, Y., Kitao, O., Nakai, H., Klene, M., Li, X., Knox, J. E., Hratchian, H. P., Cross, J. B., Bakken, V., Adamo, C., Jaramillo, J., Gomperts, R., Stratmann, R. E., Yazyev, O., Austin, A. J., Cammi, R., Pomelli, C., Ochterski, J. W., Ayala, P. Y., Morokuma, K., Voth, G. A., Salvador, P., Dannenberg, J. J., Zakrzewski, V. G., Dapprich, S., Daniels, A. D., Strain, M. C., Farkas, O., Malick, D. K., Rabuck, A. D., Raghavachari, K., Foresman, J. B., Ortiz, J. V., Cui, Q., Baboul, A. G., Clifford, S., Cioslowski, J., Stefanov, B. B., Liu, G., Liashenko, A., Piskorz, P., Komaromi, I., Martin, R. L., Fox, D. J., Keith, T., Al-Laham, M. A., Peng, C. Y., Nanayakkara, A., Challacombe, M., Gill, P. M. W., Johnson, B., Chen, W., Wong, M. W., Gonzalez, C., & Pople, J. A., *Gaussian 03*, Revision C.02, Gaussian, Inc., Wallingford CT, 2004.
- Howard, C. J., Fehsenfeld, F. C., & McFarland, M. 1974, *J. Chem. Phys.*, 60, 5086.
- Jones, P. A., Cunningham, M. R., Godfrey, P. D., & Cragg, D. M. 2007, *MNRAS*, 374, 579.
- Koizumi, H. & Armentrout, P. B. 2003, *J. Chem. Phys.*, 119, 12819.
- Koizumi, H., Muntean, F., & Armentrout, P. B. 2004, *J. Chem. Phys.*, 120, 756.
- Kuan, Y.-J., Charnley, S. B., Huang, H.-C., Tseng, W.-L., & Kisiel, Z. *ApJ* 2003, 593, 848.

- Linstrom, P. J., & Mallard, W. G. Eds., NIST Chemistry WebBook, *NIST Standard Reference Database* Number 69, National Institute of Standards and Technology, Gaithersburg MD, 20899, <http://webbook.nist.gov>, (retrieved November 3, 2009).
- Martinez Jr., O., Yang, Z., Betts, N. B., Snow, T. P., & Bierbaum, V. M. 2009, *ApJ*, 705, L172.
- McCarthy, M. C., Gottlieb, C. A., Gupta, H., & Thaddeus, P. 2006, *ApJ*, 652, L141.
- Remijan, A. J., Hollis, J. M., Lovas, F. J., Cordiner, M. A., Millar, T. J., Markwick-Kemper, A. J., & Jewell, P. R. 2007, *ApJ*, 664, L47.
- Ren, Y. & Yamataka, H. 2007, *J. Org. Chem.*, 72, 5660.
- Snow, T. P. & Bierbaum, V. M. 2008, *Annu. Rev. Anal. Chem.*, 1, 229.
- Snow, T. P. & McCall, B. J. 2006, *ARA&A*, 44, 367.
- Snow, T. P., Stepanovic M., Betts, N. B., Eichelberger, B. R., Martinez Jr. O., & Bierbaum, V. M. 2009, *Astrobio.*, 9, 1001.
- Snyder, L. E., Lovas, F. J., Hollis, J. M., Friedel, D. N., Jewell, P. R., Remijan, A., Ilyushin, V. V., Alekseev, E. A., & Dyubko, S. F. 2005, *ApJ*, 619, 914.
- Thaddeus, P., Gottlieb, C. A., Gupta, H., Brünken, S., McCarthy, M. C., Agúndez, M., Guélin, M., & Cernicharo, J. 2008, *ApJ*, 677, 1132.
- Trainor, D. W., Ham, D. O., & Kaufman, F. 1973, *J. Chem. Phys.*, 58, 4599.
- Villano, S. M., Eyet, N., Lineberger W. C., & Bierbaum, V. M. 2009, *J. Am. Chem. Soc.*, 131, 8227.
- Walsh, C., Harada, N., Herbst, E., & Millar, T. J. 2009, *ApJ*, 700, 752.
- Wu, X. P., Sun, X. M., Wei, X. G., Ren, Y., Wong, N. B., & Li, W. K. 2009, *J. Chem. Theory Comput.*, 5, 1597.
- Yang, Z., Eichelberger, B., Martinez Jr., O., Stepanovic, M., Snow, T. P., & Bierbaum, V. M. 2010a, *J. Am. Chem. Soc.*, 132, 5812.
- Yang, Z., Snow, T. P., & Bierbaum, V. M. 2010b, *Phys. Chem. Chem. Phys.*, 12, 13091.

## Chapter 7

### Experimental and Theoretical Studies of Reactions Between H Atoms and Nitrogen-Containing Carbon-Chain Anions

#### 7.1 Introduction

Although the physical conditions in the interstellar medium (ISM) are seemingly unfavorable for reactions (e.g., low particle density and temperature), a very rich chemistry exists in these regions (Snow & McCall 2006; Snow & Bierbaum 2008; Herbst & van Dishoeck). More than 160 molecular species have been detected in the ISM, and it is very likely that many more undetected neutral and ionic species exist in space (Williams 2002). Therefore an understanding of gas-phase ion chemistry is a critical aspect of astrochemical studies. Among the discovered species, six anions have been detected in the denser regions of the ISM, i.e.,  $\text{HC}_n^-$  ( $n = 2, 4, \text{ and } 6$ ) and  $\text{C}_n\text{N}^-$  ( $n = 1, 3, \text{ and } 5$ ) (McCarthy et al. 2006; Brünken et al. 2007; Cernicharo et al. 2007 & 2008; Remijan et al. 2007; Thaddeus et al. 2007; Agúndez et al. 2010), indicating that anions are involved in the chemical reactions within the ISM. Study of the corresponding ion-neutral reactions, especially with abundant species (i.e., atomic and molecular hydrogen) is crucial to understanding the ion chemistry and chemical transformations. Rate constants are important for astrochemical modeling to establish the reaction networks among species in the ISM.

Our recent studies indicate that associative detachment (AD) is a common pathway for anion-H atom reactions. For example, reactions involving some typical molecular anions proceed through AD (Snow et al. 2009; Yang et al. 2010c); however, carbon chain anions exhibit both AD ( $\text{HC}_n^-$ ,  $n = 2, 4, 6, \text{ and } 7$  and  $\text{C}_n^-$ ,  $n = 2, 4 - 10$ ) and association ( $\text{C}_n^-$ ,  $n = 7 - 10$ )

pathways (Barckholtz et al. 2001). These reactions can be critical in determining the ionization balance between anions and free electrons (Snow & McCall 2006; Snow & Bierbaum 2008; Walsh et al. 2009).

In addition to the reaction mechanisms, reaction efficiencies are important characteristics of anion-atom reactions. In reactions between carbon-chain anions, i.e.,  $\text{HC}_n^-$  ( $n = 2, 4, 6,$  and  $7$ ) and  $\text{C}_n^-$  ( $n = 2, 4 - 10$ ), and H atoms, reaction efficiencies are generally around 0.3–0.4; there is no obvious trend between efficiencies and characteristics of reactions, (e.g., reaction exothermicities, electronic spin states of reactants, and size of anions). In contrast, reactions between some typical molecular anions and H atoms exhibit some clear trends; reaction efficiencies are largely proportional to the logarithm of the reaction exothermicity. In addition, other factors may also exist, including the charge density on the reactive site of the anion, the characteristics of the potential energy surfaces along the approach of the reactants, and the angular momentum conservation of the anion-H atom collision. Therefore, additional studies of anion-H atom reactions are necessary to obtain both fundamental understanding and a general overview of these reactions.

In the current work, experimental and theoretical studies were carried out for three categories of anions that are classified by the number of N atoms in the structures. These anions include  $\text{C}_n\text{N}^-$  ( $n = 1 - 6$ ),  $\text{C}_n\text{N}_2^-$  ( $n = 1, 3, 4,$  and  $5$ ), and  $\text{C}_n\text{N}_3^-$  ( $n = 2$  and  $4$ ). A series of *ab initio* theoretical calculations was carried out at several levels of theory to explore the reaction mechanisms and investigate the factors influencing the reaction efficiencies.

## 7.2 Experimental Methods

Ions were generated using the cold-cathode discharge method of ionization (Leopold et al. 1987). A graphite rod is biased relative to the source flow tube at  $\sim -4$  kV ( $\sim 10$  mA DC),

producing a discharge; liquid water flows through a hollow sleeve portion of a stainless steel rod supporting the graphite, maintaining a stable discharge by conductively cooling the graphite rod. Helium serves as a carrier gas and N<sub>2</sub> serves as a discharge medium. The addition of N<sub>2</sub> also results in chemical ionization leading to the formation of the C<sub>n</sub>N<sub>x</sub><sup>-</sup> ions of our study. Due to the very low intensity of anions generated under our current experimental conditions, the anions were not mass-selected with the selected ion flow tube (SIFT) quadrupole mass filter; instead, all anions were allowed to pass through the quadrupole, using the RF-only mode, and then injected into the reaction flow tube through a Venturi inlet. The ions were entrained in helium buffer gas (0.4 Torr, 200 std cm<sup>3</sup> s<sup>-1</sup>) at 298 K, and relaxed by multiple collisions. The ion-neutral reaction was initiated by adding H atoms to the flow tube; the reactant ions were monitored with a quadrupole mass filter coupled with an electron multiplier. Because the relative population of H atoms is about 10<sup>6</sup> higher than anions, the reactions occur under pseudo-first order conditions, such that the presence of other anions has no influence on our measurements. However, the possible product ions can not be discriminated from other existing ions; therefore, product ions and branching ratios of reactions were not investigated in this study.

The reactant hydrogen atoms are formed via thermal dissociation (Martinez et al. 2009; Trainor et al. 1973). A flow of H<sub>2</sub> gas (~9 std cm<sup>3</sup> s<sup>-1</sup>, Airgas Inc., 99.999%) is passed through a molecular sieve trap immersed in liquid nitrogen, over a heated tungsten filament, and through a second trap and filament assembly. Teflon tubing (0.25 inch ID), used to minimize recombination, then transfers the H atoms from the thermal dissociator into the reaction flow tube. The inlet is positioned 35 cm downstream of the Venturi inlet to allow development of the laminar profile and collisional relaxation of ions, and 70 cm upstream of the ion sampling orifice to allow adequate reaction time. The concentration of hydrogen atoms was determined by

monitoring the loss of chloride ions in the AD reaction with hydrogen atoms. The rate constant for the reaction  $\text{Cl}^- + \text{H} \rightarrow \text{HCl} + e^-$  has been reported in studies from the NOAA laboratory in Boulder (Ferguson et al. 1969; Fehsenfeld et al. 1973; Howard et al. 1974), which are in good agreement, indicating that this reaction provides an excellent calibration for the hydrogen atom concentration. The error bars shown in Tables 7.1 and 7.2 represent one standard deviation of the mean of 2–4 measurements of the anion-H atom reactions under varied conditions of helium and H atom concentration. This error is combined with the uncertainty in the H atom concentration measurement and systematic errors, and the total error is estimated as  $\pm 50\%$ .

### 7.3 Theoretical Calculations

To obtain the structures and energies of species involved in the current study, theoretical calculations were carried out using the *Gaussian 03* suite of programs (Frisch et al. 2004). In order to obtain reliable energetics with limited computational resources, the geometry optimization and frequency analyses were calculated at the B3LYP/aug-cc-pVTZ level of theory, whereas the single-point energy calculations were carried out at the CCSD(T)/aug-cc-pVDZ level of theory for the optimized structures. Zero-point energy (ZPE) and thermal-energy (298 K) corrections were included using the same level of theory for geometry optimization. This level of theory provides a good combination of computational accuracy and efficiency, and it has been successfully employed in our previous study of carbon-chain anions with N and O atom (Yang et al. 2010a). The computational results were used to construct the reaction coordinate plots of four selected systems and to calculate the enthalpies of all reactions involved in the current study.

### 7.4 Results and Discussion

Reactant anions were allowed to react with H atoms, where the anions include deprotonated nitrogen-containing carbon-chain species  $\text{C}_n\text{N}^-$  ( $n = 1 - 6$ ),  $\text{C}_n\text{N}_2^-$  ( $n = 1, 3, 4$ , and

**Table 7.1** Kinetic data for reactions between  $C_nN^-$  ( $n=1-6$ ) and H atom.

Anion <sup>a</sup>	$k_{\text{exp}}$ ( $10^{-10}$ cm <sup>3</sup> /s)	Efficiency <sup>b</sup> ( $k_{\text{exp}}/k_{\text{PPI}}$ )	$\Delta H^{\text{a,c}}$ {0 K kcal/mol} [298 K kcal/mol]
CN <sup>-</sup> (S)	$5.9 \pm 0.1$	0.27	HCN (S) {-33.3} [-33.2] HNC (S) {-19.5} [-19.2]
C <sub>2</sub> N <sup>-</sup> (T)	$6.0 \pm 0.2$	0.26	HC <sub>2</sub> N (S) {-20.7} [-20.3] HC <sub>2</sub> N (T) {-32.5} [-31.9] CC(H)N (S) {-22.7} [-22.7] <i>c</i> -HC <sub>2</sub> N (S) {-19.3} [-19.2] <i>c</i> -HC <sub>2</sub> N (T) {-31.8} [-31.6] CN <sup>-</sup> (S) + CH (D) {-12.2} [-10.4]
C <sub>3</sub> N <sup>-</sup> (S)	$5.4 \pm 0.1$	0.23	HC <sub>3</sub> N (S) {-30.4} [-30.3]
C <sub>4</sub> N <sup>-</sup> (T)	$4.9 \pm 1.3$	0.21	HC <sub>4</sub> N (S) {-11.8} [-11.5] HC <sub>4</sub> N (T) {-24.5} [-24.0] <i>c</i> -CC(H)C <sub>2</sub> N (S) {-29.5} [-29.7] C <sub>2</sub> CHCN (D) {-16.4} [-16.2] C <sub>3</sub> <sup>-</sup> (D) + HCN (S) {-9.0} [-7.7]
C <sub>5</sub> N <sup>-</sup> (S)	$6.4 \pm 0.2$	0.26	HC <sub>5</sub> N (S) {-26.3} [-26.2]
C <sub>6</sub> N <sup>-</sup> (T)	$8.0 \pm 0.8$	0.32	HC <sub>6</sub> N (S) {-10.5} [-10.1] HC <sub>6</sub> N (T) {-24.9} [-24.7] C <sub>4</sub> C(H)CN (S) {-10.3} [-10.2] C <sub>2</sub> C(H)C <sub>3</sub> N (S) {-10.9} [-10.8] CC(H)C <sub>4</sub> N (S) {-24.4} [-24.6] CN <sup>-</sup> (S) + C <sub>5</sub> H (D) {-25.4} [-24.2]

<sup>a</sup> The ground state of reactant anions. Calculations were performed at the CCSD(T)/aug-cc-pVDZ//B3LYP/aug-cc-pVTZ level of theory including zero-point energy corrections. Letters in parentheses indicate the spin state of the species, *i.e.*, singlet (S), doublet (D), and triplet (T).

<sup>b</sup>  $k_{\text{PPI}}$  is the point-polarizable ion model theoretical rate constant (Eichelberger et al. 2003).

<sup>c</sup> Energies are relative to the corresponding reactants (ground-state anion and the H atom). The letter “c” as a prefix for a chemical formula indicates the cyclic structure. The numbers in parentheses indicate the calculated reaction enthalpies at 0 and 298 K.

**Table 7.2** Kinetic data for reactions between  $C_nN_2^-$  ( $n=1, 3-5$ ) and H atom.

Anions <sup>a</sup>	$k_{\text{exp}}$ ( $10^{-10}$ cm <sup>3</sup> /s)	Efficiency <sup>b</sup> ( $k_{\text{exp}}/k_{\text{PPI}}$ )	$\Delta H^{\text{a,c}}$ {0 K kcal/mol} [298 K kcal/mol]
NCN <sup>-</sup> (D)	$5.6 \pm 0.1$	0.23	HNCN (D) {-25.1} [-24.7]
NC <sub>3</sub> N <sup>-</sup> (D)	$5.1 \pm 0.8$	0.22	NCC(H)CN (D) {-25.5} [-25.3]
NC <sub>4</sub> N <sup>-</sup> (D)	$4.8 \pm 0.1$	0.20	NCC(H)C <sub>2</sub> N (D) {-11.9} [-11.9] CN <sup>-</sup> (S) + HC <sub>3</sub> N (S) {-43.5} [-42.7] C <sub>3</sub> N <sup>-</sup> (S) + HNC (S) {-32.5} [-31.5] C <sub>3</sub> N <sup>-</sup> (S) + HCN (S) {-46.4} [-45.5]
NC <sub>5</sub> N <sup>-</sup> (D)	$6.1 \pm 0.9$	0.25	NC <sub>2</sub> HC <sub>3</sub> N (D) {-18.5} [-18.6] C <sub>4</sub> N <sup>-</sup> (S) + HNC (S) {-6.5} [-5.5]

<sup>a</sup> The ground state of reactant anions. Calculations were performed at the CCSD(T)/aug-cc-pVDZ//B3LYP/aug-cc-pVTZ level of theory including zero-point energy corrections. Letters in the parentheses indicate the spin state of the species, *i.e.*, singlet (S), doublet (D), and triplet (T).

<sup>b</sup>  $k_{\text{PPI}}$  is the point-polarizable ion model theoretical rate constant (Eichelberger et al. 2003).

<sup>c</sup> Energies are relative to the corresponding reactants (ground state anion and the H atom). The letters in parentheses indicate the calculated reaction enthalpies at 0 and 298 K.

5), and  $C_nN_3^-$  ( $n = 2$  and  $4$ ); none of the anions react with  $H_2$ . The reactions proceed mainly by AD, in which the H atom bonds to the anion and an electron is ejected without further rearrangement ( $A^- + H \rightarrow AH + e^-$ ), although fragmentation is also likely to occur in some cases. Rate constants and efficiencies for reactions of the carbanions with H atoms are summarized in Table 7.1. Reaction efficiencies are reported as the ratio of experimental rate constant ( $k_{\text{exp}}$ ) to  $k_{\text{PPI}}$ , a point-polarizable-ion (PPI) model adjustment to traditional Langevin theory as detailed elsewhere (Eichelberger et al. 2003). Reaction enthalpies were calculated as summarized in Tables 7.1 and 7.2 as well as Tables 7.3 and 7.4. In general, the reaction efficiencies of  $C_nN^-$  ( $n = 1-6$ ) and  $C_nN_2^-$  ( $n = 1, 3, 4,$  and  $5$ ) systems are comparable, and there is no clear trend between reaction efficiencies and structures or reaction exothermicities. However,  $C_nN_3^-$  ( $n = 2$  and  $4$ ) are not reactive with H atoms. Therefore, detailed computational studies are necessary for a fundamental understanding of possible mechanisms and structures of species involved in reactions between nitrogen-containing carbon-chain anions and H atoms.

#### 7.4.1 Reactions of $C_nN^-$ ( $n = 1-6$ )

The reactions of  $C_nN^-$  ( $n = 1-6$ ) with H atoms occur mainly via AD: H atom bonds to the anions, and detachment of an electron produces neutral nitriles. Theoretical calculations were carried out at the CCSD(T)/aug-cc-pVDZ //B3LYP/aug-cc-pVTZ level of theory to investigate the energetics and structures of the reactant anions, probe reaction mechanisms, and calculate the reaction exothermicities. Due to the limited computational resources, complete calculations were not carried out for all possible structures; instead, we focused on the species that are more important for our study. For example, calculations were performed for  $C_nN^-$  ( $n = 1-4$ ) of all possible permutations of structure at both singlet and triplet states, and results show

**Table 7.3** Complete computational results for reactions between  $C_nN^-$  ( $n = 1-6$ ) and H atom.

Anion <sup>a</sup>	$\Delta E^b$ {0 K kcal/mol} [298 K kcal/mol]	
	AH <sup>-</sup>	$\Delta H$
CN <sup>-</sup> (S) {0.0}	HCN <sup>-</sup> (D) {-17.7}	HCN (S) {-33.3} [-33.2]
CN <sup>-</sup> (T) {129.2}	HNC <sup>-</sup> (D) {-6.8}	HCN (S) {-19.5} [-19.2]
C <sub>2</sub> N <sup>-</sup> (S) {23.6}	HC <sub>2</sub> N <sup>-</sup> (D) {-75.9}	HC <sub>2</sub> N (S) {-20.7} [-20.3]
C <sub>2</sub> N <sup>-</sup> (T) {0.0}	HC <sub>2</sub> N <sup>-</sup> (Q) {-19.8}	HC <sub>2</sub> N (T) {-32.5} [-31.9]
CNC <sup>-</sup> (S) {38.2}	HNC <sub>2</sub> <sup>-</sup> (D) {-50.6}	HNC <sub>2</sub> (S) {2.7} [3.2]
CNC <sup>-</sup> (T) {15.9}	HNC <sub>2</sub> <sup>-</sup> (Q) {6.8}	HNC <sub>2</sub> (T) {1.6} [2.0]
	CC(H)N <sup>-</sup> (D) {-24.3}	CC(H)N (S) {-22.7} [-22.7]
	CC(H)N <sup>-</sup> (Q) {-9.6}	CC(H)N (T) {21.6} [21.7]
	<i>c</i> -HC <sub>2</sub> N <sup>-</sup> (D) {-27.3}	<i>c</i> -HC <sub>2</sub> N (S) {-19.3} [-19.2]
	<i>c</i> -HC <sub>2</sub> N <sup>-</sup> (Q) {33.2}	<i>c</i> -HC <sub>2</sub> N (T) {-31.8} [-31.6]
		CN <sup>-</sup> (S) + CH (D) {-12.2} [-10.4]
C <sub>3</sub> N <sup>-</sup> (S) {0.0}	HC <sub>3</sub> N <sup>-</sup> (D) {-33.1}	HC <sub>3</sub> N (S) {-30.4} [-30.3]
C <sub>3</sub> N <sup>-</sup> (T) {83.8}	HC <sub>3</sub> N <sup>-</sup> (Q) {34.6}	HC <sub>3</sub> N (T) {58.8} [59.2]
CNC <sub>2</sub> <sup>-</sup> (S) {31.6}	HNC <sub>3</sub> <sup>-</sup> (D) {-8.9}	HNC <sub>3</sub> (S) {17.7} [18.3]
CNC <sub>2</sub> <sup>-</sup> (T) {107.6}	HNC <sub>3</sub> <sup>-</sup> (Q) {71.4}	HNC <sub>3</sub> (T) {74.9} [75.4]
	CC(H)CN <sup>-</sup> (D) {-28.8}	CC(H)CN (S) {12.4} [12.8]
	CC(H)CN <sup>-</sup> (Q) {43.0}	CC(H)CN (T) {53.4} [53.5]
	C <sub>2</sub> C(H)N <sup>-</sup> (D) {-9.7}	C <sub>2</sub> C(H)N (S) {59.4} [59.6]
	C <sub>2</sub> C(H)N <sup>-</sup> (Q) {50.4}	C <sub>2</sub> C(H)N (T) {91.4} [91.7]
		CN <sup>-</sup> (S) + C <sub>2</sub> H (D) {26.7} [28.4]
		C <sub>2</sub> <sup>-</sup> (D) + HCN (S) {26.0} [27.3]
C <sub>4</sub> N <sup>-</sup> (S) {4.9}	HC <sub>4</sub> N <sup>-</sup> (D) {-73.6}	HC <sub>4</sub> N (S) {-11.8} [-11.5]
C <sub>4</sub> N <sup>-</sup> (T) {0.0}	HC <sub>4</sub> N <sup>-</sup> (Q) {-24.2}	HC <sub>4</sub> N (T) {-24.5} [-24.0]
CNC <sub>3</sub> <sup>-</sup> (S) {25.7}	HNC <sub>4</sub> <sup>-</sup> (D) {-48.0}	HNC <sub>4</sub> (S) {15.5} [15.9]
CNC <sub>3</sub> <sup>-</sup> (T) {31.8}	HNC <sub>4</sub> <sup>-</sup> (Q) {1.5}	HNC <sub>4</sub> (T) {19.8} [20.2]

$C_2NC_2^-$ (S) {53.6}	$C_3CHN^-$ (D) {-19.4}	$C_3CHN$ (S) {17.6} [17.5]
$C_2NC_2^-$ (T) {50.5}	$C_3CHN^-$ (Q) {33.3}	$C_3CHN$ (T) {41.1} [41.4]
	$C_2CHCN^-$ (D) {-80.4}	$C_2CHCN$ (S) {-16.4} [-16.2]
	$C_2CHCN^-$ (Q) {-7.1}	$C_2CHCN$ (T) {8.9} [9.1]
	<i>c</i> - $CC(H)C_2N^-$ (D) {-51.3}	<i>c</i> - $CC(H)C_2N$ (S) {-29.5} [-29.7]
	<i>c</i> - $CC(H)C_2N^-$ (Q) {6.6}	<i>c</i> - $CC(H)C_2N$ (T) {16.5} [16.7]
		$CN^-$ (S) + $C_3H$ (D) {-0.8} [0.8]
		$C_2N^-$ (S) + $C_2H$ (D) {45.0} [46.4]
		$C_3N^-$ (S) + $CH$ (D) {22.1} [23.5]
		$C_3^-$ (D) + $HCN$ (S) {-9.0} [-7.7]
$C_5N^-$ (S) {0.0}	$HC_5N^-$ (D) {-42.1}	$HC_5N$ (S) {-26.3} [-26.2]
$C_5N^-$ (T) {73.2}	$HC_5N^-$ (Q) {12.4}	$HC_5N$ (T) {42.4} [43.2]
$CNC_4^-$ (S) {31.6}	$HNC_5^-$ (D) {-12.8}	$HNC_5$ (S) {31.7} [32.4]
$C_2NC_3^-$ (S) {56.6}	$HNC_5^-$ (Q) {34.9}	$HNC_5$ (T) {75.8} [76.5]
	$C_4C(H)N^-$ (D) {-11.4}	$C_4C(H)N$ (S) {67.3} [67.6]
	$C_4C(H)N^-$ (Q) {9.9}	$C_4C(H)N$ (T) {89.5} [89.8]
	$C_3CHCN^-$ (D) {-42.1}	$C_3C(H)CN$ (S) {17.5} [17.7]
	$C_3CHCN^-$ (Q) {9.9}	$C_3C(H)CN$ (T) {49.8} [49.9]
	$C_2CHC_2N^-$ (D) {-23.9}	$C_2C(H)C_2N$ (S) {43.3} [43.4]
	$C_2CHC_2N^-$ (Q) {17.7}	$C_2C(H)C_2N$ (T) {71.8} [71.9]
	$CC(H)C_3N^-$ (D) {-25.5}	$CN^-$ (S) + $C_4H$ (D) {30.3} [31.8]
	$CC(H)C_3N^-$ (Q) {35.7}	$C_2N^-$ (T) + $C_3H$ (D) {87.6} [89.1]
		$C_3N^-$ (S) + $C_2H$ (D) {32.3} [33.9]
		$C_4N^-$ (S) + $CH$ (D) {92.2} [93.8]
$C_6N^-$ (S) {4.5}	$HC_6N^-$ (D) {-79.5}	$HC_6N$ (S) {-10.5} [-10.1]
$C_6N^-$ (T) {0.0}	$HC_6N^-$ (Q) {-35.3}	$HC_6N$ (T) {-24.9} [-24.7]
	$HNC_6^-$ (D) {-50.1}	$HNC_6$ (S) {19.1} [19.6]
	$HNC_6^-$ (Q) {-10.7}	$HNC_6$ (T) {25.7} [26.2]
	$C_4C(H)CN^-$ (D) {-83.2}	$C_4C(H)CN$ (S) {-10.3} [-10.2]
	$C_4C(H)CN^-$ (Q) {-28.0}	$C_4C(H)CN$ (T) {11.2} [11.4]

---

$C_3C(H)C_2N^-(D)$ {-40.2}	$C_3C(H)C_2N(S)$ {23.7} [23.9]
$C_3C(H)C_2N^-(Q)$ {-33.0}	$C_3C(H)C_2N(T)$ {30.0} [30.3]
$C_2C(H)C_3N^-(D)$ {-76.9}	$C_2C(H)C_3N(S)$ {-10.9} [-10.8]
$C_2C(H)C_3N^-(Q)$ {-6.9}	$C_2C(H)C_3N(T)$ {15.4} [15.6]
$CC(H)C_4N^-(D)$ {-58.9}	$CC(H)C_4N(S)$ {-24.4} [-24.6]
$CC(H)C_4N^-(Q)$ {-29.3}	$CC(H)C_4N(T)$ {17.3} [17.4]
	$CN^-(S) + C_5H(D)$ {-25.4} [-24.2]
	$C_2N^-(S) + C_4H(D)$ {49.8} [50.8]
	$C_3N^-(S) + C_3H(D)$ {6.0} [7.3]
	$C_4N^-(S) + C_2H(D)$ {33.5} [34.9]
	$C_5N^-(S) + CH(D)$ {23.2} [24.6]

---

<sup>a</sup>Calculated at the CCSD(T)/aug-cc-pVDZ//B3LYP/aug-cc-pVTZ level of theory including zero-point energy corrections. The letter “c” as a prefix to the chemical formulas indicates the cyclic structure. Letters in the parentheses indicate the spin state of the species, *i.e.*, singlet (S), doublet (D), triplet (T), and quartet (Q). Energies are relative to the ground state anions.

<sup>b</sup>Energies are relative to reactants (H atom and the ground state anions). The letters in the parentheses indicate the calculated reaction enthalpies at 0 and 298 K.

**Table 7.4** Complete computational results for reactions between  $C_nN_2^-$  ( $n = 1, 3-5$ ) and H atom.

Anions <sup>a</sup>	$\Delta E^a$ {0 K kcal/mol}[298 K kcal/mol]	
	AH <sup>-</sup>	AH
NCN <sup>-</sup> (D) {0.0}	HNCN <sup>-</sup> (S) {-81.2}	HNCN (D) {-25.1} [-24.7]
CN <sub>2</sub> <sup>-</sup> (D) {45.4}	HNNC <sup>-</sup> (T) {-16.1}	HNCN (Q) {46.4} [46.8]
NCN <sup>-</sup> (Q) {59.1}	NC(H)N <sup>-</sup> (S) {-5.0}	NC(H)N (D) {13.6} [13.8]
CN <sub>2</sub> <sup>-</sup> (Q) {82.9}	NC(H)N <sup>-</sup> (T) {-4.3}	NC(H)N (Q) {91.9} [91.6]
NC <sub>3</sub> N <sup>-</sup> (D) {0.0}	HNC <sub>3</sub> N <sup>-</sup> (S) {-58.8}	HNC <sub>3</sub> N (D) {5.1} [5.7]
NC <sub>3</sub> N <sup>-</sup> (Q) {66.9}	HNC <sub>3</sub> N <sup>-</sup> (T) {-9.7}	HNC <sub>3</sub> N (Q) {56.4} [56.8]
CNC <sub>2</sub> N <sup>-</sup> (D) {27.1}	NC(H)C <sub>2</sub> N <sup>-</sup> (S) {-16.1}	NCHC <sub>2</sub> N (D) {27.2} [27.1]
CNC <sub>2</sub> N <sup>-</sup> (Q) {88.3}	NC(H)C <sub>2</sub> N <sup>-</sup> (T) {-13.9}	NCHC <sub>2</sub> N (Q) {93.2} [93.5]
C <sub>2</sub> NCN <sup>-</sup> (D) {41.8}	NCC(H)CN <sup>-</sup> (S) {-88.5}	NCC(H)CN (D) {-25.5} [-25.3]
C <sub>2</sub> NCN <sup>-</sup> (Q) {101.8}	NCC(H)CN <sup>-</sup> (T) {-21.0}	NCC(H)CN (Q) {69.0} [69.2]
C <sub>3</sub> N <sub>2</sub> <sup>-</sup> (D) {81.5}		CN <sup>-</sup> (S) + HC <sub>2</sub> N (S) {4.0} [5.6]
C <sub>3</sub> N <sub>2</sub> <sup>-</sup> (Q) {106.8}		C <sub>2</sub> N <sup>-</sup> (T) + HCN (S) {26.8} [28.0]
C <sub>2</sub> N <sub>2</sub> C <sup>-</sup> (D) {82.1}		
C <sub>2</sub> N <sub>2</sub> C <sup>-</sup> (Q) {145.3}		
C <sub>4</sub> N <sub>2</sub> <sup>-</sup> (D) {76.0}	HNC <sub>4</sub> N <sup>-</sup> (S) {-41.9}	HNC <sub>4</sub> N (D) {7.5} [7.8]
C <sub>4</sub> N <sub>2</sub> <sup>-</sup> (Q) {121.8}	HNC <sub>4</sub> N <sup>-</sup> (T) {-26.7}	HNC <sub>4</sub> N (Q) {62.1} [62.6]
C <sub>3</sub> NCN <sup>-</sup> (D) {37.4}	NC(H)C <sub>3</sub> N <sup>-</sup> (S) {-38.0}	NC(H)C <sub>3</sub> N (D) {4.8} [4.7]
C <sub>3</sub> NCN <sup>-</sup> (Q) {100.8}	NC(H)C <sub>3</sub> N <sup>-</sup> (T) {-19.8}	NC(H)C <sub>3</sub> N (Q) {66.1} [66.2]
C <sub>2</sub> NC <sub>2</sub> N <sup>-</sup> (D) {51.2}	NCC(H)C <sub>2</sub> N <sup>-</sup> (S) {-11.6}	NCC(H)C <sub>2</sub> N (D) {-11.9} [-11.9]
C <sub>2</sub> NC <sub>2</sub> N <sup>-</sup> (Q) {94.1}	NCC(H)C <sub>2</sub> N <sup>-</sup> (T) {42.2}	NCC(H)C <sub>2</sub> N (Q) {41.4} [41.7]
CNC <sub>3</sub> N <sup>-</sup> (D) {22.9}		CN <sup>-</sup> (S) + HC <sub>3</sub> N (S) {-43.5} [-42.7]
CNC <sub>3</sub> N <sup>-</sup> (Q) {83.3}		C <sub>2</sub> N <sup>-</sup> (S) + HC <sub>2</sub> N (T) {55.5} [56.5]
NC <sub>4</sub> N <sup>-</sup> (D) {0.0}		C <sub>3</sub> N <sup>-</sup> (S) + HNC (S) {-32.5} [-31.5]
NC <sub>4</sub> N <sup>-</sup> (Q) {59.3}		C <sub>3</sub> N <sup>-</sup> (S) + HCN (S) {-46.4} [-45.5]
C <sub>2</sub> N <sub>2</sub> C <sub>2</sub> <sup>-</sup> (D) {123.8}		

---

C <sub>2</sub> N <sub>2</sub> C <sub>2</sub> <sup>-</sup> (Q) {147.1}		
c-C <sub>3</sub> NCN <sup>-</sup> (D) {88.2}		
c-C <sub>3</sub> NCN <sup>-</sup> (Q) {111.3}		
c-C <sub>2</sub> NC <sub>2</sub> N <sup>-</sup> (D) {107.7}		
c-C <sub>2</sub> NC <sub>2</sub> N <sup>-</sup> (Q) {158.6}		
CC(CN) <sub>2</sub> <sup>-</sup> (D) {10.2}		
CC(CN) <sub>2</sub> <sup>-</sup> (Q) {80.3}		

---

NC <sub>5</sub> N <sup>-</sup> (D) {0.0}	HNC <sub>5</sub> N <sup>-</sup> (S) {-58.3}	HNC <sub>5</sub> N (D) {11.1} [11.4]
NC <sub>5</sub> N <sup>-</sup> (Q) {48.6}	HNC <sub>5</sub> N <sup>-</sup> (T) {-14.7}	HNC <sub>5</sub> N (Q) {54.9} [55.3]
(CN) <sub>2</sub> C <sub>3</sub> <sup>-</sup> (D) {2.1}	NCC(H)C <sub>3</sub> N <sup>-</sup> (S) {-87.2}	NCC(H)C <sub>3</sub> N (D) {-18.5} [-18.6]
(CN) <sub>2</sub> C <sub>3</sub> <sup>-</sup> (Q) {77.2}	NCC(H)C <sub>3</sub> N <sup>-</sup> (T) {-44.9}	NCC(H)C <sub>3</sub> N (Q) {47.9} [48.0]
	NC <sub>2</sub> C(H)C <sub>2</sub> N <sup>-</sup> (S) {-33.6}	NC <sub>2</sub> C(H)C <sub>2</sub> N (D) {35.9} [35.8]
	NC <sub>2</sub> C(H)C <sub>2</sub> N <sup>-</sup> (T) {-26.3}	NC <sub>2</sub> C(H)C <sub>2</sub> N (Q) {34.2} [34.5]
		CN <sup>-</sup> (S) + HC <sub>4</sub> N (S) {2.3} [3.6]
		C <sub>2</sub> N <sup>-</sup> (T) + HC <sub>3</sub> N (S) {64.2} [64.9]
		C <sub>3</sub> N <sup>-</sup> (S) + HC <sub>2</sub> N (S) {12.6} [13.7]
		C <sub>4</sub> N <sup>-</sup> (T) + HCN (S) {-6.5} [-5.5]

---

<sup>a</sup>Calculated at the CCSD(T)/aug-cc-pVDZ//B3LYP/aug-cc-pVTZ level of theory including zero-point energy corrections. The letter “c” as a prefix to the chemical formulas indicates the cyclic structure. Letters in the parentheses indicate the spin state of the species, *i.e.*, singlet (S), doublet (D), triplet (T), and quartet (Q). Energies are relative to the ground state anions.

<sup>b</sup>Energies are relative to reactants (H atom and the ground state anions). The letters in the parentheses indicate the calculated reaction enthalpies at 0 and 298 K.

that the ground state of the reactant anions is a singlet for  $C_nN^-$  ( $n = 1$  and  $3$ ) and a triplet for  $C_nN^-$  ( $n = 2$  and  $4$ ); all ground-state species have a linear structure and the nitrogen atom is located at the end of the carbon chains. This trend has previously been reported from other experimental and theoretical studies of  $C_nN^-$  ( $n = 2 - 7$ ) (Pascoli & Lavendy 1999; Garand et al. 2009). Therefore, full structure-exploring and energy calculations of  $C_5N^-$  and  $C_6N^-$  were not performed; only structures with energies close to the ground states were investigated, as summarized in Table 7.1 and Table 7.3.

The reaction efficiencies of all  $C_nN^-$  ( $n = 1 - 6$ ) anions are similar (0.21–0.32) with no obvious trend. Although the associative products are most likely, it is possible that fragmentation pathways may exist. However, due to the very low reactant-ion intensity, fragmentation processes cannot be confirmed from the current experimental results.

As mentioned above,  $C_nN^-$  anions can be classified into two groups by the number of C atoms in the ground-state structures: singlet ( $n = 1, 3,$  and  $5$ ) and triplet ( $n = 2, 4,$  and  $6$ ). Among these ions, all in the first group of species,  $C_nN^-$  ( $n = 1, 3,$  and  $5$ ), have been detected in the ISM. Reactions of these anions with H atom is of great interest to astrochemistry. The reaction coordinate plot of  $CN^- + H$  is shown in Figure 7.1 as an example of reactions in this category, where the energy landscapes of all possible reactions are indicated. The H atom can bind to either C or N atom in  $CN^-$ , and reaction proceeds through AD processes. According to calculations, the addition of H atom to the carbon atom of  $CN^-$  is barrierless, and the AD products ( $HCN + e^-$ ) are exothermic ( $-33.3 \text{ kcal mol}^{-1}$ ). In contrast, the energy barrier ( $1.0 \text{ kcal mol}^{-1}$ ) for addition of H atom to the nitrogen atom of  $CN^-$  is likely to inhibit this reaction channel, such that the formation of the isomeric product HNC is not favorable even though it

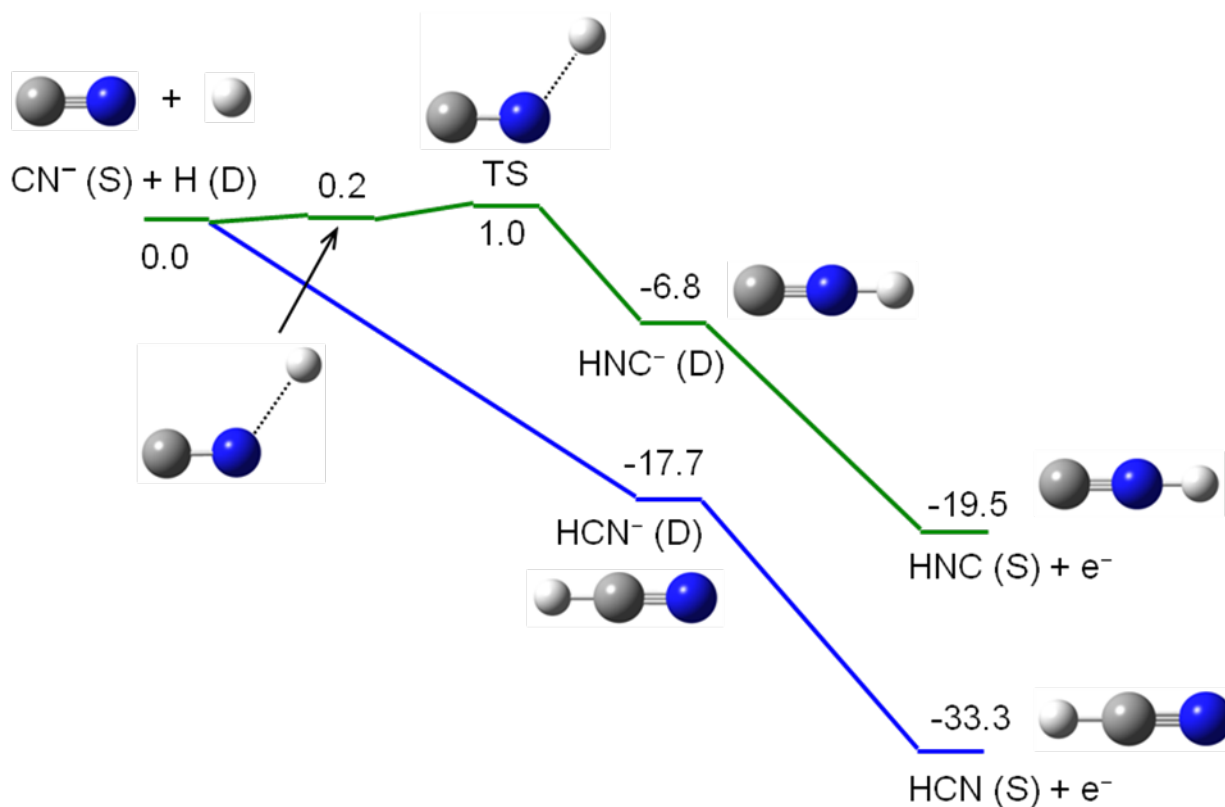


**Figure 7.1** The reaction coordinate plot (in kcal mol<sup>-1</sup>, 0 K) for CN<sup>-</sup> + H in which H atom binds to C (blue line) and N (green line), respectively. Calculations were performed at the CCSD(T)/aug-cc-pVDZ//B3LYP/aug-cc-pVTZ level of theory. Letters in the parentheses indicate the spin state of the species, *i.e.*, singlet (S) and doublet (D).

is an exothermic process ( $-19.5 \text{ kcal mol}^{-1}$ ):



The parenthetical letter after the chemical formula indicates the spin state of the species, *i.e.*, singlet (S), doublet (D), triplet (T), and quartet (Q).

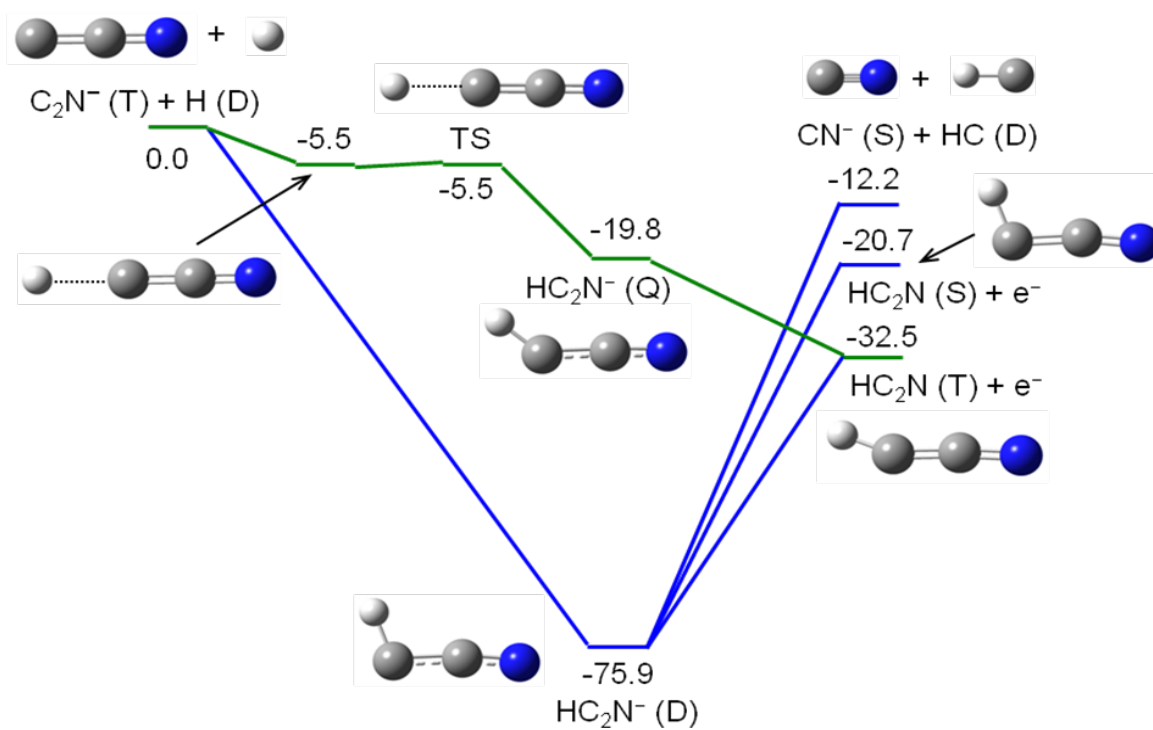
Similar reaction pathways are expected for  $\text{C}_3\text{N}^-$  and  $\text{C}_5\text{N}^-$ ; however, the formation of the corresponding neutral isocyanides ( $\text{HNC}_3$  and  $\text{HNC}_5$ ) is endothermic, and only the exothermic products ( $\text{HC}_3\text{N}$  and  $\text{HC}_5\text{N}$ ) are shown in Table 7.1.

As an example of reactions in the second category, the reaction coordinate plot of  $\text{C}_2\text{N}^- + \text{H}$  is shown in Figure 7.2 including all possible reactions. Whereas H atom is an open-shell species with a doublet spin state, the  $\text{C}_2\text{N}^-$  ion has a triplet ground state and therefore reactions may proceed through spin-allowed doublet and quartet pathways. The H atom can bind to each of the three atoms in  $\text{C}_2\text{N}^-$ , *i.e.*, C1, C2, and N3, respectively, as shown in Figure 7.2(a) through 7.2(c). For example, Figure 7.2(a) shows the reaction coordinate diagram for adding H atom to C1 of the anion, and the reaction proceeds through the spin-allowed quartet reaction adduct ( $\text{HC}_2\text{N}^-$ ), and forms a triplet neutral  $\text{HC}_2\text{N}$  and an electron through an electron detachment process:

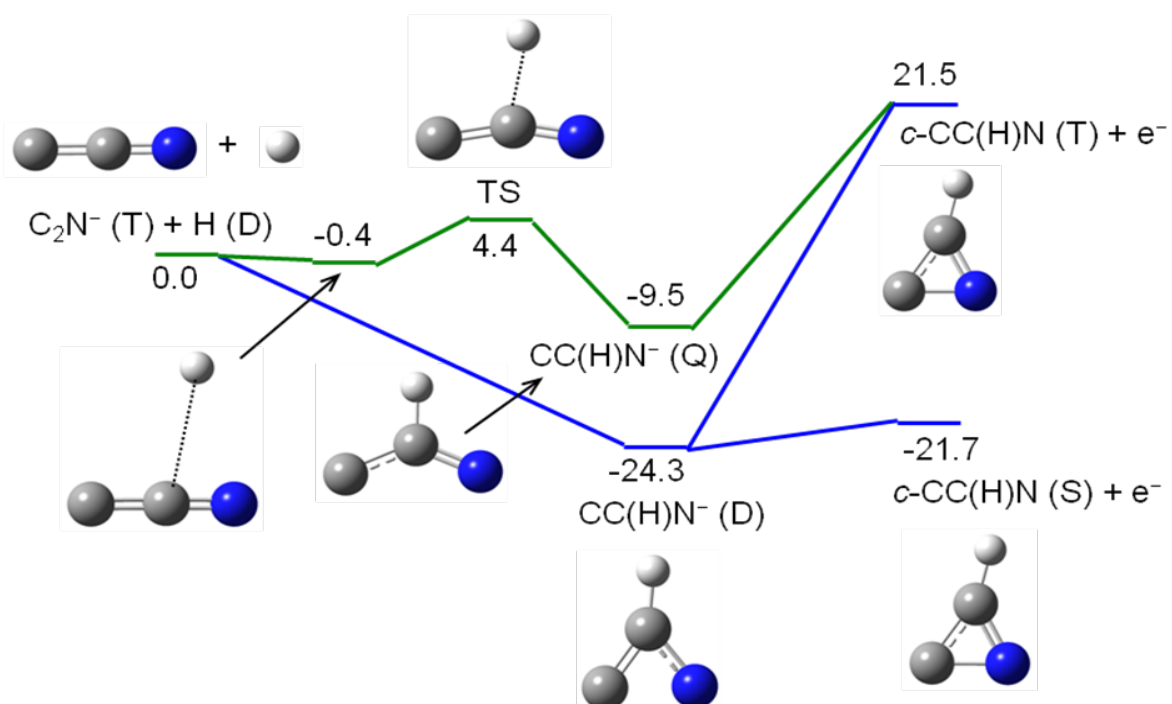


Alternatively, the spin-allowed reaction can proceed through doublet-state pathways: the doublet adduct ( $\text{HC}_2\text{N}^-$ ), can either fragment into smaller species ( $\text{CN}^-$  and  $\text{HC}$ ) or form singlet

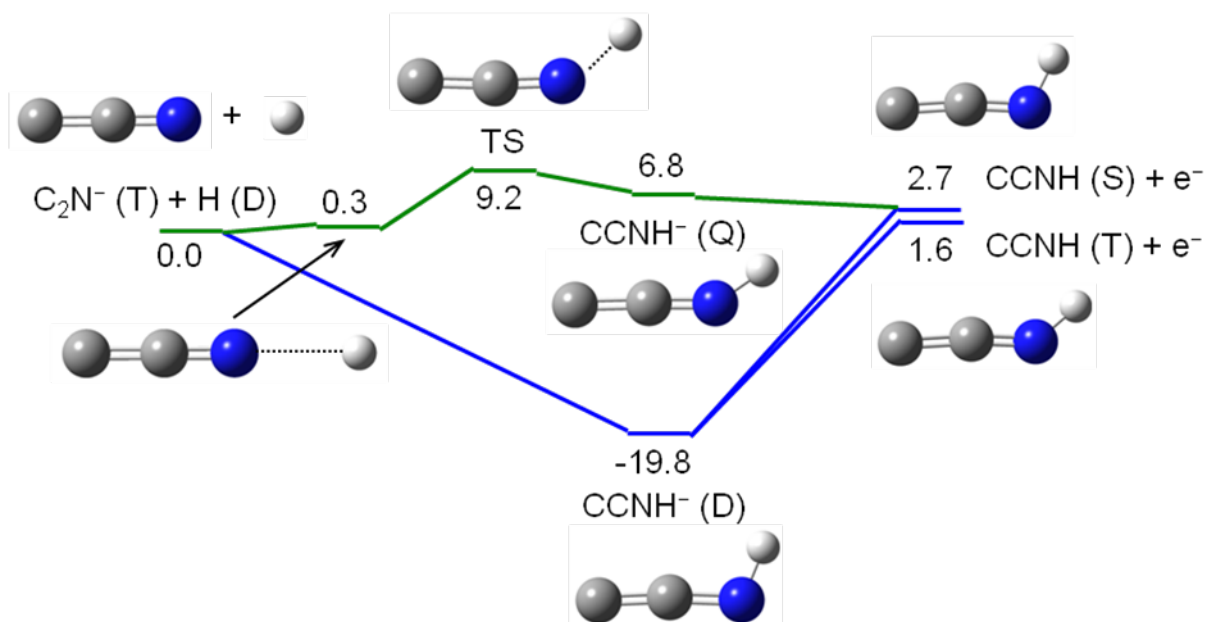
a)



b)

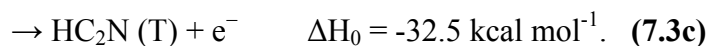
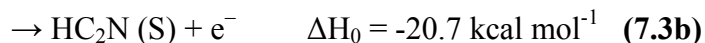
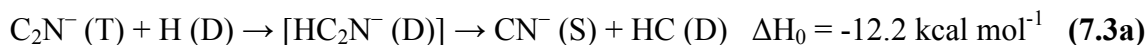


c)



**Figure 7.2** The reaction coordinate plot (in  $\text{kcal mol}^{-1}$ , 0 K) for  $C_2N^- + H$  in which H atom binds to (a) C1, (b) C2, and (c) N3, respectively. Calculations were performed at the CCSD(T)/aug-cc-pVDZ//B3LYP/aug-cc-pVTZ level of theory. Letters in the parentheses indicate the spin state of the species, *i.e.*, singlet (S), doublet (D), triplet (T), and quartet (Q). Only spin-allowed reactions are investigated, where the green and blue lines indicate the high-spin (quartet) and low-spin (doublet) processes, respectively.

and/or triplet HC<sub>2</sub>N neutral molecules through an electron detachment process:



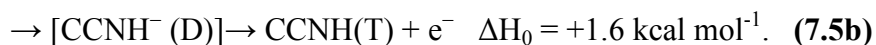
Because both quartet and doublet pathways are essentially barrierless and exothermic, they are likely to contribute to the total reactions. However, due to the coexistence of all reactant anions, the possible CN<sup>-</sup> product ion cannot be discriminated from the CN<sup>-</sup> existing among the reactants, such that this reaction pathway cannot be confirmed from the current experiments.

Figure 7.2(b) represents the reaction coordinate plot for H atom bonding to C2 of the anion. The spin-allowed quartet pathway possesses a high-energy transition state (4.4 kcal mol<sup>-1</sup>) and endothermic products (21.5 kcal mol<sup>-1</sup>). Therefore, it is not likely to be prominent under experimental conditions where all reactants have a thermal distribution of the internal and kinetic energies. In contrast, one of the spin-allowed doublet pathways is barrierless and exothermic, and the reaction leads to the formation of the cyclic neutral species *c*-CC(H)N in the singlet state (The letter “*c*” as a prefix for a chemical formula indicates the cyclic structure discussed here and in the remainder of this chapter.



In Figure 7.2(c) H atom bonds to N3 of the anion, and the spin-allowed reaction pathways have either higher energy transition states or slightly endothermic products:





Neither channel is likely to have significant contribution to the total reaction.

In principle, spin conversion may occur when potential energy curves of different spin states cross. However, the conversion efficiency is generally very low and spin-forbidden reaction pathways are not likely to be important when compared with the spin-allowed reactions (Harvey 2007; Yang et al. 2010a). Additionally, only the ground state reactant anions are investigated in this study, whereas other possible species are not included. For example, according to our calculations as shown in Table 7.3, compared to the most stable  $\text{C}_2\text{N}^-$  ion (triplet, 0.0 kcal/mol), the relative energies of other species  $\text{C}_2\text{N}^-$  (singlet),  $\text{CNC}^-$  (singlet), and  $\text{CNC}^-$  (triplet) are 23.6, 38.2, and 15.9 kcal mol<sup>-1</sup>, respectively. Considering the experimental conditions where ions are produced by using a DC discharge operated at ~4 kV, it is possible that other minor species may coexist with ground-state  $\text{C}_2\text{N}$ . Similar pathways are expected in reactions of other anions with H atom, and further detailed discussion is not included. Instead, the reactions that are related to the ground-state reactants were investigated, and the exothermic products are shown in Table 7.1. Additional computational information for this category of species is listed in Table 7.3.

#### 7.4.2 Reactions of $\text{C}_n\text{N}_2^-$ (n = 1, 3, 4, and 5)

Similar theoretical calculations were performed to investigate reactions of species in this category as summarized in Tables 7.2 and 7.4. The reaction efficiencies of all  $\text{C}_n\text{N}_2^-$  (n = 1, 3 – 5) anions are similar (0.20 – 0.25). According to our calculations, the ground states of the reactant anions are doublets, and both N atoms are located at the termini of the chain structures. In general, AD is the most exothermic pathway (-18.6 – -25.3 kcal mol<sup>-1</sup>), in which the H atom

bonds to either the terminal N atoms in  $\text{CN}_2^-$ , or the middle C atoms in  $\text{C}_3\text{N}_2^-$  and  $\text{C}_5\text{N}_2^-$ . The only exception is for the reaction of  $\text{C}_4\text{N}_2^-$ . Here the fragmentation pathway leading to  $\text{C}_3\text{N}^-$  and HCN formation is the most exothermic channel ( $\Delta H_0 = -46.4 \text{ kcal mol}^{-1}$ , reaction 7.6):



$$\Delta H_0 = -46.4 \text{ kcal mol}^{-1}. \quad (7.6)$$

In this reaction the H atom adds to the first C atom in  $\text{C}_4\text{N}_2^-$  and forms the singlet transient adduct  $\text{NC}(\text{H})\text{C}_3\text{N}^-$  ( $-38.0 \text{ kcal mol}^{-1}$ ). This fragments into  $\text{C}_3\text{N}^-$  and HCN via a transition state ( $-35.4 \text{ kcal mol}^{-1}$ ). Again, due to the coexistence of all reactant anions, the possible product ions ( $\text{C}_3\text{N}^-$ ) can not be discriminated from the reactant ions. This reaction pathway cannot be proved from the current experiments.

The only possible exothermic AD pathway is the formation of neutral  $\text{NCC}(\text{H})\text{C}_2\text{N} (\text{D})$  ( $\Delta H_0 = -11.9 \text{ kcal mol}^{-1}$ , reaction 7.7), in which the H atom adds to the second C atom in  $\text{C}_4\text{N}_2^-$  and forms a singlet transient adduct  $\text{NCC}(\text{H})\text{C}_2\text{N}^-$  ( $-11.6 \text{ kcal mol}^{-1}$ ) which subsequently becomes the corresponding neutral molecule by ejecting an electron:



$$\Delta H_0 = -11.9 \text{ kcal mol}^{-1}. \quad (7.7)$$

### 7.4.3 Reactions of $\text{C}_n\text{N}_3^-$ ( $n = 2$ and $4$ )

Our experimental results indicate that both  $\text{C}_2\text{N}_3^-$  and  $\text{C}_4\text{N}_3^-$  are not reactive with H atom. Theoretical calculations were carried out to investigate the reaction coordinate plots, and results are shown in Figure 7.3(a) and 7.3(b). Calculations indicate that  $\text{C}_2\text{N}_3^-$  has a singlet

a)

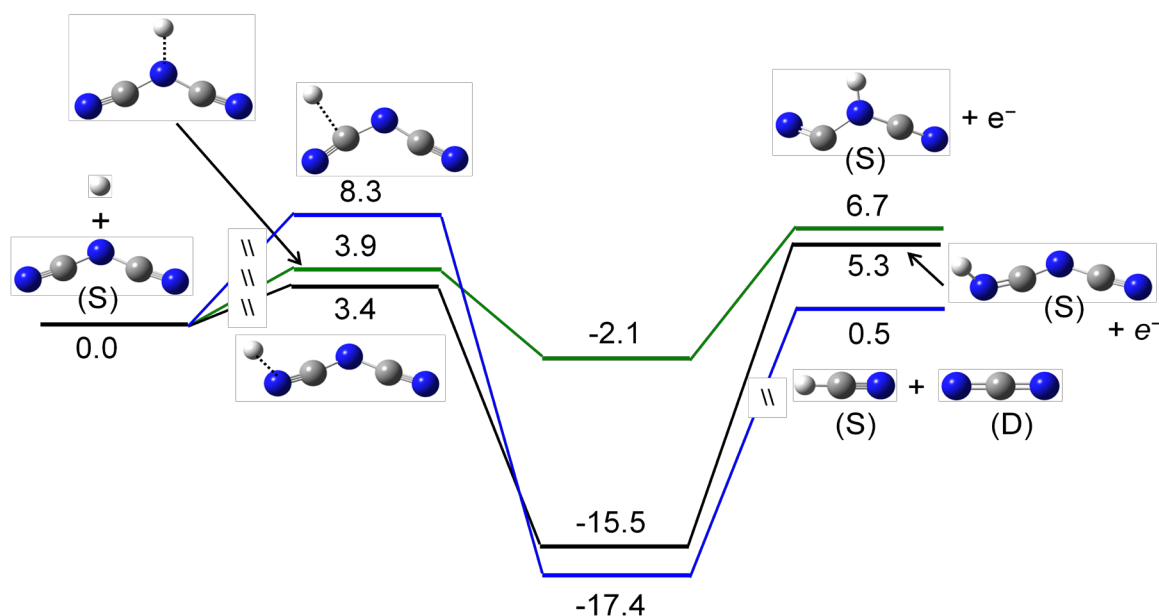


**Figure 7.3a** The reaction coordinate plot (in kcal mol<sup>-1</sup>, 0 K) for NCNCN<sup>-</sup> + H. Calculations were performed at the CCSD(T)/aug-cc-pVDZ//B3LYP/aug-cc-pVTZ level of theory. Letters in the parentheses indicate the spin state of the species, *i.e.*, singlet (S) and doublet (D). Only spin-allowed reactions are investigated, where different reaction pathways are shown in different colors. The loosely-bound ion-neutral complexes prior to the transition states are not shown. The transition states prior to the fragmentation products (7.3 kcal mol<sup>-1</sup> for HCN formation channel) are not shown.

b)

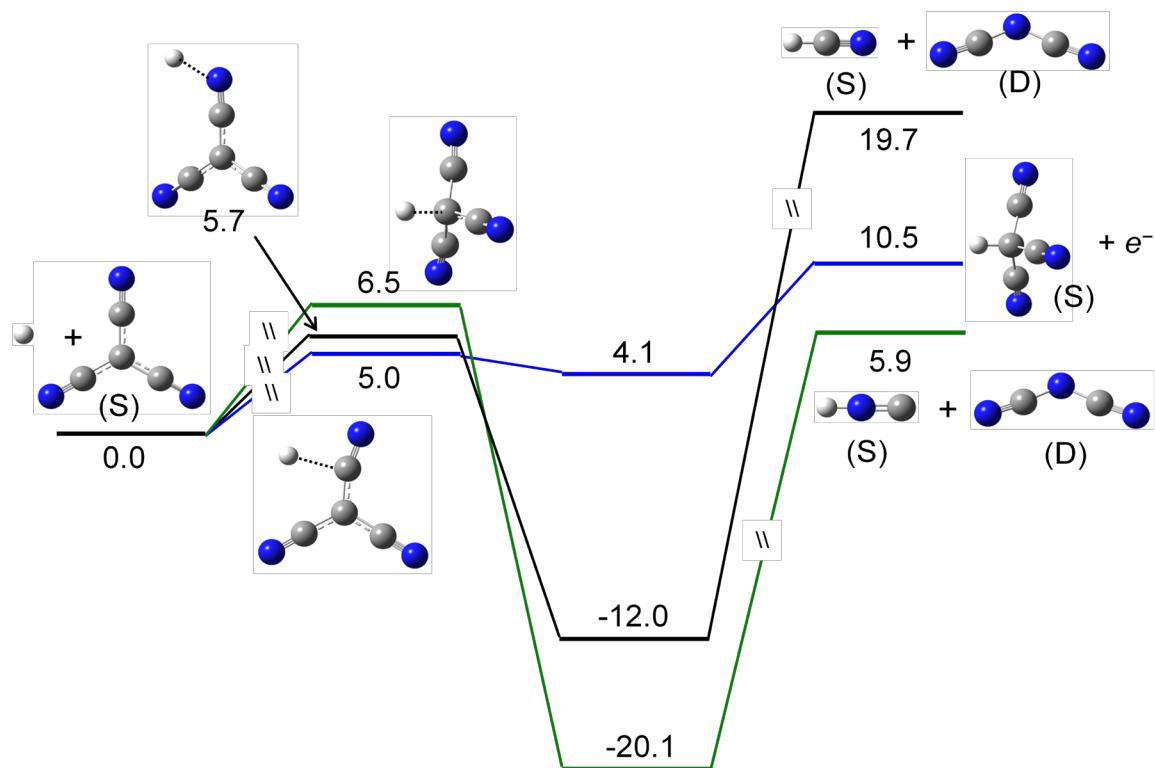


**Figure 7.3b** The reaction coordinate plot (in  $\text{kcal mol}^{-1}$ , 0 K) for  $\text{C(CN)}_3^- + \text{H}$ . Calculations were performed at the CCSD(T)/aug-cc-pVDZ//B3LYP/aug-cc-pVTZ level of theory. Letters in the parentheses indicate the spin state of the species, *i.e.*, singlet (S) and doublet (D). Only spin-allowed reactions are investigated, where different reaction pathways are shown in different colors. The loosely-bound ion-neutral complexes prior to the transition states are not shown. The transition states prior to the fragmentation products (10.5 and 22.9  $\text{kcal mol}^{-1}$  for HCN and HNC formation channels, respectively) are not shown.

ground state, which has a V-shaped conformation with C and N atoms appearing alternately in the structure (NCNCN<sup>-</sup>) as shown in Figure 7.3(a). In principle, the association of C<sub>2</sub>N<sub>3</sub><sup>-</sup> with H atom may proceed through three different possible pathways by adding the H atom to C and N atoms at 3 different positions. However, all three reaction pathways are prohibited because of endothermic transition states (3.4 – 8.3 kcal mol<sup>-1</sup>) along the approach of reactants. For example, adding the H atom to the terminal N atom in C<sub>2</sub>N<sub>3</sub><sup>-</sup> requires overcoming an energy barrier that is 3.4 kcal mol<sup>-1</sup> above the total energy of the reactants. Under our experimental conditions, reactants have a thermal distribution of kinetic and internal energies, therefore the majority of reactants do not possess sufficient energy to surmount this barrier height. Similarly, there are endothermic transition states that prohibit H atom from adding to the other two positions and these transition states are above the total energy of reactants by 8.3 and 3.9 kcal mol<sup>-1</sup> along the approach of the H atom to the C atom and the middle N atom in the structure, respectively. In addition, the AD products are endothermic (5.3 and 6.7 kcal mol<sup>-1</sup>), whereas the thermoneutral fragmentation products (HCN and NCN<sup>-</sup>) are associated with a higher-energy transition state prior to the dissociation (7.3 kcal mol<sup>-1</sup>, not shown). Therefore, the endothermic reactions and unfavorable transition states prohibit the reactions.

The reaction coordinate plot of C<sub>4</sub>N<sub>3</sub><sup>-</sup> with H atom is shown in Figure 7.3(b), whereas the complete computational results are summarized in Table 7.5. The ground state reactant anion (C(CN)<sub>3</sub><sup>-</sup>) has a planar branched structure in its singlet state. Presumably H atom can attach at three different positions of the anion. Similarly, anion-H atom association is prohibited by the high-energy transition states (5.0 – 6.5 kcal mol<sup>-1</sup>) along the approach of reactants. The endothermic products (5.9 – 19.7 kcal mol<sup>-1</sup>) and the associated high-energy transition states (not

**Table 7.5** Complete computational results for reactions between  $C_nN_3^-$  ( $n = 2$  and 4) and H atom.

Anions <sup>a</sup>	$\Delta E^a$ {0 K kcal/mol} [298 K kcal/mol]	
	AH <sup>-</sup>	AH
$C_2N_3^-$ (S) {114.6}	HNCNCN <sup>-</sup> (S) {-18.6}	HNCNCN (D) {2.9} [3.2]
$CN_2CN^-$ (S) {49.6}	NCNHCN <sup>-</sup> (S) {-20.5}	
$NCNCN^-$ (S) {0.0}		
$NCNCN^-$ (T) {75.9}		
$NC_2N_2^-$ (S) {86.5}		
$NC_2N_2^-$ (T) {84.2}		
$CNCN_2^-$ (S) {79.1}		
$CNCN_2^-$ (T) {102.6}		
$CN_3C^-$ (S) {91.3}		
$CN_3C^-$ (T) {108.2}		
$C_3N_2CN^-$ (S) {99.3}	HC(CN) <sub>3</sub> <sup>-</sup> (S) {4.1}	HC(CN) <sub>3</sub> (S) {10.5} [10.8]
$C_2NCNCN^-$ (S) {81.8}	C(CN) <sub>2</sub> CNH <sup>-</sup> (S) {-12.4}	HC(CN) <sub>3</sub> (T) {105.7} [106.1]
$C_2NCNCN^-$ (T) {120.6}	C(CN) <sub>2</sub> C(H)N <sup>-</sup> (S) {-20.1}	C(CN) <sub>2</sub> CNH (S) {22.4} [22.4]
$C_2N_2C_2N^-$ (S) {129.0}		C(CN) <sub>2</sub> CNH (T) {54.9} [55.3]
$C_2N_2C_2N^-$ (T) {139.8}		C(CN) <sub>2</sub> C(H)N (S) {40.7} [40.7]
$C_2N_3C_2^-$ (S) {99.7}		C(CN) <sub>2</sub> C(H)N (T) {71.9} [72.2]
$C_2N_3C_2^-$ (T) {201.3}		CN <sup>-</sup> (S) + NCC(H)CN (S) {13.7} [15.0]
$C(CN)_3^-$ (S) {0.0}		NC <sub>3</sub> N <sup>-</sup> (S) + HCN (S) {5.9} [7.1]
$C(CN)_3^-$ (T) {72.0}		NC <sub>3</sub> N <sup>-</sup> (S) + HNC (S) {19.7} [21.1]
$NC_3NCN^-$ (S) {23.6}		
$NC_2NC_2N^-$ (S) {56.3}		
$NC_2NC_2N^-$ (T) {79.8}		

<sup>a</sup>Calculated at the CCSD(T)/aug-cc-pVDZ//B3LYP/aug-cc-pVTZ level of theory including zero-point energy corrections. Letters in the parentheses indicate the spin state of the species, *i.e.*, singlet (S), doublet (D), triplet (T), and quartet (Q). Energies are relative to the ground state anions.

<sup>b</sup>Energies are relative to reactants (H atom and the ground state anions). The letters in the parentheses indicate the calculated reaction enthalpies at 0 and 298 K.

shown in the figure) prior to the dissociation (10.5 and 22.9 kcal mol<sup>-1</sup> for HCN and HNC formation channels, respectively) are additional possible factors inhibiting the reactivity.

#### 7.4.4 Astrophysical Implications

It has been suggested that in the dense regions of the ISM large organics should be predominantly in the anionic form (Bakes & Tielens 1994; Lepp & Dalgarno 1988). In contrast, hydrogen atom is abundant in the diffuse atomic clouds (Snow & McCall 2006; Snow & Bierbaum 2008). Therefore, it is likely that the anion-H atom reactions may occur in the boundary regions between dense and diffuse clouds. The laboratory studies of the corresponding reactions can provide both general rules of stability and a fundamental understanding of reaction mechanisms in the ISM. Our experimental results show that the efficiencies of all anion-H atom reactions of reactive species, i.e., C<sub>n</sub>N<sup>-</sup> (n = 1 – 6) and C<sub>n</sub>N<sub>2</sub><sup>-</sup> (n = 1, 3 – 5), range between 0.20 and 0.32, whereas C<sub>n</sub>N<sub>3</sub><sup>-</sup> (n = 2 and 4) ions are not reactive. As discussed above, the approach of reactants to form the transient species is a critical step during reaction. Similar efficiencies (0.3–0.4) were determined in reactions of bare, C<sub>n</sub><sup>-</sup> (n = 2, 4 – 10) and monohydride, HC<sub>n</sub><sup>-</sup> (n = 4, 6, and 7) carbon-chain anions with H atoms where no obvious trend was seen (Barkholtz et al. 2001). Although a systematic computational study of these systems has not yet been performed, barrierless exothermic pathways are likely to exist in these reactions.

Bare carbon-chain anions generally are not stable in the interstellar regions with high H atom densities. Anions can be destroyed via AD by forming neutral molecules; larger ions can be removed by fragmentation pathways, leading to the formation of smaller anions which can be eventually destroyed through AD. However, nitrogen-rich carbon-chain anions may exhibit an unusually-high stability and would survive in these regions. Although C<sub>4</sub>N<sub>3</sub><sup>-</sup> is invisible to radio

astronomy due to its lack of a permanent dipole,  $C_2N_3^-$  has a V-shaped structure ( $C_{2V}$ ) and consequently has a permanent dipole moment that might lead to its identification via rotational spectra.

Although H atom is regarded as a very reactive species, the efficiencies of all carbanion-H atom reactions that have been studied are less than unity. Angular momentum conservation is likely to be a universal factor influencing reaction efficiency that is similar to reactions between molecular carbanions and H atoms as reported in our previous study (Yang et al. 2010c). This constraint decreases the efficiencies of reactions involving very light species, and can be used as a general guide in the study of ion-H atom reactions.

## 7.5 Conclusions

In this study, we have characterized reactions of the nitrogen-containing carbon-chain anions including species that were recently detected in the ISM (i.e.,  $CN^-$ ,  $C_3N^-$ , and  $C_5N^-$ ). These studies not only enhance our understanding of the chemistry of the species discovered, but also provide guidelines to predict the characteristics of other possible species that may exist in the ISM. According to our experimental and theoretical studies of 12 deprotonated nitriles ( $C_nN^-$  ( $n = 1 - 6$ ),  $C_nN_2^-$  ( $n = 1, 3, 4,$  and  $5$ ), and  $C_nN_3^-$  ( $n = 2$  and  $4$ )), reacting with H atom, the dominant reaction channel is AD. However, fragmentation pathways are also possible in some cases. Our results indicate that the reaction efficiencies of  $C_nN^-$  ( $n = 1 - 6$ ) and  $C_nN_2^-$  ( $n = 1, 3, 4,$  and  $5$ ) systems are comparable, and there is no clear trend between reaction efficiencies and structures or reaction exothermicities. However,  $C_nN_3^-$  ( $n = 2$  and  $4$ ) are not reactive with H atoms. This is attributed to the existence of high energy barriers along the approach of reactants and to the endothermicity of the reaction. Similar mechanisms likely exist in our previous

studies of bare and monohydride carbon-chain anions, e.g.,  $C_n^-$  ( $n = 2, 4 - 10$ ) and  $HC_n^-$  ( $n = 2, 4, 6, \text{ and } 7$ ); the existence of barrierless reaction channels insures that the reaction proceeds through energetically accessible pathways (Barckholtz et al. 2001). Additionally, the angular momentum conservation of anion-H atom collision may be a universal effect which decreases the reaction efficiency of all reactions involving the light H atom. This study of anion-H atom reactions enhances our understanding from both experimental and theoretical perspectives, and enriches our knowledge of negative ion chemistry in the ISM.

## 7.6 References

- Agúndez, M., Cernicharo, J., Guélin, M., Kahane, C., Roueff, E., Klos, J., Aoiz, F. J., Lique, F., Marcelino, N., Goicoechea, J. R., González García, M., Gottlieb, C. A., McCarthy, M. C., & Thaddeus, P. 2010, *A&A*, 517, L2
- Bakes, E. L. O., & Tielens, A. G. G. M. 1994, *ApJ*, 427, 822
- Barckholtz, C., Snow, T. P., & Bierbaum, V. M. 2001, *ApJ*, 547, L171
- Brünken, S., Gupta, H.; Gottlieb, C. A.; McCarthy, M. C.; Thaddeus, P. 2007, *ApJ*, 664, L43
- Cernicharo, J., Guélin, M., Agúndez, M., Kawaguchi, K., McCarthy, M., & Thaddeus, P. 2007, *A&A*, 467, L37
- Cernicharo, J., Guélin, M., Agúndez, M., McCarthy, M. C., & Thaddeus, P. 2008, *ApJ*, 688, L83
- Eichelberger, B. R., Snow, T. P., & Bierbaum, V. M. 2003, *J. Am. Soc. Mass Spectrom.*, 14, 501
- Fehsenfeld, F. C., Howard, C. J., & Ferguson, E. E. 1973, *J. Chem. Phys.*, 58, 5841
- Ferguson, E. E., Fehsenfeld, F. C., & Schmeltekopf, A. L. 1969, *Adv. At. Mol. Phys.*, 5, 1
- Frisch, M. J., et al. 2004, *Gaussian 03* (Wallingford: Gaussian).
- Garand, E., Yacovitch, T. I., & Neumark, D. M. 2009, *J. Chem. Phys.*, 130, 064304.
- Harvey, J. N. 2007, *Phys. Chem. Chem. Phys.*, 9, 331
- Herbig, G. H. 1995, *ARA&A*, 33, 19
- Herbst, E., & van Dishoeck E. F. 2009, *ARA&A*, 47, 427
- Howard, C. J., Fehsenfeld, F. C., & McFarland, M. 1974, *J. Chem. Phys.*, 60, 5086
- Kuan, Y.-J., Charnley, S. B., Huang, H.-C., Tseng, W.-L., & Kisiel, Z. 2003, *ApJ*, 593, 848
- Leopold, D. G.; Ho, J., & Lineberger, W. C. 1987, *J. Chem. Phys.* 86, 1715
- Lepp, S., & Dalgarno, A. 1988, *ApJ*, 324, 553
- Martinez Jr., O., Yang, Z., Betts, N. B., Snow, T. P., & Bierbaum, V. M. 2009, *ApJ*, 705, L172
- McCarthy, M. C., Gottlieb, C. A., Gupta, H., & Thaddeus, P. 2006, *ApJ*, 652, L141
- Pascoli G., & Lavendy H. 1999, *Chem. Phys. Lett.*, 312, 333

Remijan, A. J., Hollis, J. M., Lovas, F. J., Cordiner, M. A., Millar, T. J., Markwick-Kemper, A. J., & Jewell, P. R. 2007, *ApJ*, 664, L47

Snow, T. P., & McCall, B. J. 2006, *ARA&A*, 44, 367

Snow, T. P., & Bierbaum, V. M. 2008, *Annu. Rev. Anal. Chem.*, 1, 229

Snow, T. P., Stepanovic M., Betts, N. B., Eichelberger, B. R., Martinez Jr. O., & Bierbaum, V. M. 2009, *Astrobio.*, 9, 1001

Thaddeus, P., Gottlieb, C. A., Gupta, H.; Brünken, S., McCarthy, M. C., Agúndez, M., Guélin, M., & Cernicharo, J. 2007, *ApJ*, 677, 1132

Trainor, D. W., Ham, D. O., & Kaufman, F. 1973, *J. Chem. Phys.*, 58, 4599

Van Doren, J. M., Barlow, S. E., DePuy, C. H., & Bierbaum, V. M. 1987, *Int. J. Mass Spectrom. Ion Proc.*, 81, 85

Walsh, C., Harada, N., Herbst, E., & Millar, T. J. 2009, *ApJ*, 700, 752

Williams, D. A., & Viti, S. 2002, *Annu. Rep. Prog. Chem. Sect. C*, 98, 87

Yang, Z., Eichelberger, B., Martinez Jr., O., Stepanovic, M., Snow, T. P., & Bierbaum, V. M. 2010a, *J. Am. Chem. Soc.*, 132, 5812

Yang, Z., Snow, T. P., & Bierbaum, V. M. 2010b, *Phys. Chem. Chem. Phys.*, 12, 13091

Yang, Z., Eichelberger, B., Carpenter, M. Y., Martinez Jr., O., Snow, T. P., & Bierbaum, V. M. 2010c, *ApJ*, 723, 1325

## Bibliography

- Abel, T., Anninos, P., Zhang, Y., & Norman, M. L. 1997, *New Astron.*, 2, 181.
- Adams, N. G. & Smith, D. 1976, *Int. J. Mass Spectrom. Ion Proc.*, 21, 349.
- Adams, N. G., & Smith, D. 1976, *J. Phys. B*, 9, 1439.
- Adams, N. G., & Smith, D. 1977, *Chem. Phys. Lett.*, 47, 383.
- Adams, W. S. 1941, *ApJ*, 93, 11.
- Agúndez, M., Cernicharo, J., Guélin, M., Kahane, C., Roueff, E., Klos, J., Aoiz, F. J., Lique, F., Marcelino, N., Goicoechea, J. R., González García, M., Gottlieb, C. A., McCarthy, M. C., & Thaddeus, P. 2010, *A&A* 517:L2.
- Agúndez, M., Cernicharo, J., Guélin, M., Kahane, C., Roueff, E., Klos, J., Aoiz, F. J., Lique, F., Marcelino, N., Goicoechea, J. R., González García, M., Gottlieb, C. A., McCarthy, M. C., & Thaddeus, P. 2010, *A&A*, 517, L2.
- Allamandola, L. J., Tielens, A. G. G. M., & Barker, J. 1989, *ApJ Suppl. Ser.*, 71, 733.
- Anicich, V. G. 1993, *ApJ Supp.*, 84, 215.
- Anicich, V. G. 1993, *J. Phys. Chem. Ref. Data.*, 22, 1469.
- Anicich, V. G., & Huntress, W. T., Jr. 1986, *ApJS*, 62, 553.
- Anicich, V. G., Huntress, W. T., & Futrell, J. H. 1976, *Chem. Phys. Lett.*, 40, 233.
- Anicich, V. G., Huntress, W. T., & McEwan, M. J. 1986, *J. Phys. Chem.*, 90, 2446.
- Bakes, E. L. O., & Tielens, A. G. G. M. 1994, *ApJ*, 427, 822
- Barckholtz, C., Snow, T. P., & Bierbaum, V. M. 2001, *ApJ*, 547, L171.
- Betowski, D., Payzant, J. D., Mackay, G. I., & Bohme, D. K. 1975, *Chem. Phys. Lett.*, 31, 321.
- Bieniek, R. J., & Dalgarno, A. 1979, *ApJ*, 228, 635.
- Bierbaum, V. M. 2003, in *Encyclopedia of Mass Spectrometry*, ed. P.B. Armentrout (Amsterdam: Elsevier), 940.
- Black, J. H. 1978, *ApJ*, 222, 125.
- Bohme, D. K., & Young, L. B. 1971, *Can. J. Chem.*, 49, 2918.

- Bohme, D. K., Rakshit, A. B., & Schiff, H. I. 1982, *Chem. Phys. Lett.*, 93, 592.
- Bolden, R. C., & Twiddy, N. D. 1972, *Faraday Discussions of the Chemical Society*, 53, 192.
- Bromm, V. 2010, *Science* 329, 45.
- Browne, J. C., & Dalgarno, A. 1969, *J. Phys. B: At. Mol. Phys.*, 2, 885.
- Brünken, S., Gupta, H., Gottlieb, C. A., McCarthy, M. C.; & Thaddeus, P. 2007, *ApJ.*, 664, L43.
- Burley, J. D., & Armentrout, P. B. 1988, *Int. J. Mass Spectrom. Ion Proc.*, 84, 157.
- CDMS 2010, <http://www.astro.uni-koeln.de/cdms/>.
- Cernicharo, J., Guélin, M., Agúndez, M., Kawaguchi, K., McCarthy, M., & Thaddeus, P. 2007, *A&A*, 467, L37.
- Cernicharo, J., Guélin, M., Agúndez, M., McCarthy, M. C., & Thaddeus, P. 2008, *ApJ*, 688, L83.
- Chandrasekhar, S. 1944, *ApJ*, 100, 176.
- Chandrasekhar, S., & Breen, F. H. 1946, *ApJ*, 104, 430.
- Chemical Kinetics Database, NIST, 2000, Standard Reference Database 17, Version 7.0 (Web Version), Release 1.5, <http://kinetics.nist.gov/kinetics/index.jsp>.
- Chong, S.-L., & Franklin, J. L. 1971, *J. Chem. Phys.*, 54, 1487.
- Chyba, C. F. & Hand, K. P. 2005, *Annu. Rev. Astron. Astrophys.*, 43, 31.
- Čížek, M., Horáček, J., & Domcke, W. 1998, *J. Phys. B: At. Mol. Opt. Phys.*, 31, 2571.
- Cunningham, M. R., Jones, P. A., Godfrey, P. D., Cragg, D. M., Bains, I., Burton, M. G., Calisse, P., Crighton, N. H. M., Curran, S. J., Davis, T. M., Dempsey, J. T., Fulton, B., Hidas, M. G., Hill, T., Kedziora-Chudczer, L., Minier, V., Pracy, M. B., Purcell, C., Shobbrook, J., & Travouillon, T., 2007, *MNRAS*, 376, 1201.
- Dalgarno, A., & Black, J. H. 1976, *Rep. Prog. Phys.*, 39, 573.
- Dalgarno, A., & Browne, J. C. 1967, *ApJ*, 149, 231.
- DePuy, C. H., & Bierbaum, V. M. 1981, *J. Am. Chem. Soc.*, 103, 5034.
- Douglas, A. E. & Herzberg, G. 1941, *ApJ*, 94, 381.
- Dunkin, D. B., Fehsenfeld, F. C., & Ferguson, E. E. 1970, *J. Chem. Phys.*, 53, 987.

- Ehrenfreund, P., & Charnley, S. B. 2000, *Annu. Rev. Astron. Astrophys.*, 38, 427.
- Eichelberger, B. R., Snow, T. P., & Bierbaum, V. M. 2003, *J. Am. Soc. Mass Spectrom.*, 14, 501.
- Fehsenfeld, F. C., & Ferguson, E. E. 1972, *J. Chem. Phys.*, 56, 3066.
- Fehsenfeld, F. C., Evenson, K. M., & Broida, H. P. 1965, *Rev. Sci. Instrum.* 36, 29.
- Fehsenfeld, F. C., Howard, C. J., & Ferguson, E. E. 1973, *J. Chem. Phys.*, 58, 5841.
- Fehsenfeld, F. C., Schmeltekopf, A. L., & Ferguson, E. E. 1966, *J. Chem. Phys.*, 45, 23.
- Ferguson, E. E., Fehsenfeld, F. C., & Schmeltekopf, A. L. 1969, *Adv. At. Mol. Phys.*, 5, 1.
- Field, D. 2000, *A&A*, 362, 774.
- Franklin, J. L., & Munson, M. S. B. 1964, in *Proc. Tenth Symp. (International) on Combustion*, ed. W. G. Berl (Pittsburgh: Combustion Inst.), 1488.
- Friedman, L. 1968, *Ann. Rev. Phys. Chem.*, 19, 273.
- Frisch, M. J., Trucks, G. W., Schlegel, H. B., Scuseria, G. E., Robb, M. A., Cheeseman, J. R., Montgomery, Jr., J. A., Vreven, T., Kudin, K. N., Burant, J. C., Millam, J. M., Iyengar, S. S., Tomasi, J., Barone, V., Mennucci, B., Cossi, M., Scalmani, G., Rega, N., Petersson, G. A., Nakatsuji, H., Hada, M., Ehara, M., Toyota, K., Fukuda, R., Hasegawa, J., Ishida, M., Nakajima, T., Honda, Y., Kitao, O., Nakai, H., Klene, M., Li, X., Knox, J. E., Hratchian, H. P., Cross, J. B., Bakken, V., Adamo, C., Jaramillo, J., Gomperts, R., Stratmann, R. E., Yazyev, O., Austin, A. J., Cammi, R., Pomelli, C., Ochterski, J. W., Ayala, P. Y., Morokuma, K., Voth, G. A., Salvador, P., Dannenberg, J. J., Zakrzewski, V. G., Dapprich, S., Daniels, A. D., Strain, M. C., Farkas, O., Malick, D. K., Rabuck, A. D., Raghavachari, K., Foresman, J. B., Ortiz, J. V., Cui, Q., Baboul, A. G., Clifford, S., Cioslowski, J., Stefanov, B. B., Liu, G., Liashenko, A., Piskorz, P., Komaromi, I., Martin, R. L., Fox, D. J., Keith, T., Al-Laham, M. A., Peng, C. Y., Nanayakkara, A., Challacombe, M., Gill, P. M. W., Johnson, B., Chen, W., Wong, M. W., Gonzalez, C., & Pople, J. A., *Gaussian 03*, Revision C.02, Gaussian, Inc., Wallingford CT, 2004.
- Galli, D., & Palla, F. 1998, *A&A*, 335, 403.
- Garand, E., Yacovitch, T. I., Neumark, D. M. 2009, *J. Chem. Phys.*, 130, 064304.
- Gerlich, D. & Smith, M. 2006, *Phys. Scr.*, 73, C25.
- Gioumousis, G., & Stevenson, D. P. 1958, *J. Chem. Phys.*, 29, 294.
- Glassgold, A. E. 1996, *Annu. Rev. Astron. Astrophys.*, 34, 241.
- Glover, S. C. O., & Abel, T. 2008, *MNRAS*, 388, 1627.

- Glover, S. C., Savin, D. W., & Jappsen, A.-K. 2006, *ApJ*, 640, 553.
- Harvey, J. N. 2007, *Phys. Chem. Chem. Phys.*, 9, 331.
- Heger, M. L. 1922, *Lick. Obs. Bull.*, 337, 141.
- Hemsworth, R. S., Bolden, R. C., Shaw, M. J., & Twiddy, N. D. 1970, *Chem. Phys. Lett.*, 5, 237.
- Henning, Th., & Salama, F. 1998, *Science*, 282, 2204.
- Herbig, G. H. 1995, *Ann. Rev. Astron. Astrophys.*, 33, 19.
- Herbst, E. & van Dishoeck, E. F. 2009, *Ann. Rev. Astron. & Astrophys.*, 47, 427.
- Herbst, E. 1993, *Rep. Prog. Phys.*, 56, 1209.
- Herbst, E. 1995, *Annu. Rev. Phys. Chem.*, 46, 27.
- Herbst, E. 2001, *Chem. Soc. Rev.*, 30, 168.
- Herbst, E. 2005, *J. Phys.: Conf. Ser.*, 4, 17.
- Herbst, E. 2007, Ohio State Chemical Database, available at (<http://www.physics.ohio-state.edu/~eric>), listed under “gas phase model”.
- Herbst, E. 2010, <http://www.physics.ohio-state.edu/~eric/>.
- Herbst, E., & Klemperer, W. 1973, *ApJ*, 185, 505.
- Herbst, E., & van Dishoeck E. F. 2009, *ARA&A*, 47, 427.
- Herod, A. A., & Harrison, A. G. 1970, *Int. J. Mass Spectrom. Ion Proc.*, 4, 415.
- Hollenbach, D. J., & Thronson, Jr., H. A., eds. 1987, *Interstellar Processes*, Reidel, Dordrecht.
- Howard, C. J., Fehsenfeld, F. C., & McFarland, M. 1974, *J. Chem. Phys.*, 60, 5086
- IAU Symposium 197 1999, *Astrochemistry: From Molecular Clouds to Planetary Systems*, ed. Minh, Y. C. & Van Dishoeck, E. F., Sheridan Books, Chelsea, MI.
- IAU Symposium 231 2005; *Astrochemistry: Recent Successes and Current Challenges*, eds. Dariusz, C. L., Blake, G. A., & Herbst, E., Cambridge University Press, Cambridge, U.K.
- Ikezoe, Y., Matsuoka, S., Takebe, M., & Viggiano, A 1987, *Gas Phase Ion-Molecule Reaction Rate Constants Through 1986*, Maruzen, Tokyo.
- Ishikawa, Y., Binning, R. C., & Ikegami, T. 2001, *Chem. Phys. Lett.*, 343, 413

- IUPAC 42<sup>nd</sup> Congress Symposium, *Astrochemistry*, Glasgow, Scotland, U.K., 2-7 August 2009.
- Jones, P. A., Cunningham, M. R., Godfrey, P. D., & Cragg, D. M. 2007, MNRAS, 374, 579.
- KIDA (*KInetic Database for Astrochemistry*) 2010, <http://kida.obs.u-bordeaux1.fr/>.
- Klemperer, W. 1997, Faraday Lecture, Proc. Roy. Inst., London, 209.
- Kreckel, H., Bruhns, H., Čížek, M., Glover, S. C. O., Miller, K. A., Urbain, X., & Savin, D. W. 2010, Science 329, 69.
- Kuan, Y.-J., Charnley, S. B., Huang, H.-C., Tseng, W.-L., & Kisiel, Z. 2003, ApJ, 593, 848.
- Kwok, S. 2006, *Physics and Chemistry of the Interstellar Medium*, ed. Murdzek, J., University Science Books, Sausalito, CA.
- Langevin, P. 1905, Annal. Chim. Phys., 5, 245.
- Launay, J. M., Le Dourneuf, M., & Zeippen, C. J. 1991, A&A, 252, 842
- Le Teuff, Y. H., Millar, T. J., & Markwick, A. J. 2000, A&A Suppl. Ser., 146, 157.
- Leopold, D. G.; Ho, J., & Lineberger, W. C. 1987, J. Chem. Phys. 86, 1715.
- Lepp, S., & Dalgarno, A. 1988, ApJ, 324, 553
- Lepp, S., Stancil, P. C., & Dalgarno, A. 2002, J. Phys. B: At. Mol. Opt. Phys., 35, R57.
- Lepp, S., & Shull, J. M. 1984, ApJ, 280, 465.
- Liddy, J. P., Freeman, C. G., & McEwan, M. J. 1977, MNRAS, 180, 683.
- Lide, D. R. 2008, *CRC Handbook of Chemistry and Physics* (89<sup>th</sup> ed.; Boca Raton, FL: CRC Press; Taylor & Francis Group)
- Linstrom, P. J., & Mallard, W. G. (ed.) 2010, *NIST Chemistry WebBook*, NIST Standard Reference Database Number 69 (Gaithersburg, MD: NIST) 20899 (<http://webbook.nist.gov>).
- Lovas, F. J., Bass, J. E., Dragoset, R. A., Olsen, K. J. 2009, *NIST Recommended Rest Frequencies for Observed Interstellar Molecular Microwave Transitions*, <http://www.nist.gov/phylab/data/micro/index.cfm>.
- M., Cernicharo, J. 2007, ApJ, 677, 1132.
- Mackay, G. I., Betowski, L. D., Payzant, J. D., Schiff, H. I., & Bohme, D. K. 1976, J. Phys. Chem., 80, 2919.
- Mackay, G. I., Tanaka, K., & Bohme, D. K. 1977, Int. J. Mass Spectrom. Ion Proc., 24, 125.

- Mackenzie Peers, A., & Milhaud, J. 1974, *Int. J. Mass Spectrom. Ion Proc.*, 15, 145.
- Markwick-Kemper, A. J. 2005, in *Proc. IAU Symp. 231, Astrochemistry: Recent Successes and Current Challenges*, ed. D. C. Lis, G. A. Blake, & E. Herbst (Cambridge Univ. Press: Cambridge), 204.
- Martinez Jr., O., Yang, Z., Betts, N. B., Snow, T. P., & Bierbaum, V. M. 2009, *ApJ*, 705, L172.
- Martinez, O., Yang, Z., Demarais, N. J., Snow, T. P., & Bierbaum, V. M. 2010, *ApJ*, 720, 173.
- Martinez, O., Jr., Betts, N. B., Villano, S. M., Eyet, N., Snow, T. P., & Bierbaum, V. M. 2008, *ApJ*, 686, 1486.
- McCarthy, M. C., Gottlieb, C. A., Gupta, H., & Thaddeus, P. 2006, *ApJ*, 652, L141.
- McKellar, A. 1940, *Publ. Astron. Soc. Pac.*, 52, 187.
- Melton, C. E., & Neece, G. A. 1971, *J. Am. Chem. Soc.*, 93, 6757.
- Millar, T. J., & Williams, D. A., eds. 1993, *Dust and Chemistry in Astronomy*, Institute of Physics, Bristol.
- Miller, T. M., Wetterskog, R. E., & Paulson, J. F. 1984, *J. Chem. Phys.*, 80, 4922.
- Müller, H. S. P., Schlöder, F., Stutzki, J., & Winnewisser, G. 2005, *J. Mol. Struct.*, 742, 215.
- Müller, H. S. P., Thorwirth, S., Roth, D. A., & Winnewisser, G. 2001, *A&A*, 370, L49.
- Münch, D. 1945, *ApJ*, 102, 385.
- NIST Computational Chemistry Comparison and Benchmark Database (CCCBDB) 2010*, NIST Standard Reference Database Number 101, Release 15a, April 2010, ed. R. D. Johnson III (<http://cccbdb.nist.gov/>).
- Otto, R., Mikosch, J., Trippel, S., Weidemüller, M., & Wester, R. 2008, *Phys. Rev. Lett.*, 101, 063201.
- Pascoli G., Lavendy H. 1999, *Chem. Phys. Lett.*, 312, 333.
- Peeters, E., Allamandola, L. J., Hudgins, D. M., Hony, S., & Tielens, A. G. G. M. 2004, *Proceedings: Astrophysics of Dust*, ed. Witt, A. N., Clayton, C. G., Draine, B. T., 309, 141.
- Perez, J., Ramirez-Arizmendi, L. E., Petzold, C. J., Guler, L. P., Nelson, E. D., & Kenttamaa, H. I. 2000, *Int. J. Mass Spectrom.*, 198, 173.
- Rakshit, A. B., Stock, H. M. P., Wareing, D. P., & Twiddy, N. D. 1978, *J. Phys. B*, 11, 4237.

- Rehde, D. 2010, *Chemistry in Space: From Interstellar Matter to the Origin of Life*, Wiley-VCH, Weinheim, Germany.
- Remijan, A. J., Hollis, J. M., Lovas, F. J., Cordiner, M. A., Millar, T. J., Markwick-Kemper, A. J., & Jewell, P. R. 2007, *ApJ*, 664, L47.
- Ren, Y. & Yamataka, H. 2007, *J. Org. Chem.*, 72, 5660.
- Rincon, M., Pearson, J., & Bowers, M. T. 1987, *Int. J. Mass Spectrom. Ion Proc.*, 80, 133.
- Ross, T., Baker, E. J., Snow, T. P., Destree, J. D., Rachford, B. L., Drosback, M. M., & Jensen, A. G. 2008, *ApJ*, 684, 358
- Sablier, M. & Rolando, C. 1993, *Mass Spectrom. Rev.*, 12, 285.
- Sakimoto, K. 1989, *Chem. Phys. Lett.*, 164, 294.
- Savage, B. D., & Sembach, K. R., 1996, *Annu. Rev. Astron. Astrophys.*, 34, 279.
- Schiff, H. I., & Bohme, D. K. 1979, *ApJ*, 232, 740.
- Schiff, H. I., Hemsworth, R. S., Payzant, J. D., & Bohme, D. K. 1974, *ApJ*, 191, L49.
- Schmeltekopf, A. L., Fehsenfeld, F. C., & Ferguson, E. E. 1967, *ApJ*, 148, L155.
- Shaw, A. M. 2006, *Astrochemistry: from Astronomy to Astrobiology*, John Wiley & Sons, New York.
- Smith, D. 1992, *Chem. Rev.*, 92, 1473.
- Smith, D., & Adams, N. G. 1977b, *Int. J. Mass Spectrom. Ion Proc.*, 23, 123
- Smith, D., & Adams, N. G. 1977c, *Chem. Phys. Lett.*, 47, 145.
- Smith, D., & Adams, N. G. 1989, *J. Chem. Soc., Faraday Trans. 2*, 85, 1613.
- Snow, T. P. & Bierbaum, V. M. 2008, *Annu. Rev. Anal. Chem.*, 1, 229.
- Snow, T. P. & McCall, B. J. 2006, *Annu. Rev. Astro. Astrophys.*, 44, 367.
- Snow, T. P. 2001, *Spectrochem. Acta, Part A*, 75, 615.
- Snow, T. P., & Bierbaum, V. M. 2008, *Annu. Rev. Anal. Chem.*, 1, 229.
- Snow, T. P., Stepanovic M., Betts, N. B., Eichelberger, B. R., Martinez Jr. O., & Bierbaum, V. M. 2009, *Astrobio.*, 9, 1001.

- Snow, T., 2002, *Diffuse Interstellar Bands* in *Encyclopedia of Astronomy and Astrophysics*, Murdin, P. ed., Bristol Institute of Physics Publishing.
- Snyder, L. E., Lovas, F. J., Hollis, J. M., Friedel, D. N., Jewell, P. R., Remijan, A., Ilyushin, V. V., Alekseev, E. A., & Dyubko, S. F. 2005, *ApJ*, 619, 914.
- Solomon, P. M., & Klemperer, W. 1972, *ApJ*, 178, 389.
- Spitzer, L. 1978, *Physical Processes in the Interstellar Medium*, John Wiley & Sons, New York.
- Stockdale, J. A. D., Compton, R. N., & Reinhardt, P. W. 1969, *Phys. Rev.*, 184, 81.
- Stockdale, J. A. D., Compton, R. N., & Reinhardt, P. W. 1968, *Phys. Rev. Lett.*, 21, 664.
- Su, T., & Chesnavich, W. J. 1982, *J. Chem. Phys.*, 76, 5183
- Swings, P. & Rosenfeld, L. 1937, *ApJ* 86, 483.
- Tanaka, K., Mackay, G. I., Payzant, J. D., & Bohme, D. K. 1976, *Can. J. Chem.*, 54, 1643.
- Thaddeus, P., Gottlieb, C. A., Gupta, H., Brünken, S., McCarthy, M. C., Agúndez, M., Guélin, M., & Cernicharo, J. 2008, *ApJ*, 677, 1132.
- Tichy, M., Rakshit, A. B., Lister, D. G., Twiddy, N. D., Adams, N.G., & Smith, D. 1979, *Int. J. Mass Spectrom. Ion Proc.*, 29, 231
- Tielens, A. G. G. M., & Snow, T. P. eds. 1995, *The Diffuse Interstellar Bands*, Kluwer Academic Publishers, Dordrecht.
- Tielens, A. G. G. M., 2005, *The Physics and Chemistry of the Interstellar Medium*, Cambridge University Press, Cambridge, U.K.
- Trainor, D. W., Ham, D. O., & Kaufman, F. 1973, *J. Chem. Phys.*, 58, 4599
- Twiddy, N. D., Mohebati, A., & Tichy, M. 1986, *Int. J. Mass Spectrom. Ion Proc.*, 74, 251
- UMIST 2010, *The UMIST Database for Astrochemistry*, <http://www.udfa.net/>.
- Van Doren, J. M. 1987, in Ph.D. thesis *Chem. Phys.* (Boulder: Univ. Colorado), 341.
- Van Doren, J. M., Barlow, S. E., DePuy, C. H., & Bierbaum, V.M. 1987, *Int. J. Mass Spectrom. Ion Processes*, 81, 85.
- Villano, S. M., Eyet, N., Lineberger W. C., & Bierbaum, V. M. 2009, *J. Am. Chem. Soc.*, 131, 8227.
- Wakelam, V., Herbst, E., & Selsis, F. 2006, *A&A*, 451, 551.

Wall, W. F., Carraminana, A., Carrasco, L., & Goldsmith, P. F. eds., 1999, *Millimeter-wave Astronomy: Molecular Chemistry & Physics in Space*, Kluwer Academic Publishers, Dordrecht.

Walsh, C., Harada, N., Herbst, E., & Millar, T. J. 2009, *ApJ*, 700, 752.

Watson, W. D. 1973, *ApJ*, 183, L17.

Watson, W. D. 1974, *ApJ*, 188, 35

Watson, W. D. 1976, *Rev. Mod. Phys.* 48, 513.

Watson, W. D. 1977, *Acc. Chem. Res.*, 10, 221.

Wildt, R. 1939, *ApJ*, 90, 611.

Williams, D. A. & Viti, S. 2002, *Annu. Rep. Prog. Chem. Sect. C*, 98, 87.

Woodall, J., Agúndez, M., Markwick-Kemper, A. J., & Millar, T. J. 2007, *A&A*, 466, 1197;  
<http://www.udfa.net>

Woon, D. E. 2010, [www.astrochymist.org](http://www.astrochymist.org).

Wu, X. P., Sun, X. M., Wei, X. G., Ren, Y., Wong, N. B., & Li, W. K. 2009, *J. Chem. Theory Comput.*, 5, 1597.

Xu, Y., Moran, T. F., & Thomas, E. W. 1990, *Phys. Rev. A*, 41, 1408.

Yang, Z., Eichelberger, B., Carpenter, M. Y., Martinez Jr., O., Snow, T. P., & Bierbaum, V. M. 2010, *ApJ*, 723, 1325.

Yang, Z., Eichelberger, B., Martinez Jr., O., Stepanovic, M., Snow, T. P., & Bierbaum, V. M. 2010, *J. Am. Chem. Soc.*, 132, 5812.

Yang, Z., Martinez Jr., O., Carpenter, M. Y., Snow, T. P., & Bierbaum, V. M., in preparation.

Yang, Z., Snow, T. P., & Bierbaum, V. M. 2010, *Phys. Chem. Chem. Phys.*, 12, 13091.